

Université du Québec  
**Institut national de la recherche scientifique**  
Centre Énergie Matériaux Télécommunications

**Antennes Reconfigurables en Diagramme de Rayonnement à base  
de Surfaces Sélectives de Fréquence**

**(Reconfigurable Radiation Pattern Antennas Based on Frequency  
Selective Surfaces)**

Par  
**Suhair Mansoor Mahmood**

Thèse présentée pour l'obtention du grade de Philosophiae Doctor (Ph.D.) en  
Télécommunications

**Jury d'évaluation**

Examinateur externe	Dr. Chan-Wang Park Université de Québec à Rimouski (UQAR)
Examinateur externe	Dr. Khelifa Hettak Communication Research Center Canada (CRC)
Président du jury	Dr. Serioja Ovidiu Tatu INRS-Énergie Matériaux Télécommunications
Directeur de recherche	Dr. Tayeb A. Denidni INRS-Énergie Matériaux Télécommunications

## **ABSTRACT**

Reconfigurable antennas have recently formed a popular research topic. They are attracting the interest of many industry professionals. This is basically due to the growing demands for more functionality while occupying the same or even smaller physical volume. Using various antennas for wireless applications is no longer effective because having several antennas take too much space. Reconfigurable antennas are the best solution to provide a better performance in terms of flexibility, efficiency and combination of several electromagnetic spectrum applications. Frequency selective surfaces are exploited in many communication applications, especially in designing reconfigurable antennas due to their ability to control the electromagnetic field. A frequency selective surface is an important figure concept in reconfigurable antenna structures and has developed rapidly due to their unique properties in suppressing the surface wave propagation.

The main topic of this research is to design new reconfigurable radiation pattern antennas with enhanced performance by using switchable frequency selective surfaces. The antenna consists of a central radiating source surrounded by switchable frequency selective surface unit cells to give the antenna beam, shaping capability to scan 360 degree in the azimuth plane. Novel switchable frequency selective surface unit cells with various structures are designed and their characteristics are compared in both the reflective and transparent states. The reconfigurable response is the basic concept in the antenna design. This is achieved by adding PIN diodes to the lines that will connect or disconnect the unit cells and transform the frequency selective surface to be either a reflective or a transparent surface. As a consequence, switching the frequency selective surface PIN diodes leads to control the antenna beam direction.

In this thesis, two novel reconfigurable antennas with frequency selective surface unit cells are presented, each antenna works at a different frequency band. The switchable frequency selective surface utilized in the proposed antennas operates at different frequency bands. The research topic in this thesis includes investigations and techniques to increase the bandwidth and improve the radiation characteristics of the

reconfigurable antennas by using new switchable frequency selective surface unit cells. Experimental results show the preference of the proposed antennas over those presented in the literature. Thus, two new reconfigurable antennas are implemented and their enhanced performances in terms of bandwidth are proven.



## TABLE OF CONTENTS

Abstract.....	II
Table of Contents.....	V
List of Figures.....	IX
List of Tables.....	XV
1 Chapter One: Introduction.....	1
1.1 Motivations.....	1
1.2 Research problem and objectives.....	2
1.3 Thesis contribution.....	5
1.4 Literature review .....	6
1.5 Frequency selective surface applications .....	7
1.6 Frequency selective surface applications in antennas .....	11
1.7 Thesis organization.....	12
2 Chapter Two: General FSS Theory and Design .....	14
2.1 Introduction .....	14
2.2 Frequency selective surfaces .....	14
2.3 Frequency selective surface design.....	15
2.4 Switchable frequency selective surfaces .....	16
2.5 PIN diodes integration in FSS.....	18
2.5.1 Pin diode lumped elements influence on FSS performance.....	18
2.5.2 PIN diodes impact on FSS performance .....	21
2.6 Conclusion .....	24
3 Chapter Three: frequency selective surface unit cells.....	26

3.1	Introduction .....	26
3.2	Switchable frequency selective surface unit cell design.....	28
3.2.1	Planar strip switchable FSS unit-cell.....	29
3.2.2	Square switchable FSS unit-cell .....	32
3.2.3	Circular switchable FSS unit-cell.....	38
3.2.4	Triangle switchable FSS unit-cell .....	42
3.3	FSS structures comparison.....	47
3.4	Conclusion .....	50
4	Chapter Four: Reconfigurable Radiation Pattern Antenna (one) .....	52
4.1	Introduction .....	52
4.2	Reconfigurable radiation pattern antenna application .....	53
4.3	FSS unit-cell design at $f_2$ .....	53
4.4	Nonagon reconfigurable pattern antenna design .....	58
4.5	Antenna measurements and results .....	60
4.6	Matching and realized gain bandwidth relation .....	62
4.7	Radiation pattern measurements .....	67
4.8	Reconfigurable antenna bandwidth.....	70
4.9	Conclusion .....	75
5	Chapter Five: Reconfigurable Radiation Pattern Antenna (two) .....	76
5.1	Introduction .....	76
5.2	FSS unit-cell design at $f_1$ .....	76
5.3	Pattern reconfigurable antenna design and steering mechanism .....	82
5.4	Experimental results and discussion.....	86

5.5	Conclusion .....	89
6	Chapter Six: Conclusions and future work .....	90
6.1	Introduction .....	90
6.2	Conclusions .....	90
6.3	Future work.....	92
7	CHAPITRE Seven: Résumé .....	94
7.1	Motivations.....	94
7.2	Problème et objectifs de recherche.....	95
7.3	Contributions de la thèse .....	97
7.4	Surfaces sélectives de fréquence .....	98
7.5	Antenne reconfigurable en diagramme de rayonnement .....	100
7.5.1	Introduction .....	100
7.5.2	Conception de la cellule unitaire FSS à la fréquence $f_2$ .....	101
7.6	Antenne reconfigurable de forme ennégone .....	103
7.6.1	Fabrication et résultats de mesure .....	105
7.6.2	Diagrammes de rayonnement mesurés .....	106
7.7	La deuxième antenne reconfigurable en diagramme de rayonnement ..	109
7.7.1	Introduction .....	109
7.7.2	La Cellule de FSS à la fréquence $f_1$ .....	110
7.7.3	Configuration de l'antenne cylindrique reconfigurable .....	116
7.7.4	Résultats expérimentaux et discussions .....	121
7.8	Conclusions .....	124
8	References .....	126



## LIST OF FIGURES

Figure 1-1 Communication links using steerable antennas [69] .....	1
Figure 1-2 An F-117 Nighthawk stealth strike aircraft flying over Nevada in August 2002 [36]. .....	8
Figure 1-3 The French stealth frigate Surcouf (1997-present day) [37].....	8
Figure 1-4 Japan – Misawa Cryptology operation center [38]. .....	9
Figure 1-5 USA San Antonio with FSS installed to cover the antennas. ....	9
Figure 1-6 FSS glass windows for buildings [41].....	10
Figure 1-7 FSS applications in RCS control [43]. .....	11
Figure 2-1 FSS filter responses (a) Low-pass. (b) High-pass. (c) Band-stop. (d) Band-pass. [50]......	15
Figure 2-2 An arbitrary FSS unit cell with its transmission coefficient. Dimensions of the unit cell is about 16 mm.....	16
Figure 2-3 Switchable frequency selective surface with PIN diodes integrated, unit cell dimensions = 14X18.7 mm.....	17
Figure 2-4 Proposed FSS structure. Dimensions (millimeters): W = 10, L = 10, Wd = 5.25, Wf = 1.5, Sb = 1.85, S = 0.5. (a) FSS with discontinuous lines in reflective state. (b) FSS with continuous lines in transparent state. (c) FSS with PIN diode. .....	19
Figure 2-5 Frequency response of the proposed switchable FSS.....	20
Figure 2-6 Ring FSS. (a) Proposed continuous FSS. (b) Proposed discontinuous FSS. (c) Conventional ring FSS. (d) Conventional ring FSS with four gaps. (e) Switchable conventional FSS. (f) Switchable proposed FSS. Dimensions (in millimetres) are M = 1.5, L = 10, K = 0.5, P = 2.475, S = 0.5, R = 2.15 .....	22
Figure 2-7 Transmission coefficient of ring FSS with single PIN diode .....	23
Figure 2-8 Transmission coefficient of ring FSS with four PIN diodes.....	23

Figure 3-1 Proposed FSS unit cell structure.....	27
Figure 3-2 Reflective and transparent performance for $f_1$ and $f_2$ . .....	28
Figure 3-3 Conventional strip line FSS unit cell-Dimensions (mm): M=1.5, L=10, Y=.5, K=0.5, Y=0.5. ....	29
Figure 3-4 Strip line FSS transmission coefficient for line width 1.5mm .....	30
Figure 3-5 Strip line FSS transmission coefficient for line width 0.5mm .....	30
Figure 3-6 Strip line FSS transmission coefficient in the reflective and transparent states.....	31
Figure 3-7 Strip line FSS transmission coefficient in the reflective and transparent states at $f_1$ .....	32
Figure 3-8 Square switchable FSS unit cells -Dimensions (mm): M=1.5, L=10, Y=0.5, K=0.5, P=2.375, S=0.5, A=5.25 .....	33
Figure 3-9 Square FSS transmission coefficient in the transparent and reflective state. ....	35
Figure 3-10 Square FSS transmission coefficient in the reflective state at $f_2$ .....	36
Figure 3-11 Square FSS transmission coefficient in the transparent state at $f_2$ .....	36
Figure 3-12 Square FSS transmission coefficient in the transparent state at $f_1$ .....	37
Figure 3-13 Square FSS transmission coefficient in the reflective state at $f_1$ .....	38
Figure 3-14 Ring FSS unit cells. Dimensions: M=1.5, L=10, Y=0.5, K=0.5, P=2.375, S=0.5, R=2.625. (mm).....	39
Figure 3-15 Circular FSS transmission coefficient in the transparent and reflective state at $f_2$ .....	40
Figure 3-16 Circular FSS transmission coefficient in the reflective state at $f_2$ .....	40
Figure 3-17 Circular FSS transmission coefficient in the transparent state at $f_2$ .....	41
Figure 3-18 Circular FSS transmission coefficient in the transparent state at $f_1$ .....	42

Figure 3-19 Circular FSS transmission coefficient in the reflective state at $f_1$ .....	42
Figure 3-20 Triangle FSS unit cells. Dimensions : $M = 1.5$ , $L = 10$ , $Y = 0.5$ , $K = 0.5$ , $P = 2.375$ , $S = 0.5$ , $H = 5.25$ (mm).....	43
Figure 3-21 Triangular FSS transmission coefficient in the transparent and reflective state at $f_2$ .....	44
Figure 3-22 Triangle FSS transmission coefficient in the reflective state at $f_2$ . ....	44
Figure 3-23 Triangle FSS transmission coefficient in the transparent state at $f_2$ .....	45
Figure 3-24 Triangle FSS transmission coefficient in the transparent state at $f_1$ .....	46
Figure 3-25 Triangle FSS transmission coefficient in the reflective state at $f_1$ .....	46
Figure 3-26 FSS structures transmission coefficient in the transparent state at $f_1$ .....	47
Figure 3-27 FSS structures transmission coefficient in the reflective state at $f_1$ .....	48
Figure 3-28 Proposed FSS unit cells.....	49
Figure 4-1 FSS unit cell. Dimensions in millimetres: $W=18.7$ , $L=14$ , $W_d=8.9$ , $K=3$ , $S_c=1$ , $L_d=8.9$ , $S_b=0.8$ , $S=0.5$ , $W_f=3$ .....	54
Figure 4-2 FSS transmission coefficient. Dimensions changed in (B): $W_d=6$ , $L_d=6$ mm .....	55
Figure 4-3 FSS transmission coefficient. Dimensions changed in (C): $W_d=11$ , $L_d=11$ mm .....	56
Figure 4-4 Simulated transmission coefficient of the proposed FSS unit cell. © 2016 IEEE .....	56
Figure 4-5 Y-Z plane, FSS electric field distribution in the reflective state. © 2016 IEEE .....	57
Figure 4-6 Y-Z plane, FSS electric field distribution in the transparent state. © 2016 IEEE .....	58
Figure 4-7 Proposed reconfigurable antenna, total length is 170mm and radius is	

R=30mm. (a) photo of the antenna. (b) The dipole feed inside the antenna. ....	59
Figure 4-8 Measured reflection coefficient of the antenna and dipole. © 2016 IEEE ...	61
Figure 4-9 Simulated and measured realized gain of the proposed antenna. © 2016 IEEE .....	61
Figure 4-10 Measured results for Antenna-I (a) Measured reflection coefficient [54]-page 2235. ....	63
Figure 4-11 Measured results for Antenna-II: (a) Measured reflection coefficient [54]-page 2235. ....	64
Figure 4-12 Measured gains for Antenna-I and II compared to the simulation. [54] -page 2236. ....	64
Figure 4-13 Measured reflection coefficients of the three fabricated antenna prototypes compared to the simulated one. [34]-page 672. © 2013 IEEE .....	65
Figure 4-14 Measured realized gains of the three fabricated antenna prototypes compared to the simulated one. [34]-page 672. © 2013 IEEE .....	65
Figure 4-15 Simulation and measurement results of S11 . [65] - page 171. © 2015 IEEE .....	66
Figure 4-16 Simulation and measurement results: realized gain in H-plane. [65] - page 172. © 2015 IEEE .....	66
Figure 4-17 Measured H-plane pattern, co-polar, through 300MHz. © 2016 IEEE .....	67
Figure 4-18 Measured H-plane pattern, cross-polar. © 2016 IEEE .....	68
Figure 4-19 Measured E-plane radiation pattern, through 300MHz. © 2016 IEEE.....	68
Figure 4-20 United States frequency spectrum. ....	70
Figure 4-21 Measured radiation pattern E-plane.....	71
Figure 4-22 Measured radiation pattern H-plane.....	71
Figure 4-23 FSS unit cell Transmission coefficient [65]. © 2015 IEEE .....	72

Figure 4-24 Measured radiation pattern N=3 (a) H-Plane (b) E-plane [65]. © 2015 IEEE .....	73
Figure 4-25 Measured radiation pattern in N=7 (a) H-Plane (b) E-plane [65]. © 2015 IEEE .....	73
Figure 4-26 FSS unit cell Transmission coefficient [31]. © 2013 IEEE .....	74
Figure 4-27 Measured radiation pattern E-plane [31]. © 2013 IEEE .....	74
Figure 5-1 Proposed FSS unit cell structure. (a) Transparent state. (b) Reflective state. ....	77
Figure 5-2 FSS transmission coefficients for reflective and transparent states, with and without integrated PIN diodes. ....	78
Figure 5-3 Measured and simulated transmission coefficients for the transparent state. ....	79
Figure 5-4 FSS measured and simulated transmission coefficients in the reflective and transparent states with diodes.....	80
Figure 5-5 (a) Electric field distribution for the transparent state in the Y-Z plane. (b) Electric field distribution for the reflective state in the Y-Z plane. ....	81
Figure 5-6 Top view of the realized cylindrical structure. dL is width of the FSS unit cell, $\theta=0.1976$ rad = $11.32^\circ$ , t=24.969mm, r=25.4648mm, F=2.25GHz, k0=47.156 [1/M], $\Delta\phi=k_0(r-t)=0.0233$ rad = $1.34^\circ$ (phase shift between points A and B).....	83
Figure 5-7 Proposed antenna (a) Photo of the fabricated antenna.(b) The FSS shield hole for the RF-cable entrance.(c) Top and side view antenna design.....	84
Figure 5-8 H-plane radiation pattern for six angles .....	85
Figure 5-9 Antenna beam-steering mechanism .....	86
Figure 5-10 Measured reflection coefficient .....	87
Figure 5-11 Measured H-plane radiation pattern.....	88

Figure 5-12 Measured E-plane radiation pattern.....	88
Figure 7-1 Liens de communication en utilisant des antennes reconfigurables [69]. ....	94
Figure 7-2 La structure de la cellule FSS proposée. .....	99
Figure 7-3 le coefficient de transmission simulé de la cellule FSS, pour f1et f2.....	100
Figure 7-4 Structure de la cellule unitaire de FSS. Dimensions en millimètre: W=18.7, L=14, Wd=8.9, K=3, Sc=1, Ld=8.9, Sb=0.8, S=0.5, Wf=3.....	101
Figure 7-5 le coefficient de transmission simulé de la cellule FSS.....	102
Figure 7-6 L'antenne reconfigurable proposée, la longueur totale est 170mm et un rayon R=30mm. (a) la photo de l'antenne. (b) le dipôle d'alimentation à l'intérieur de l'antenne.....	104
Figure 7-7 Le coefficient de réflexion mesuré de l'antenne et du dipôle.....	105
Figure 7-8 Le gain simulé et mesuré de l'antenne proposée.....	106
Figure 7-9 Diagramme de rayonnement co-pol mesuré dans le plan H à travers la bande 300MHz.....	107
Figure 7-10 Diagramme de rayonnement cross-pol mesuré dans le plan H à travers la bande 300MHz.....	107
Figure 7-11 Diagrammes de rayonnement mesurés à travers la bande 300MHz .....	108
Figure 7-12 La structure de la cellule FSS proposée. (a) état transparent. (b) état réfléchissant.....	110
Figure 7-13 les coefficients de transmission des FSS pour les états transparent et réfléchissant, avec et sans les diodes PIN intégrées. .....	112
Figure 7-14 Les coefficients de transmissions simulés et mesures pour l'état transparent .....	113
Figure 7-15 Les coefficients de transmission simulés et mesurés de la cellule FSS dans l'état réfléchissant et transparent. .....	114

Figure 7-16 (a) La distribution du champ électrique à l'état transparent dans le plan Y-Z. (b) La distribution du champ électrique à l'état réfléchissant dans le plan Y-Z .....	115
Figure 7-17 Vue d'en haut de la structure cylindrique dL est la largeur de la cellule FSS, $\theta=0.1976$ rad = $11.32^\circ$ , $t=24.969\text{mm}$ , $r=25.4648\text{mm}$ , $F=2.25\text{GHz}$ , $k_0=47.156 \text{ m}^{-1}$ , $\Delta\phi=k_0(r-t)=0.0233$ rad = $1.34^\circ$ (le déphasage entre le point A and B) .....	118
Figure 7-18 Antenne proposée (a) Photographie de l'antenne fabriquée, (b) Le trou du bouclier FSS pour le câble RF de l'entrée.....	119
Figure 7-19 Diagramme de rayonnement pour six angle .....	120
Figure 7-20 Mécanisme de pilotage de faisceau de l'antenne .....	121
Figure 7-21 Coefficient de réflexion mesuré.....	122
Figure 7-22 Diagramme de rayonnement mesuré dans le plan H, à travers 300 MHz. .....	123
Figure 7-23 Diagramme de rayonnement mesuré dans le plan E, à travers 300 MHz	123

## LIST OF TABLES

Table 2-1 Switchable FSS transmitted and reflected power percentages with PIN diodes integrated.....	21
Table 2-2 Single pin diode unit cell .....	25
Table 2-3 Four pin diode unit cell .....	25
Table 3-1 Switchable FSS unit cells comparison .....	51
Table 4-1 Comparison of the antennas .....	69
Table 6-1 Comparison of the antennas .....	92
Tableau 7-1 Comparaison des antennes .....	109
Tableau 7-2 Comparaison des antennes .....	125

# 1 CHAPTER ONE: INTRODUCTION

## 1.1 Motivations

Many military and civil applications for reconfigurable antennas can be seated in industry [1-3]. For example, communication between a satellite and a moving transportation object needs to have a steerable antenna to keep the connection stable [4]. Steerable antennas change its radiation direction according to the object position to stay on track. Reconfigurable antennas can allow the delivery of broadband internet access to passengers in many transmission categories as shown in the Fig. 1-1. Also, GPS connection and other types of important links of communications could be delivered [5].

In near future, the demand for broadband is insatiable not just for home and office users but also for mobile users, as Cisco Systems, San Jose, California, estimates that [6]:

*"About three quarters of the world's mobile data traffic will become video by the year 2019, and the smart phone average will generate about 4.0GB of traffic per month by the year 2019".* This highlights the need for wideband reconfigurable antennas to cover the expanded high data rate.

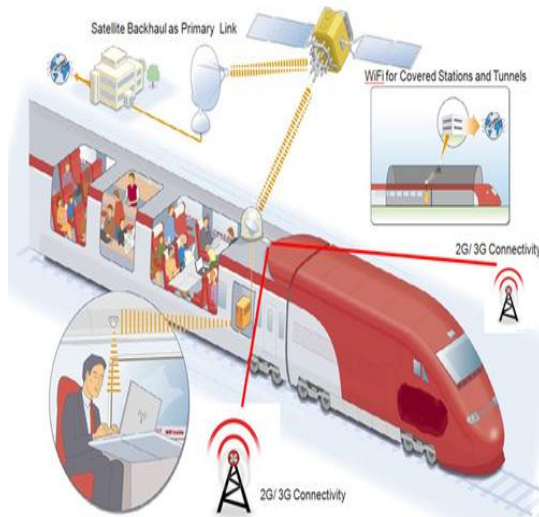


Figure 1-1 Communication links using steerable antennas [69].

Steering the antenna could be done by either mechanical or electronic methods. Mechanical steering is achieved by repositioning and moving the antenna to reach the intended characteristics. However, the mechanical approach is criticized by its low speed and complex system installation.

Phased arrays have been used for many years as reconfigurable antennas; they can steer the antenna pattern in an electronic manner. The phase shifters steer the antenna beam when integrating active switching components such as PIN diodes, RF micro electro mechanical systems (RF MEMS) or any other switchable components. These switching components limit the speed and losses of the antenna due to their undesired parasitic elements. Both the mechanical and electronic methods result in extreme expensive and complex systems [7]. Therefore, intensive research has been made in many directions to find other alternatives and different approaches in this field. One of these alternatives is to use frequency selective surface (FSS) in reconfigurable antennas. This approach offers more functionality for an antenna, more versatility, robustness, less cost and a significant save in size and space [5, 8]. Thus, research in this field is very important and is one of the most popular fields nowadays. The thesis proposes reconfigurable antennas based on FSS with enhanced operating bandwidth.

## 1.2 Research problem and objectives

Reconfigurable antennas have been around since 1930 [9], they are becoming even more interesting for industry. They draw high attention because these antennas give additional functionality and more flexible properties while occupying smaller physical volume compared with traditional smart antennas [10].

Reconfigurable antennas can modify their operating frequency, polarization, impedance bandwidth and radiation pattern in an independent way to conform required operations [5]. However, due to the antennas complication, the developments of these antennas created significant challenges to the engineers designing them besides the required supporting system designs.

Frequency selective surfaces (FSSs) play an important role in reconfigurable antenna designs due to their influence on the wave propagation in planar antennas and other three dimensional antennas [11, 12]. A frequency selective surface is known as a high impedance surface due to its ability to suppress the propagation of the incident waves at its operational frequency. Also, the structure can reduce the influence of mutual coupling in array applications [13, 14].

Many FSSs are exploited in designing reconfigurable antennas for various communication applications because of their variable influence on the electromagnetic field [14]. FSSs are composed of periodic structures performing a forbidden region [15]. Electromagnetic waves cannot propagate through the structure in the forbidden region, (the forbidden region is the frequency band that the structure blocks the waves). This response will be changed if a defect is made in the periodicity of the FSS, in this case, the electromagnetic wave will penetrate through the defect [16]. A FSS is used as a partial reflective or transparent surface in many antenna designs to improve the performance of the antenna in many aspects, such as the antenna gain and the radiation pattern [17].

The goal of this work is to present new switchable frequency selective surface unit cells to form the basic components of the reconfigurable antennas. The transmission coefficient of each proposed unit cell is studied to figure out the best performance for the unit cell that achieves the desired reconfigurable antenna characteristics. In reconfigurable antenna designs, the frequency selective surface unit cell characteristic is the primary influential parameter that affects the sweeping radiation pattern functionality. Thus, in chapter three, an extensive study is done on the proposed FSS characteristics.

Objective of the thesis are summarized in the following points:-

- 1- Design of four different switchable FSSs are proposed and their parameters are investigated. A comparison is made in terms of transmission coefficient and bandwidth for the proposed unit cells in both the resonance and non-resonance frequency bands. The switchable FSS characteristics are investigated to show the difference between each design. This comparative study is important to choose the suitable switchable frequency selective surface characteristics for the intended reconfigurable antenna application.
- 2- Design and fabrication of a reconfigurable antenna based on switchable FSS. The switchable frequency selective surface operates at resonance frequency and the antenna operates at 3.6 GHz. The antenna can sweep the whole azimuth plane with 9 equidistant angles and has enhanced bandwidth.
- 3- Design and fabrication of a reconfigurable antenna operating at 2.1GHz with a more compact size than the antenna mentioned in 2. This means that the antenna is smaller in size and operates at less frequency band. This is rare because when shifting the antenna to a lower operating frequency, its size is expected to be larger. The proposed antenna can sweep the whole azimuth plane over 16 equidistant angles. The switchable FSS used in this antenna design operates in the first non-resonance frequency band and the antenna is characterized by its enhanced bandwidth.

### **1.3 Thesis contribution**

The thesis deals with using significant switchable FSS properties to form an antenna with directive reconfigurable radiation pattern. This research is important because it overcomes the problems associated with communication system performances by combining several functions in a single element [18] and enhances the antenna bandwidth.

The significance of this thesis results arises from the following points:

- To improve the reconfigurable antenna performance and its functionality, two new switchable frequency selective surface unit cells are proposed in two different frequency bands. These switchable frequency selective surfaces are essential parts in the designed antennas.
- To increase the functionality of the reconfigurable antenna by achieving enhanced bandwidth along with suitable back lobe level and low side lobe level in the directive radiation pattern case.
- Due to the switchable FSS small size, the antenna size is reduced and more directive positions are achieved in the whole azimuth plane with enhanced performance.

## 1.4 Literature review

The idea of reconfiguring antenna is relatively old. In the early 1930s, the nulls of two element arrays have been steered by using a calibrated variable phase shifter to find their arrived signal direction [9]. In 1979, “reconfigurability” has been defined as “the ability to adjust beam shapes upon command” [19]. Since then the topic attracted the interest of many researchers and professionals. Here, most of the work done in this field is summarized to distinguish the thesis contribution as compared to similar available antenna designs in literature.

As stated, reconfigurable radiation pattern antenna using FSS is the topic of this thesis. FSS are used because of their variable reaction toward electromagnetic waves. This variable reaction influences the antenna radiation pattern when surrounding a radiating source and leads to sweep its beam. Therefore by changing the periodicity of the structure the antenna radiation pattern could be controlled. Several types of structures are used in this type of application, Electromagnetic band gap structures (EBG) or called Photonic band gap materials (PBG) and Frequency selective surface (FSS) [20, 21].

Several researchers have studied the cylindrical electromagnetic band-gap as a partially reflecting surface (PRS) when surrounding an omni-directional antenna. This application has been introduced in 2004 to increase the directivity of the E-plane beam [22, 23]. In 2006, Boutayeb has designed a reconfigurable antenna by designing a monopole surrounded with an EBG cylinder shield of wires reported in [24]. Afterwards, the idea of integrating active elements has been reported in [25, 26]. These achievements led to the idea of controlling the reconfigurable antenna beam remotely [27]. At this stage, the cylindrical reconfigurable antenna attracted many scholars due to its high gain as compared to the central radiating source antenna and the simple method of steering the beam in an electric manner [28-30]. Liang Zhang has presented a reconfigurable antenna with a single and a dual beam mode. This has been done by integrating varactor diodes to switch the FSS [31]. Habib has made a different approach by changing the EBG direction that faces the radiating source. He changed the EBG shield

direction and made it aligned with the cascading layers toward the propagation [32, 33]. Niro-Jazi has presented a low-power consumption antenna with a design guideline. The guideline has been done by modeling a corner reflector antenna, a semi cylindrical reflector and a cylindrical FSS antenna to estimate the overall reconfigurable antenna design dimensions [34].

In this thesis two novel reconfigurable antennas are proposed in two frequency ranges based on a cylindrical frequency selective surface. The main research contribution is to enhance the antenna bandwidth. Tables are presented to show the bandwidth enhancement and results are compared to other related work in literature. Fractional bandwidth is increased to reach 13.33%. The largest bandwidth reported in literature was 4.49% presented at 2013 by Liang Zhang in [31]. The proposed two antennas have a fractional bandwidth of 8.45% and 13.33% with enhanced performance as proven in the thesis.

## 1.5 Frequency selective surface applications

In 2014, ASD Reports (a market research group in Amsterdam, the Netherlands) estimated that the metamaterials market would increase at a compound annual growth rate of over 41% from 2015 till 2025 to reach \$ 643 million by 2025 [35]. This is due to their continuous raise in applications. FSSs are part of this market with a wide application range. In the following sections some of the FSS important applications are highlighted in brief to show the structure industrial importance.

FSSs could act as a low-pass, high-pass, band-pass or band-reject filter. This characteristic opens a wide variety of applications for each FSS design. One of the important applications in military is the stealth technology that reduces the object detection by the enemy. FSSs are used for this application because it reduces the radar cross section in communication systems when covering an object. FSSs have been implemented on aircrafts and warfare ships and other military weapons [36, 37].



**Figure 1-2 An F-117 Nighthawk stealth strike aircraft flying over Nevada in August 2002 [36].**



**Figure 1-3 The French stealth frigate Surcouf (1997-present day) [37].**

Another important application is using the structure as radomes to cover the communication systems, usually antennas. Radomes work by allowing only the operational frequencies to pass through and reject the other frequencies that lie outside this band. This decreases the radar cross section for the communication equipment and hides it from the enemy. The FSS implemented at the “Cryptology operation center” in Japan-Misawa at 1960 [38] is believed to be the first FSS application.



**Figure 1-4 Japan – Misawa Cryptology operation center [38].**

Radomes are used in warfare ships such as in San Antonio ship to decrease the radar cross section of the communication system antennas. Also, most important to protect these antennas from any undesired external influences which might damage them [39].



**Figure 1-5 USA San Antonio with FSS installed to cover the antennas.**

FSSs are exploited also by the building construction sector in different aspects. Several companies such as Nippon in Japan have manufactured glass that rejects certain frequencies. This type of glass is manufactured with two choices of frequencies, either 2.45 GHz or 1.9 GHz. First frequency rejects the wireless local area network, and the second rejects the mobile communications [40].

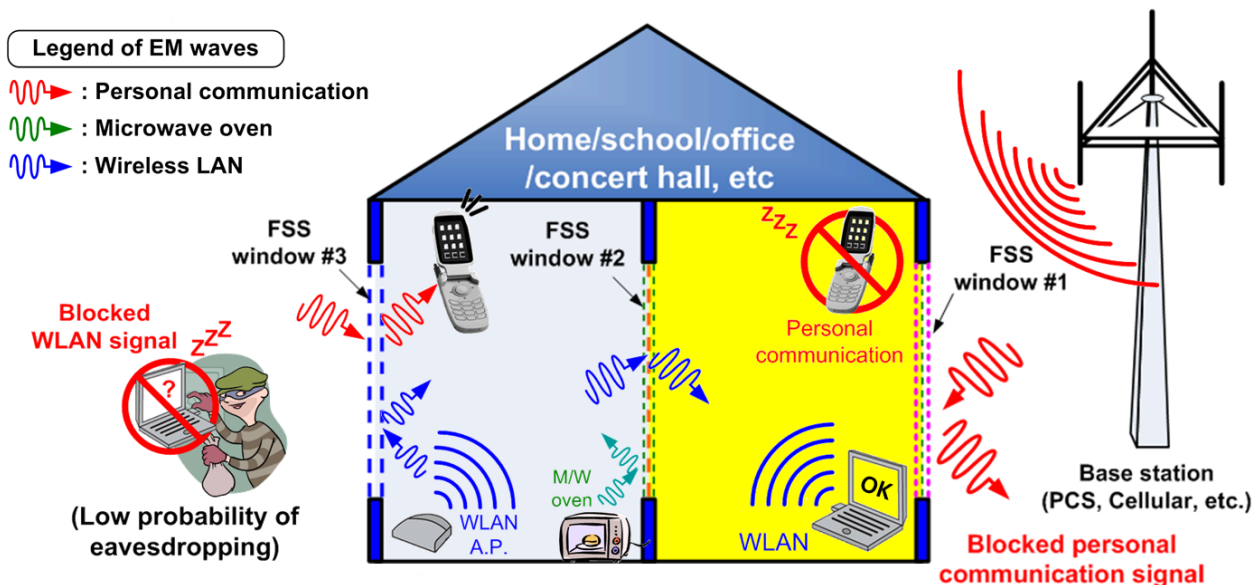


**Figure 1-6 FSS glass windows for buildings [41].**

Electromagnetic architecture of buildings is another concept that is added to the applications of FSS [2]. In this application the FSS covers the walls inside the buildings to enhance the wireless communication systems inside a single building. It is implemented in precise locations on the walls to control the impinged electromagnetic wave direction and power [42]. Here the FSSs are switched between the transparent and reflective state by adding active elements. In addition, they can be controlled remotely. As far as I know, this application is still in the research stage and is done for research purposes in several universities and can be manufactured in future.

## 1.6 Frequency selective surface applications in antennas

The main application within the thesis domain of interest is using FSSs in antenna designs. The antenna performance can be enhanced in different ways if adding FSSs to the design. The FSS will change the antenna performance in many aspects depending on the structure used and the method of integration.

Fig. 1-7 shows forms of using the FSS in reducing the radar cross section as illustrated in [43]. In Fig. 1-7 (a), an antenna is fit in an airplane and the FSS is used on the shield of the airplane. The structure will only allow the antenna operating frequencies to pass through and reject the other frequencies. In Fig. 1-7 (b) the FSS reflects only the antenna operating frequencies and allows the frequencies outside this band to pass through its surface to be absorbed and eliminated by the back layers. In Fig. 1-7 (c) the FSS reflects only the operating frequencies toward the feed and the other frequencies are absorbed and eliminated on the other side of the sub reflector. Finally, in Fig. 1-7 (d) the out of band signals are reflected and only the operating frequencies enter to the shaped band-pass FSS to reach the antenna feed.

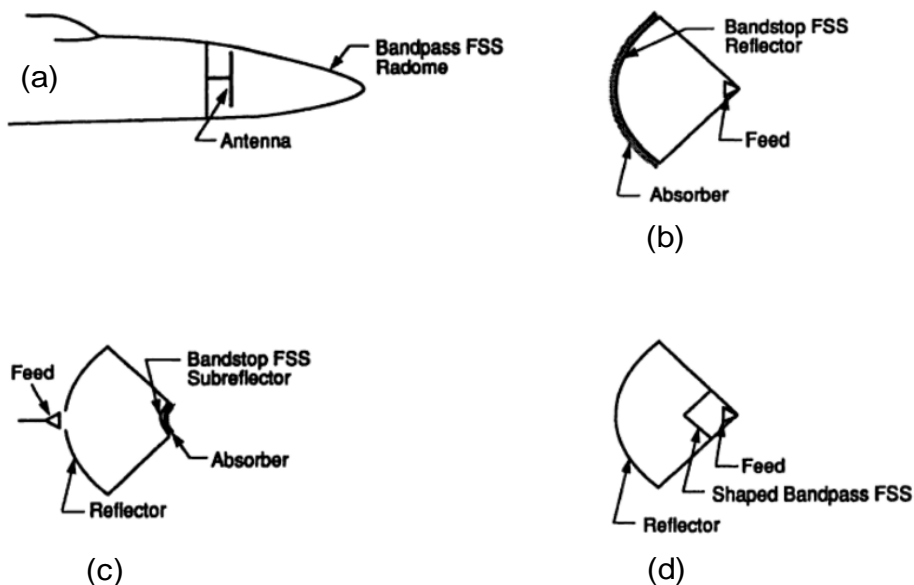


Figure 1-7 FSS applications in RCS control [43].

## 1.7 Thesis organization

### **Chapter One:** Introduction

Presents an introduction on the research topic and discusses the motivation behind studying this specific antenna. Then the research objectives are defined in details and the contribution of the research in this scientific domain is highlighted. A literature review is presented to show the background of this field of research, in particular for the group guided by Professor Tayeb Denidni. At the end of the chapter, applications for the frequency selective surfaces are presented to display the importance of this research filed in the industrial domain.

### **Chapter Two:** General FSS theory and design

A literature summary is presented in this chapter and many related concepts are illustrated. Frequency selective surfaces and their design elements are presented. The impact of adding PIN diodes to switch the switchable frequency selective surface in an electric manner is illustrated. At last, a study is made to show the influence of the switchable PIN diodes and their equivalent circuit on the unit cell performance.

### **Chapter Three:** Frequency selective surface unit cells

In this chapter, several switchable frequency selective surface designs are proposed. The designs are investigated in both the resonance frequency and the non-resonance frequency bands. Results of the proposed unit cell characteristics are compared together for both these frequency bands in terms of transparent and reflective bandwidth.

**Chapter Four:** Reconfigurable radiation pattern antenna (one)

A three dimension reconfigurable antenna is designed. Controlling the antenna beam is done by switching the frequency selective surfaces. Simulation and experimental results for the antenna performance are presented. The antenna performance is examined and the impact of each influential parameter on the antenna performance is justified in details. The antenna is characterized by its enhanced bandwidth and is compared to other similar antennas in literature to prove this enhancement.

**Chapter Five:** Reconfigurable radiation pattern antenna (two)

A second reconfigurable antenna is designed but here the switchable frequency selective surface is operating in the non-resonance frequency band. The aspect of using this FSS frequency band for antenna applications is presented for the first time in this thesis. Experimental and simulated results prove the enhancement of this antenna in terms of bandwidth.

**Chapter Six:** At last, conclusions are made and work expected to be done in the future to enrich this research field is proposed.

## **2 CHAPTER TWO: GENERAL FSS THEORY AND DESIGN**

### **2.1 Introduction**

Frequency selective surfaces (FSS) have attracted high attention in nowadays technology evolution due to their high demand in many applications. Back in the sixties, the topic was under deep studies for military application purposes [13]. The parabolic reflector antenna designed by Marconi and Franklin [44] has been the first contribution in this field. Although passive frequency selective surfaces have many applications, switchable frequency selective surfaces add extra functionality to the unit cell and open other sectors for more applications. FSSs are exploited in many antenna designs to improve their performance and control their characteristics, such as reconfigurable antennas [17], multi-band reflector antennas [45, 46], and various printed antennas [47].

### **2.2 Frequency selective surfaces**

FSS is a periodic two-dimensional or three-dimensional structure [48]. It is composed of a conductive periodic element based on a dielectric substrate [13]. The most important feature of these structures is their frequency selectivity as can be understood from the structure name. FSS controls the electromagnetic waves impinging on its surface and acts as a filter depending on the structure design [49]. These filter properties are classified in to low-pass, high-pass, band-pass and band-stop filters.

Fig. 2-1 shows the basic FSS structures and their frequency response. The gray color in the figure shows the conductive material. In Fig 2-1 (a), the patches show a capacitive equivalent structure [49], and provides low-pass filter characteristics on the impinging electromagnetic field. The FSS will allow the penetration of only the low frequencies and will block the higher frequencies from passing. On the contrary, Fig. 2-1 (b) has an inductive response and acts as a high-pass filter on the impinging electromagnetic wave. The FSS can have both the capacitive and inductive properties combined in their design. In this case, the band-stop or band-pass filter characteristics are obtained as

shown in Fig. 2-1 (c) and (d), respectively.

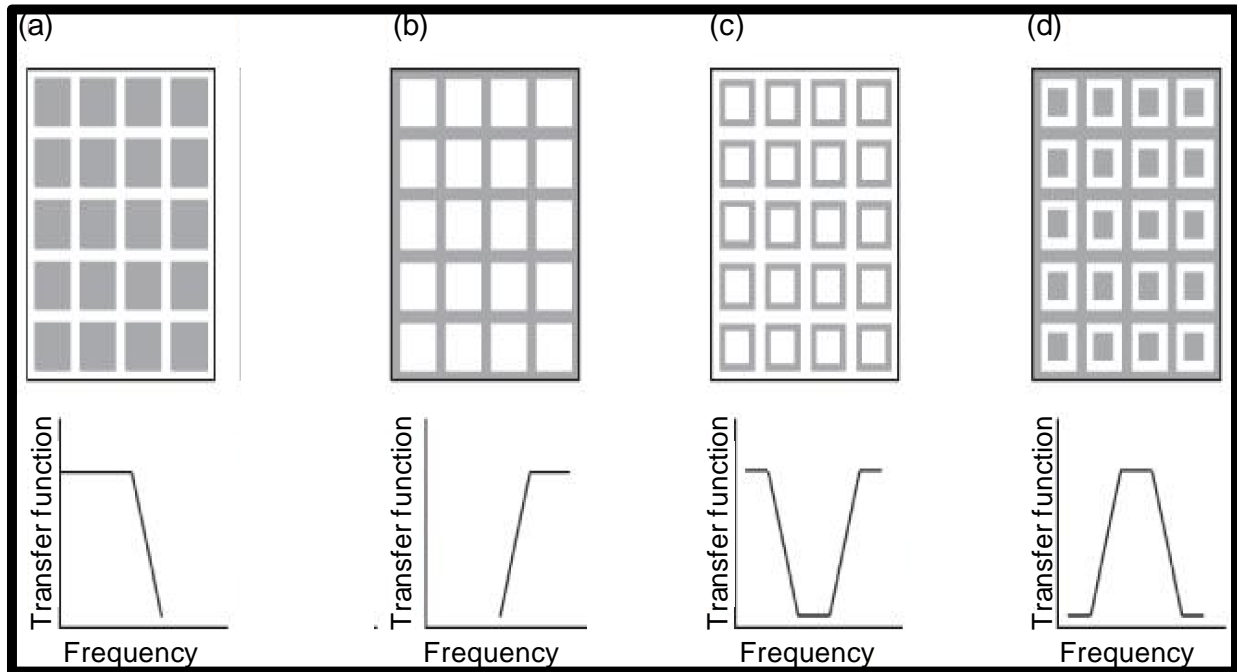


**Figure 2-1 FSS filter responses (a) Low-pass. (b) High-pass. (c) Band-stop. (d) Band-pass. [50]**

### 2.3 Frequency selective surface design

Many shapes could be considered for designing an FSS. The designed shape depends on the FSS performance and characteristics required for the intended application. The design parameters identified at the start point in the FSS design are as following: the operating frequency, the bandwidth, the impinging wave incident angle and the amount of reflected and transmitted power against frequency [5]. Therefore, each frequency selective surface should be designed according to the parameters requested for its intended application.

An example is shown in Fig 2-2 for a “smiling face” FSS. This shape is chosen to prove that any arbitrary shape gives a certain FSS performance. The transmission coefficient shows the reflective and transparent frequency bands. The “smiling face” structure gives a high-pass filter performance. The incident power is reflected in low frequencies, a maximum of 90% from the incident power is reflected around the frequency 1.8 GHz.

While, 81% of the incident power passes through the structure at frequency 7GHz and this percentage increases in higher frequencies as shown in the graph.

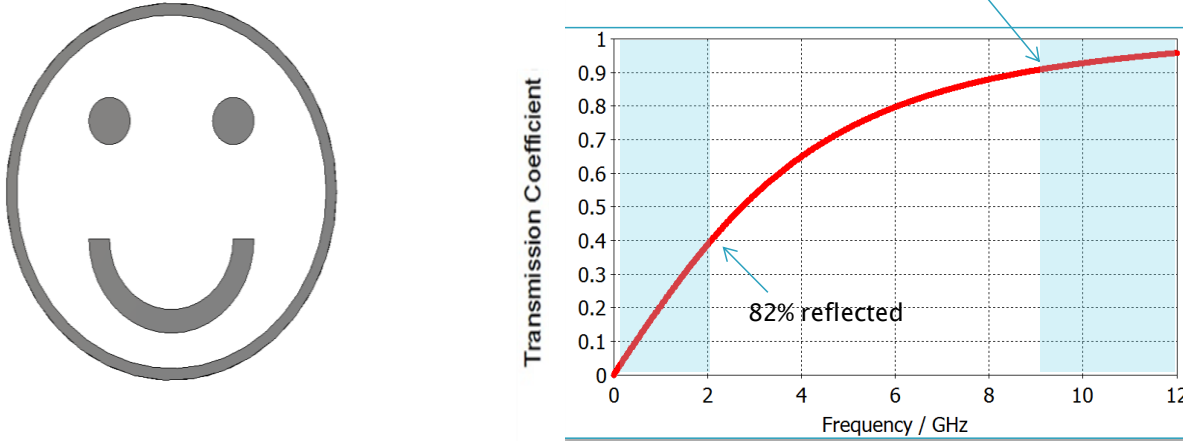


**Figure 2-2** An arbitrary FSS unit cell with its transmission coefficient. Dimensions of the unit cell is about 16 mm.

## 2.4 Switchable frequency selective surfaces

Frequency selective surfaces have a fixed frequency performance that limits the structure functionality. It would be an advantage if the structure can work over more than one frequency without replacing the hardware [21]. This can be achieved by adding switchable elements to the FSS [51]. Switching provides extra functionality to the structure because it controls the electromagnetic field as a function of time by shifting the operating frequency. Switching will convert the structure to be either a transparent or a reflective state, and vice versa. The transparent state means that the structure allows the waves to penetrate through, and the reflective state means that the structure reflects the impinged waves. Switching between the two states can be done electrically by adding active elements to the FSS; in this case it can be controlled in a remote manner. Switchable FSS designs emerged more applications such as tunable filters, phased arrays, reconfigurable antennas [52] and multi-band reflector antennas.

Designing a switchable FSS for an application is based on the intended application parameters. These parameters should be studied to decide which design has the most suitable performance to achieve the required characteristics. Some FSS applications need a wide bandwidth regardless of the transmitted power amount. Other applications require that the maximum transmitted power is identical to the maximum reflected power regardless of the bandwidth. Thus, the switchable FSS design should be adjusted to achieve certain characteristics compatible with the intended application.

Fig. 2-3 shows a switchable FSS example with a PIN diode integrated at the center to switch the structure. The transmission coefficient ( $S_{21}$ ) is shown across a wide frequency band to clarify the switching mechanism. When the PIN diodes are biased OFF, the squares are disconnected from each other and the diodes act as open circuits, here the FSS appears like an infinite array of squares that resonate at 3.87 GHz. When the diodes are forward biased, the squares are connected by the diodes forming an inductive series of unit cells [53]. This leads to shift the resonance to a higher frequency around 10.5 GHz. As a consequence, the FSS will be transparent at 3.87 GHz. This justifies why the FSS is switchable at 3.87 GHz and has either a transparent or a reflective performance depending on the PIN diode switching state.

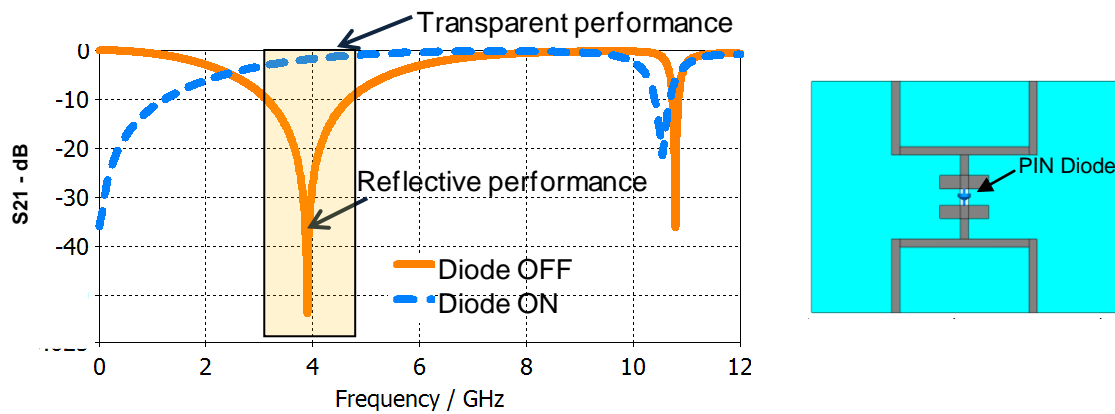


**Figure 2-3** Switchable frequency selective surface with PIN diodes integrated, unit cell dimensions = 14X18.7 mm

## 2.5 PIN diodes integration in FSS

FSS are usually switched by integrating PIN diodes to the unit cells [21]. The PIN diode parameters should be selected carefully to ensure minimum influence on the unit cell performance in both the transparent and reflective state. Although different kinds and brands of PIN diodes with various specifications are available in the market, several main parameters still limit its selection process. The main parameter that should be considered is the price. This parameter is disparate and important because of the large PIN diode numbers required for the switchable FSS designs. Diodes with appropriate specifications and suitable packaging style could be expensive. There could be many types of PIN diodes suitable for each FSS design; never the less, PIN diodes with sufficient characteristics should be targeted. In the following sub sections, two main issues are discussed to illustrate the PIN diode influence on the switchable FSS unit cell.

- First, PIN diodes are integrated to the unit cell and modeled with their equivalent lumped elements to investigate the most convenient equivalent elements that offer the performance closest to the ideal case.
- Second, the influence of reducing the number of PIN diodes for the same FSS on the overall performance is investigated. In addition, variable capacitance values are simulated to study the impact of the equivalent circuit parasitic elements on the unit cell performance.

### 2.5.1 PIN diode lumped elements influence on FSS performance

Fig. 2-4 shows the FSS unit cell with mechanical switching in (a) and (b) and when integrating the PIN diode to unit cell for electrical switching in (c). The unit cell has a square shape with a vertical line between each successive unit cell, the square length is **wd**. The continuity of the vertical line **sb**, identifies whether the FSS unit cell has a reflective or transparent surface. If the vertical line **sb** is discontinuous and has a gap as

in Fig 2-4 (a), the unit cell performs as a reflective surface and does not allow the incident electromagnetic wave to penetrate. On the contrary, if the line **sb** is continuous between the successive unit cells, as shown in Fig. 2-4 (b), it performs as a transparent surface and allows the electromagnetic wave to propagate through the structure.

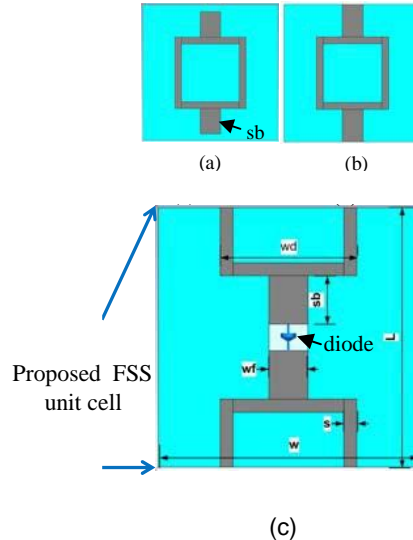


**Figure 2-4** *Proposed FSS structure. Dimensions (millimeters):  $W = 10$ ,  $L = 10$ ,  $Wd = 5.25$ ,  $Wf = 1.5$ ,  $Sb = 1.85$ ,  $S = 0.5$ . (a) FSS with discontinuous lines in reflective state. (b) FSS with continuous lines in transparent state. (c) FSS with PIN diode.*

The PIN diodes are modeled in simulation using their equivalent lumped elements RLC circuit [54]. When the PIN diode is OFF in the reversed bias, it is modeled with a series connection of the equivalent inductance and capacitance elements. When the PIN diode is ON in the forward bias, it is modeled with a resistance value of  $R = 1.8$  Ohms. The inductance value considered is  $L = 0.5$  nH. The most critical element that influences the FSS reflective state is the capacitance value. Therefore, two capacitance values are taken in to account. The capacitance values  $C = 0.001$  pF and  $C = 0.01$  pF are considered to show the impact of these two values on the switchable FSS performance.

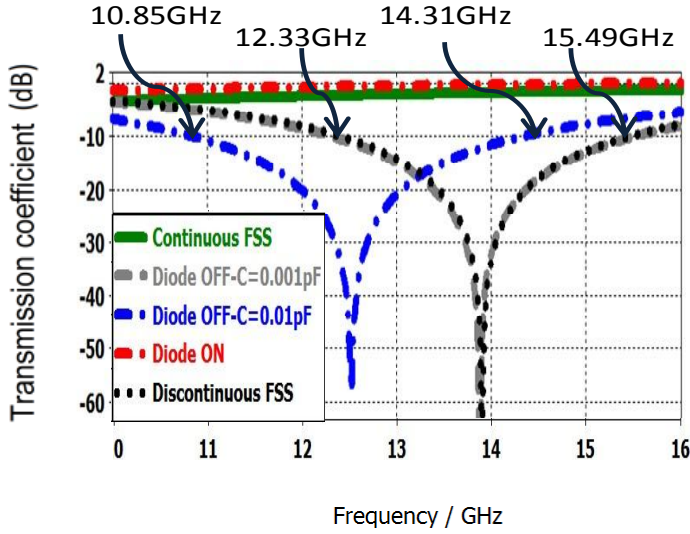


**Figure 2-5 Frequency response of the proposed switchable FSS**

Figure 2-5 shows the transmission coefficient of the switchable unit cell in the reflective and transparent state. The curves compare between the ideal case which has continuous and discontinuous lines and the case when the PIN diodes are integrated to the FSS. When the capacitance value is  $C = 0.001 \text{ pF}$ , the maximum reflected power is at 13.88 GHz. While, when the value is  $C = 0.01 \text{ pF}$  the maximum reflected power is at 12.53 GHz. In addition, the 90% reflective bandwidth for the  $C = 0.01 \text{ pF}$  case is larger by 288 MHz than the  $C = 0.001 \text{ pF}$  case. Table 2-1 shows the power percentages versus frequency for the transparent and reflective states. The frequency limits are minimum 90% for the reflected power. These frequencies are pointed out in Fig 2-5 around -10 dB.

According to Table 2.1, the power penetrating through the switchable FSS when it operates as a transparent surface is between 79% - 95.4%. When the FSS operates as a reflector it reflects minimum 90% of the incident power that is between 10.854 – 14.31 GHz for the  $C = 0.01 \text{ pF}$  case. The minimum power limit considered in the thesis is 90% for the reflective state that is convenient for most industrial applications.

Results show that the PIN diodes with capacitance value  $C = 0.001 \text{ pF}$  has a performance relative to the ideal mechanical switching case. Thus, PIN diodes with

similar parameters are recommended to be considered for fabrication.

**Table 2-1 Switchable FSS transmitted and reflected power percentages with PIN diodes integrated**

PIN diode Elements (pF)	Frequency (GHz)	Power percentage (%)	
		Transmitted	Reflected
C = 0.01	10.854	79	90
C = 0.01	14.31	95.4	90
C = 0.001	12.33	85	90
C = 0.001	15.498	98	90

### 2.5.2 PIN diodes impact on FSS performance

If large numbers of unit cells are desired in a switchable FSS application then the number and cost of active components will raise. Here, a novel switchable ring FSS is proposed with the need for less active components for a switchable FSS design. The switchable ring FSS presented in literature has four gaps and uses four active components to switch the unit cell [55-57]. In this section, the proposed ring FSS requires only one active element to switch the unit cell between the transparent and reflective states. Reducing the number of active components from four to one for each switchable FSS unit cell reduces the cost by 75%. In addition, it reduces the parasitic element effect that degrades the unit cell performance. Also, the proposed FSS requires no DC feed lines to bias the active elements, because they are already taken in to account in the unit-cell design. Whereas, the DC lines in the conventional ring FSS are designed on the back side of the substrate to feed the four diodes. These lines degrade the FSS performance, especially in the transparent state, as reported in [55]. Here, the ring FSS is switched by using only one gap for the first time in literature and adds enhanced features over the conventional ring FSS, results are presented and discussed to demonstrate these features.

Figure 2-6 (f) shows the proposed switchable ring unit-cell with one PIN diode. This is equivalent to the mechanical switching shown in Fig. 2-6 (a) and (b), with continuous and discontinuous lines, respectively. Fig. 2-6 (e) shows the conventional switchable

FSS with four PIN diodes. Its equivalent mechanical switching is shown in Fig. 2-6 (c) and (d).

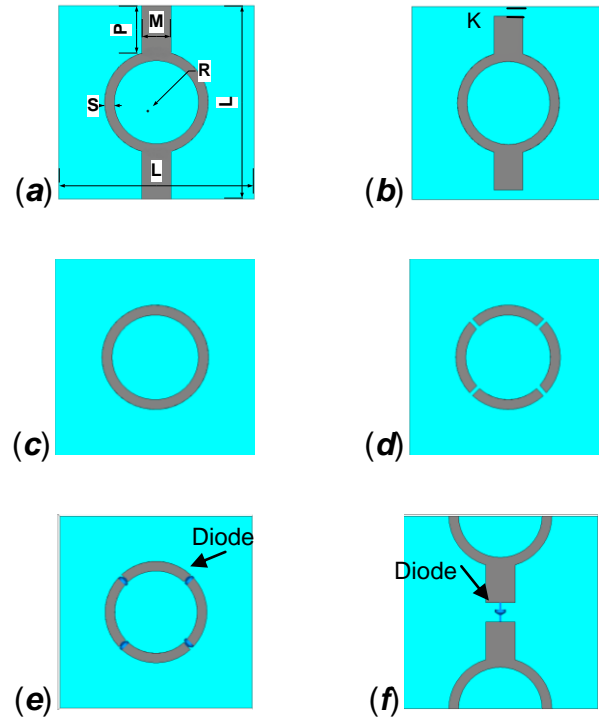


**Figure 2-6 Ring FSS.** (a) *Proposed continuous FSS.* (b) *Proposed discontinuous FSS.* (c) *Conventional ring FSS.* (d) *Conventional ring FSS with four gaps.* (e) *Switchable conventional FSS.* (f) *Switchable proposed FSS.* Dimensions (in millimetres) are  $M = 1.5$ ,  $L = 10$ ,  $K = 0.5$ ,  $P = 2.475$ ,  $S = 0.5$ ,  $R = 2.15$

Different lumped equivalent circuits are examined to model the PIN diodes integrated to the switchable FSS unit cells. The PIN diodes are modeled as a resistor in the ON state and as a capacitor in the OFF state. Varying the resistor value in the ON state has a negligible effect on the unit cell performance. Thus, it is considered to be constant and its value is  $R = 1.8 \Omega$ . When changing the value of the capacitance in the OFF state, influence is noticed on the unit cell performance. Hence, three values of capacitance are selected for the equivalent lumped elements to study their influence on the transmission coefficient. The values proposed are:  $C = 0.7 \text{ pF}$ ,  $C = 0.07 \text{ pF}$  and  $C = 0.02 \text{ pF}$ . Fig. 2-7 shows the transmission coefficient for the single active element unit cell shown in Fig 2-6 (f) when having variable capacitance values in the PIN diode OFF

state and constant resistance in the ON state. Fig. 2-8 shows the transmission coefficient with the same proposed capacitance values in the diode OFF state, but this time for the unit cell that has four PIN diodes shown in Fig 2-6 (e).

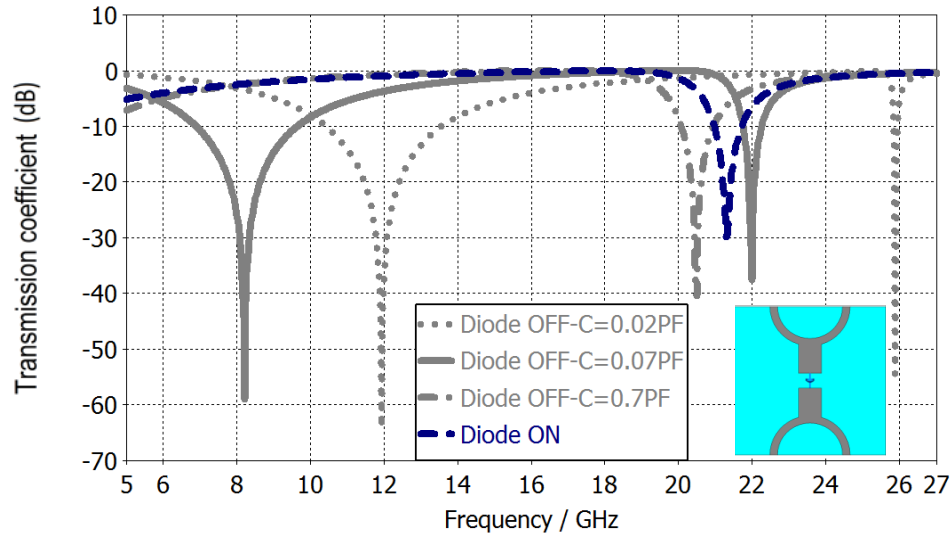


Figure 2-7 Transmission coefficient of ring FSS with single PIN diode

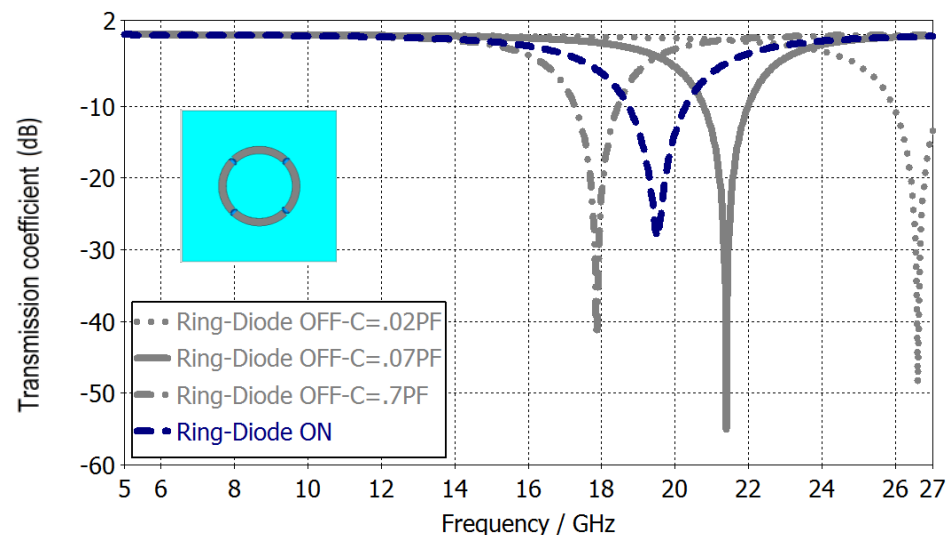


Figure 2-8 Transmission coefficient of ring FSS with four PIN diodes

It is observed from the graphs 2-7 and 2-8 that the last four nulls are similar in the shape of the curves, but differ in terms of bandwidth and center frequencies. The main difference noticed between the two graphs is the added two nulls in Fig 2-7.

Table 2-2 and 2-3 list the percentages of the transmitted power correspondent to a minimum of 90% power reflected from the incident power. When the capacitance value is  $C = 0.02 \text{ pF}$  three resonant frequencies occur at 11.94 GHz, 21.3 GHz and 25.89 GHz, as shown in Table 2-2. At the first and last resonance frequencies, the unit cell is reflective when the PIN diode is OFF and transparent when ON. At the resonance frequency 21.3 GHz, the unit-cell is reflective when the diode is ON and transparent when OFF. The same switchable states apply in Table 2-3 for the nulls at frequencies 26.64 GHz and 19.56 GHz, respectively.

## 2.6 Conclusion

FSSs are important periodic structures in nowadays technology due to the structure ability to control the electromagnetic waves. In this chapter an overview on FSSs has been presented. Switchable FSS adds more functionality and cost to the unit cell. The active elements added to switch the FSS influence directly the unit cell performance. Therefore, active-element price and characteristics should be compromised when designing the unit cell especially if large numbers are used. Demanded applications are the main aspect to design switchable FSSs to be appropriate for new technologies.

**Table 2-2 Single pin diode unit cell**

Diode Elements		Frequency	Power percentage (%)	
R ( $\Omega$ )	C (pF)	(GHz)	Transmitted	Reflected
	0.07	6.93	48	90
	0.07	9.63	64	90
	0.02	10.44	72	90
	0.02	13.54	85	90
1.8	0.7	20.02	71	90
1.8	0.07 0.02	20.97	85 79	90
1.8	0.02	21.72	83	90
	0.02	25.89	87	90

**Table 2-3 Four pin diode unit cell**

Diode Elements		Frequency	Power percentage (%)	
R ( $\Omega$ )	C (pF)	(GHz)	Transmitted	Reflected
1.8	0.02 0.07	18.75	92 67	90
1.8	0.02 0.7	20.31	87 70	90
1.8	0.07	21.99	54	90
	0.02	25.95	91.3	90
	0.02	27.18	94.7	90

### **3 CHAPTER THREE: FREQUENCY SELECTIVE SURFACE UNIT CELLS**

#### **3.1 Introduction**

The FSS topic plays an important role in technology for its various applications. In general, the idea of using FSS is based on its structure influence on the impinging electromagnetic waves [58, 59]. A switchable FSS controls the electromagnetic wave propagation in two ways. Either it allows most of the impinging electromagnetic wave to penetrate through the structure or it reflects most of the impinging waves [59]. These two states are called transparent and reflective, respectively. In our designs, switching between the two FSS states are achieved by changing the periodicity of the FSS. This is done by controlling the gaps between the successive unit cells.

Four main variant switchable FSS geometries are introduced, planar strip, square, ring and triangle. The switchable FSSs are similar in terms of size, periodic spacing and material, but they are different in terms of geometric structure. The idea behind changing the structure geometry and keeping the other components similar is to study the influence of the geometric structure on the transmission coefficient performance in both the transparent and reflective states.

The proposed switchable FSSs are designed to work in both the resonance frequency band ( $f_2$ ) and the first realized frequency that can be also called the first non-resonance frequency band ( $f_1$ ). These two frequency bands are exploited due to the following features. First, the transparent and reflective states have compatible maximum power at the first non-resonance frequency band  $f_1$ . Whereas, at the resonance frequency  $f_2$  the maximum transmitted power is not necessarily compatible in frequency with the maximum reflective power as in [34]. Second, both the reflective and transparent states have large joint bandwidth in  $f_1$  as compared to the resonance frequency  $f_2$  narrow joint bandwidth as in [31]. These features made it important to investigate the proposed designed unit cells at the non-resonance frequency  $f_1$  and at the resonance frequency bands  $f_2$  in parallel with the geometry influence on the overall performance.

A solid interior circular switchable FSS unit cell is taken as an example to illustrate furthermore the difference in the two operating bands  $f1$  and  $f2$ . Fig. 3-1 (a, b) shows a circular solid interior unit cell in the reflective and transparent state. Fig. 3-2 shows the transmission coefficient for both states. At the first realized frequency band  $f1$ , both the transparent and reflective states are almost identical and have more than 90% transmitted and reflected power in both states across a joint frequency band of about 5GHz. Whereas, at the resonance frequency  $f2$  the joint frequency could be considered between 19.8 -21.04 GHz, across a bandwidth of 1.24 GHz. In this frequency band, the reflected power is between 90%-75% and the transmitted power is more than 83% when switching between the reflective and transparent states, respectively. Never the less, a larger band could be considered for  $f2$  but the transmitted power in this case will be less than 83%. If the selected limit is around 90% reflected power then the bandwidth is about 3.8GHz and the corresponding transmitted power will vary between 68% - 83% from the incident power. Choosing the  $f2$  band depends on the application required. Either a wide bandwidth with high reflective power is chosen or a narrow bandwidth with high transparent power. From these results it could be concluded that the first non-resonance frequency band  $f1$  is preferable over the resonance frequency band  $f2$  in terms of high power accompanied with wide joint frequency bandwidth for both the reflective and transparent states.

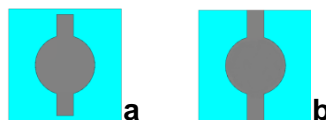


**Figure 3-1 Proposed FSS unit cell structure.**

- a) Transparent state in the  $f1$  case and reflective state in the  $f2$  case
- b) Reflective state in the  $f1$  case and transparent state in the  $f2$  case

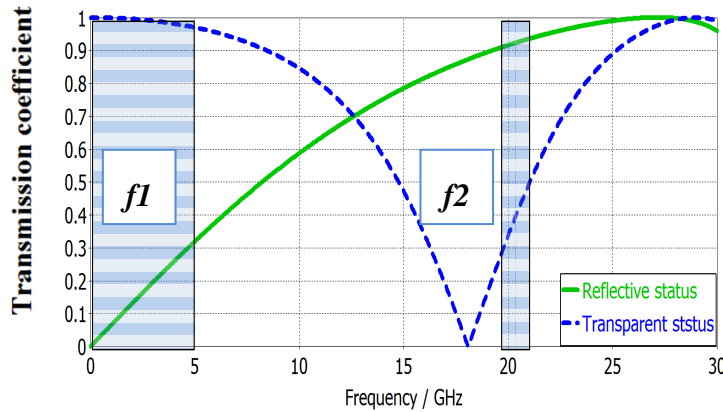


Figure 3-2 Reflective and transparent performance for  $f_1$  and  $f_2$ .

### 3.2 Switchable frequency selective surface unit cell design

In the previous section the switchable FSS performance and differences between both the resonance and non-resonance frequency bands are explained. In this section, the concept is validated by designing four switchable FSSs: planar strip, square, ring and triangle. Each configuration has a loop design and a solid interior design with thick and thin connecting lines. Each unit cell is studied in the first non-resonance frequency band  $f_1$  and in the resonance frequency band  $f_2$ . The characteristics of these two cases are examined to show the properties of each unit cell design within these frequency bands. Besides, a comparison is made between the achieved results for the proposed unit cells in both frequency bands. The comparison is presented in a table at the end of the chapter to emphasize the influence of the unit cell shape variation on the FSS properties.

Computer Simulation Technology (CST) Microwave Studio simulator is used to simulate the proposed structures. In these simulations, the incident electromagnetic wave propagation is emitted in the Z direction with normal impinging to the X - Y plane. The incident E-plane is parallel to the Y coordinate, while the H-plane is parallel to the X coordinate. The unit cells are designed on a flexible RO3003 substrate with dielectric constant of 3 and thickness of 0.13mm. This substrate is chosen due to its bending ability that is necessary to form the cylinder shape needed for the intended antenna

design application.

### 3.2.1 Planar strip switchable FSS unit-cell

In this section we consider a simple FSS structure that is a  $\lambda/2$  strip lines [13]. This unit cell is included in the thesis to compare between this simple structure and other more complicated geometric structures. Fig. 3-3 shows the line shaped FSS with unit a cell dimension of  $L = 10$  mm. The length of the gap between the successive unit cells is 1mm and two line widths are considered:  $Y = 0.5$  mm and  $M = 1.5$  mm.

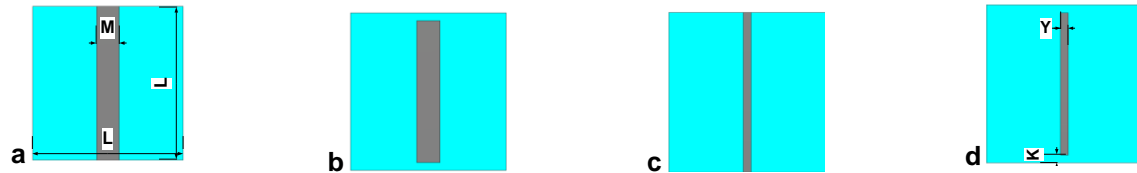


**Figure 3-3 Conventional strip line FSS unit cell-Dimensions (mm):  $M=1.5$ ,  $L=10$ ,  $Y=.5$ ,  $K=0.5$ ,  $Y=0.5$ .**

#### 3.2.1.1 Strip line results for the resonance frequency $f_2$

Figs. 3-4 and 3-5 show the FSS unit cell performance for both the proposed line widths. While, the transmission coefficient of the proposed unit cells in both the transparent and reflective states are shown in Fig. 3-6. The thin line unit cell has less bandwidth, and lower resonance frequency, but it has higher transmitted power as compared to the thick line. Switching is done in simulation by making the lines connected as shown in Figs. 3-3 a, c or disconnected as in Figs. 3-3 b, d. In other words, there are two designs one for the reflective state and one for the transparent state. This scenario is the ideal case where no losses occur due to active components. But it is not practically efficient because the structures have to be replaced during the switching process. The functional alternative is to use electronic switching by adding any active components in the place of the gap as discussed in chapter two. In chapter four and five, the FSS unit cells are

electrically switched by integrating PIN diodes to the unit cells. The FSS dimensions are constant for the unit cells presented in this chapter and only the shape of the FSSs are changed to study and compare them together at the end of the chapter. In addition, these specific dimensions are chosen to integrate the unit cells later in a reconfigurable antenna application operating in specific frequency bands.

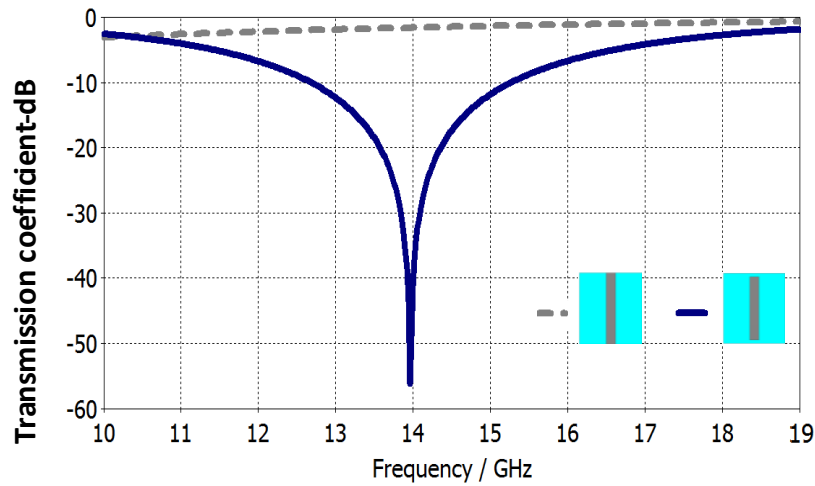


**Figure 3-4 Strip line FSS transmission coefficient for line width 1.5mm**

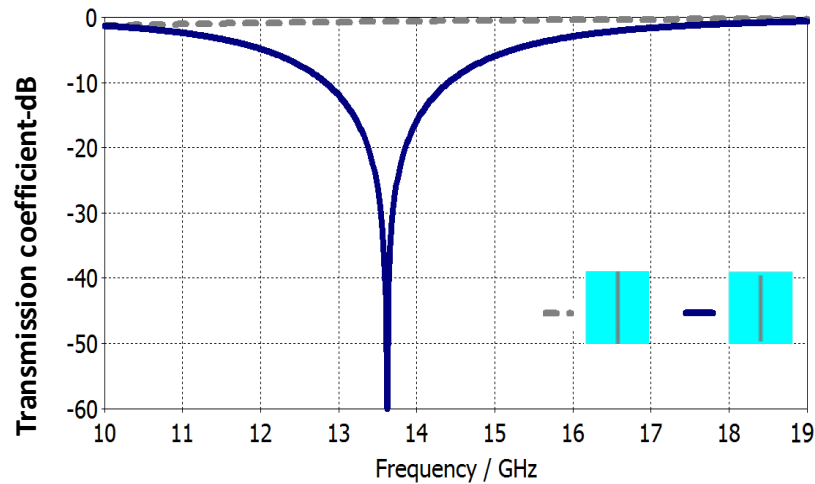


**Figure 3-5 Strip line FSS transmission coefficient for line width 0.5mm**

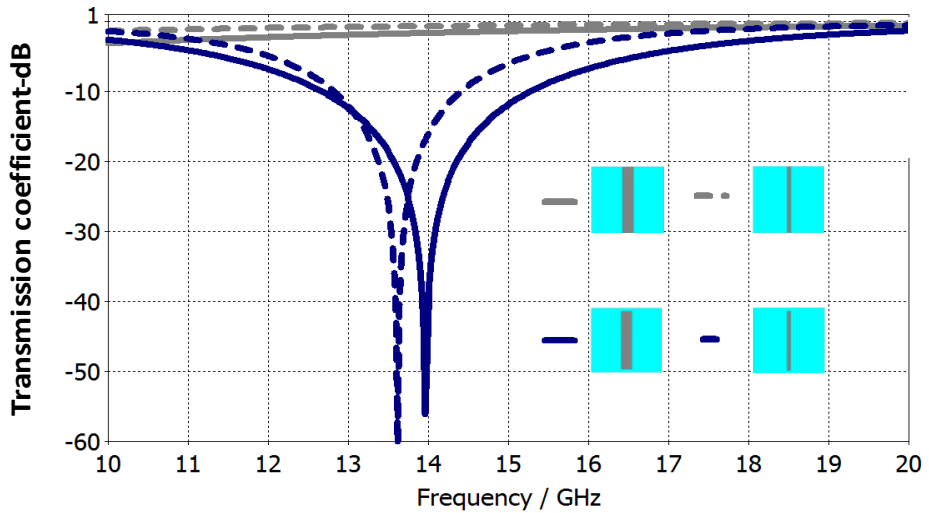


**Figure 3-6 Strip line FSS transmission coefficient in the reflective and transparent states.**

### 3.2.1.2 Strip line results for the non-resonance frequency band $f1$

At the non-resonance frequency, the FSS acts as a reflective surface when the unit cells are connected as in Figs. 3-3a and c and will block the incident electromagnetic wave. On the other hand, it is a transparent surface when there is a gap between the successive unit cells, as shown in Figs. 3-3b and d. It can be noticed that this configuration is opposite to the configuration in the resonance frequency band operating at  $f2$  where Figs. 3-3a and c present the transparent state, and Figs. 3-3b and d present the reflective state.

Fig. 3-7 shows the transmission coefficient of the unit cells for both the transparent and reflective states in the first non-resonance frequency  $f1$ . Results are provided in linear and decibel scales to make it easy to compare between the unit cell performance and other unit cells in literature.

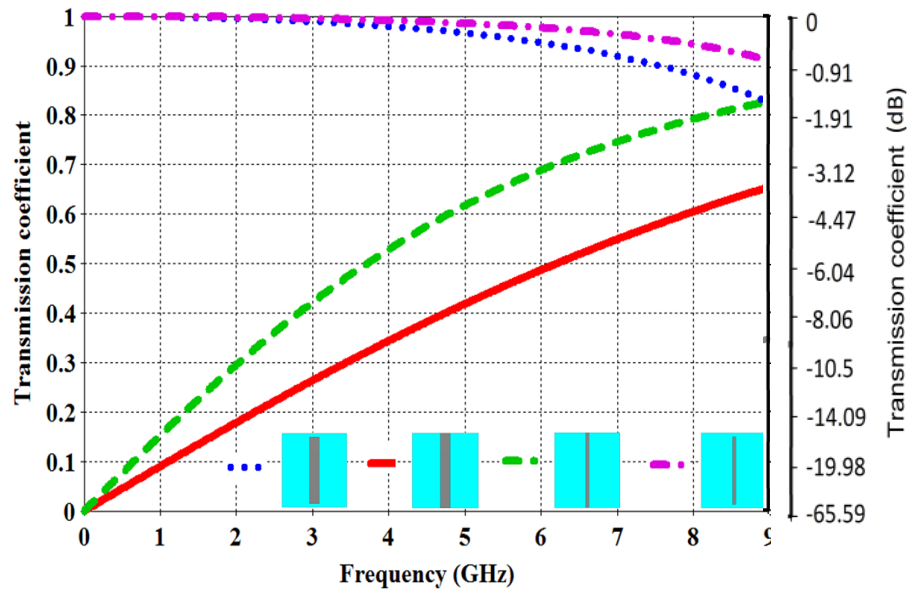


**Figure 3-7 Strip line FSS transmission coefficient in the reflective and transparent states at  $f_1$**

### 3.2.2 Square switchable FSS unit-cell

Four main switchable square FSS geometries are introduced. As mentioned, the FSSs are similar in terms of size, periodic spacing and material, but they are different in terms of geometric structure. In this chapter the FSS geometries are different while the other components are similar such as the substrate used and the unit cell dimensions. This assumption is made to investigate the impact of the structure geometry on the transmission coefficient performance in both the transparent and reflective states at the resonance and non-resonance frequency bands.

The proposed switchable square FSS unit cells are shown in figure 3-8. Different square unit cells are presented. The line  $P$  influences directly the state of the unit cell. At resonance frequency  $f_2$ , if the line  $P$  is continuous between two successive unit cells, as shown in Fig. 3-8a then the FSS performs as a transparent surface. However, if the unit cell has a gap  $K=0.5$  mm in the line  $P$  as in figure 3-8f, then the unit cell is a reflective surface and will not allow the wave to penetrate. This applies for the unit cell when operating at  $f_2$  frequency band.

Unit cells in Figs. 3-8a and b are loop switchable square FSSs with thick connecting lines in the transparent and reflective state, respectively. Figs. 3-8c and d are solid

interior square FSS with thick connecting lines. Figs. 3-8e and f are loop square FSS unit cell with thin connecting lines, and Figs. 3-8g and h show the solid interior square with thin connecting lines.

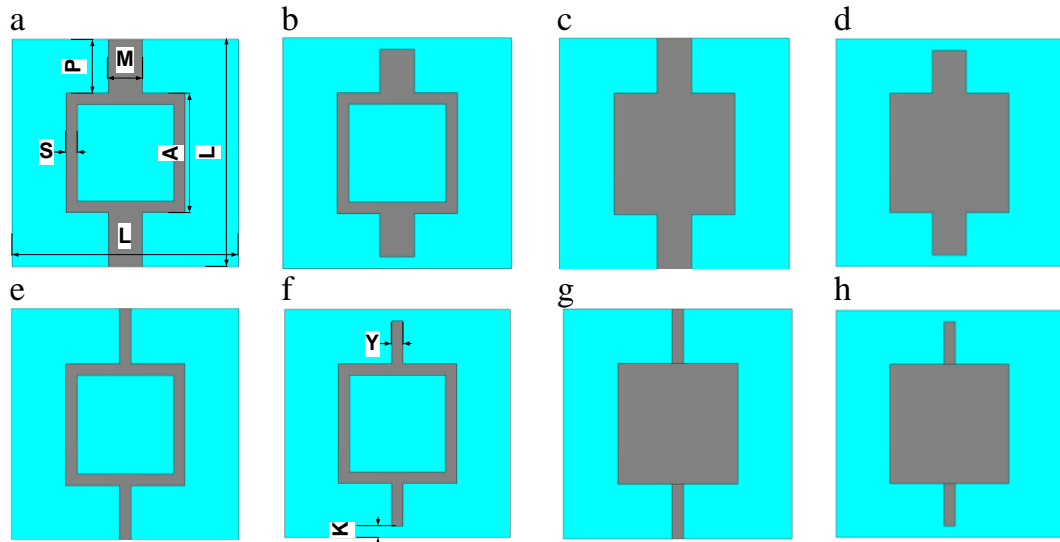
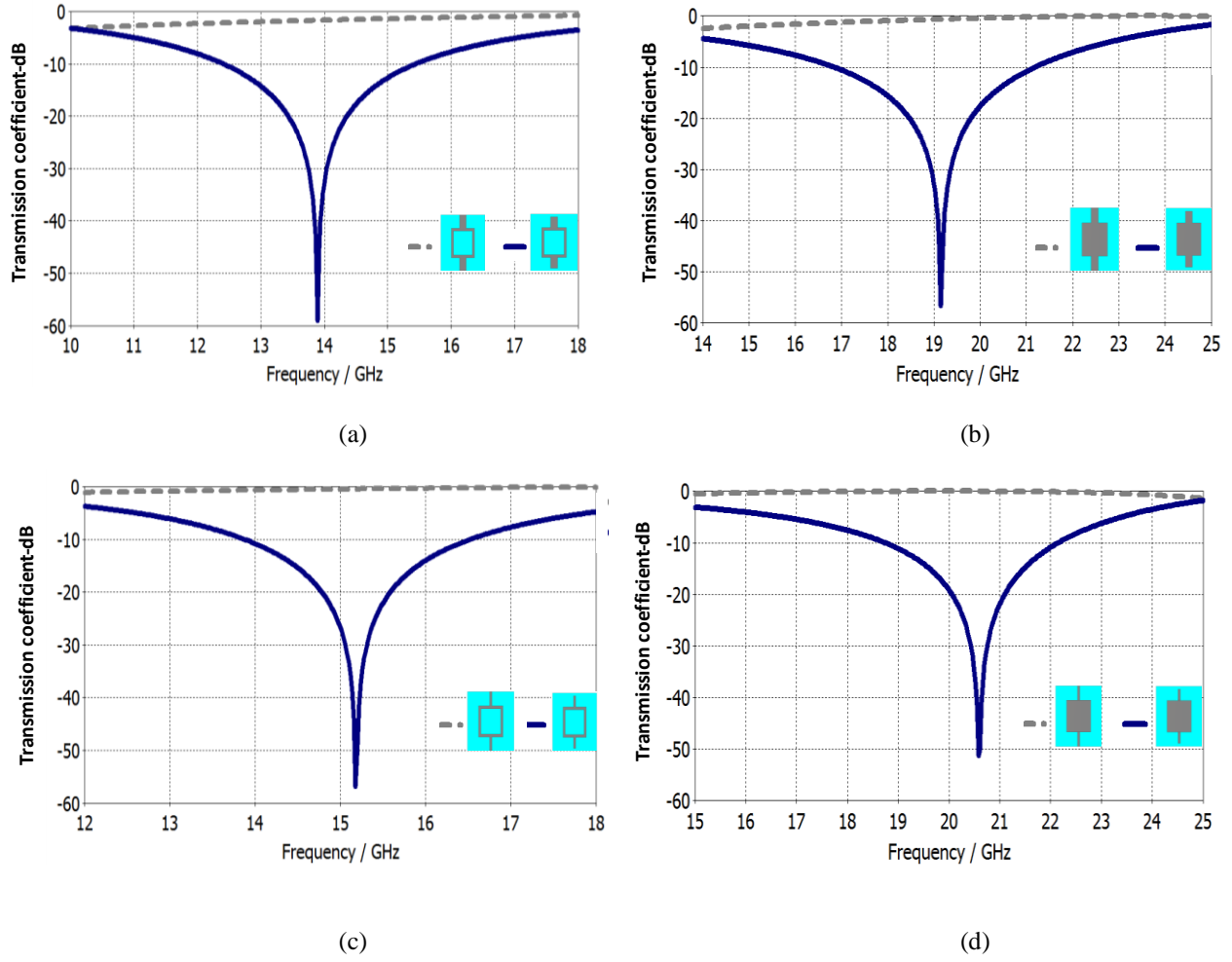


**Figure 3-8 Square switchable FSS unit cells -Dimensions (mm):  $M=1.5$ ,  $L=10$ ,  $Y=0.5$ ,  $K=0.5$ ,  $P=2.375$ ,  $S=0.5$ ,  $A=5.25$**

The width of the connecting lines are chosen to be  $M=1.5$  mm and  $Y=0.5$  mm, these dimensions are chosen to be compatible with the unit cell dimensions. They are variable to show their influence on the transmission coefficient performance in both the reflective and transparent states. Switchable FSS unit cells presented in this chapter have the same dimensions  $L=10$  mm and the same gap width 1 mm. In addition, the loop unit cells have similar thickness that is  $S=0.5$  mm, and the length of the connecting lines  $P$  is the same.

### 3.2.2.1 Square unit cells results for the resonance frequency $f_2$

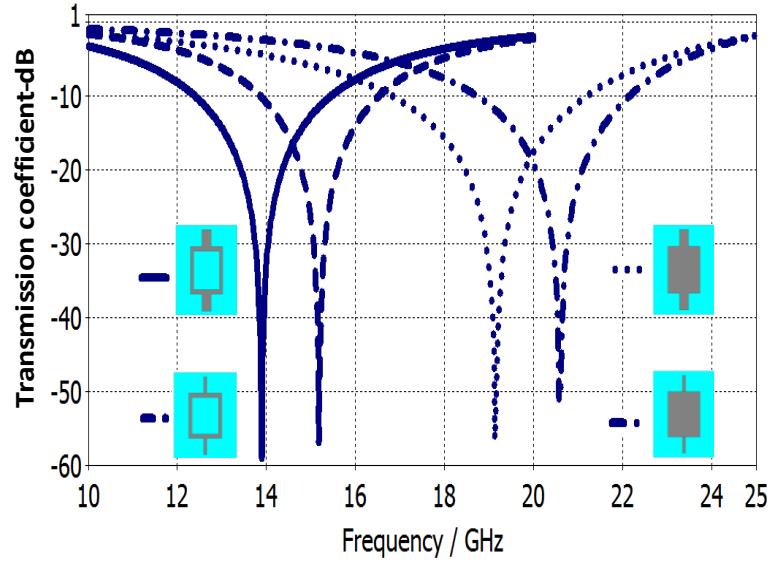
Figure 3-9a shows the transmission coefficient of the transparent and reflective state for the FSS unit cells in Figs. 3-8a and b. The resonance frequency in the reflective state is at 13.9 GHz, where most of the incident power is reflected. Figure 3-9b shows the transmission coefficient for the FSS unit cells in Figs. 3-8c and d. In the solid interior, it could be noticed that the resonance frequency is shifted upward and that the transmitted power in the transparent state is enhanced as compared to Fig. 3-9a. Figure 3-9c shows the transmission coefficient for the FSS unit cell in Figs. 3-8e and f. The resonance frequency in the reflective state is at 15.2GHz where most of the power is reflected. The resonance frequency is shifted upward compared to Fig. 3-9a. This is due to the influence of the thick connecting lines between the successive unit cells. Here, the transmitted power is enhanced more than in Figs. 3-9a and b. Fig. 3-9d shows the transmission coefficient for the FSS unit cells in Figs. 3-8g and h. The resonance frequency is shifted upward to a frequency higher than the other unit cells. This is due to the reduced width of the connecting lines and due to the solid interior unit cell design. Anyhow, the transparent curve is improved and higher power is transmitted as compared to the other switchable square FSS unit cells.



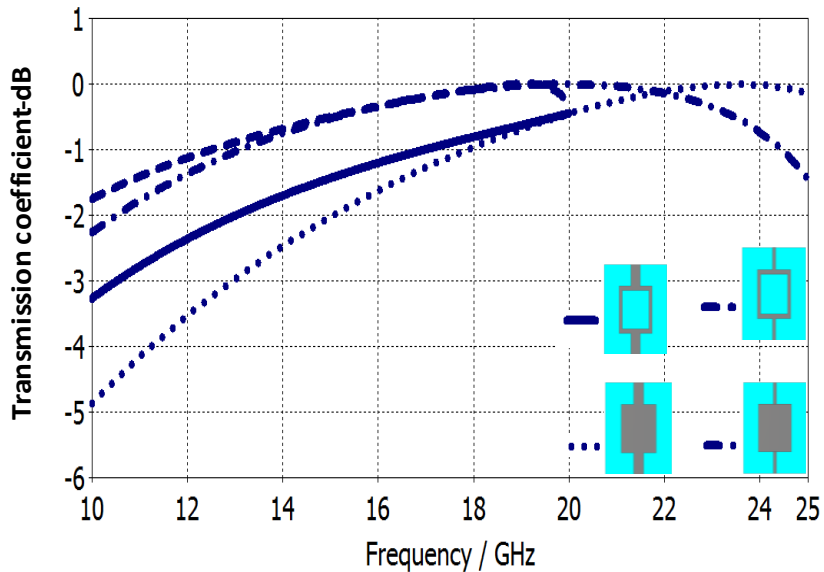
**Figure 3-9 Square FSS transmission coefficient in the transparent and reflective state.**

Fig.3-10 shows the transmission coefficient in the reflective state for the proposed square FSS unit cells presented in Fig. 3-8. The loop square with thick connecting lines gives the highest reflected power, while the solid interior with thin connecting lines gives the least reflected power. These unit cells have the lowest and highest resonance frequencies, respectively. In addition, the solid interior unit cell with thick connecting lines provides a wider bandwidth, and the square loop with thin connecting lines provides the least bandwidth when considering a minimum limit of 90% reflected power. Fig. 3-11 shows the transmission coefficient for the square unit cells in the transparent state. Because the FSS unit cells are switchable so the transparent curves are studied

specifically within the corresponding reflected 90% power frequency band. The solid interior unit-cell with thin connecting lines offer the highest transmitted power while the loop square unit-cell with the thick connecting lines offer the least transmitted power.



**Figure 3-10** Square FSS transmission coefficient in the reflective state at  $f_2$ .



**Figure 3-11** Square FSS transmission coefficient in the transparent state at  $f_2$ .

### 3.2.2.2 Square unit cells results for the non-resonance frequency band $f1$

Fig. 3-12 shows the transmission coefficient of the transparent state at the first non-resonance frequency band. Results are presented in linear scale from 1 to 0.8 to improve visibility. 90% power transmitted from the total incident power is considered the minimum limit for the bandwidth calculations. Clear from the graph that unit cell in Fig. 3-8h has the widest bandwidth while unit cell in Fig. 3-8b has the narrowest bandwidth.

Fig. 3-13 shows the transmission coefficient of the reflective state. According to this graph, the unit cell in Fig 3-8c has the widest bandwidth while unit cell in Fig. 3-8e has the narrowest bandwidth.

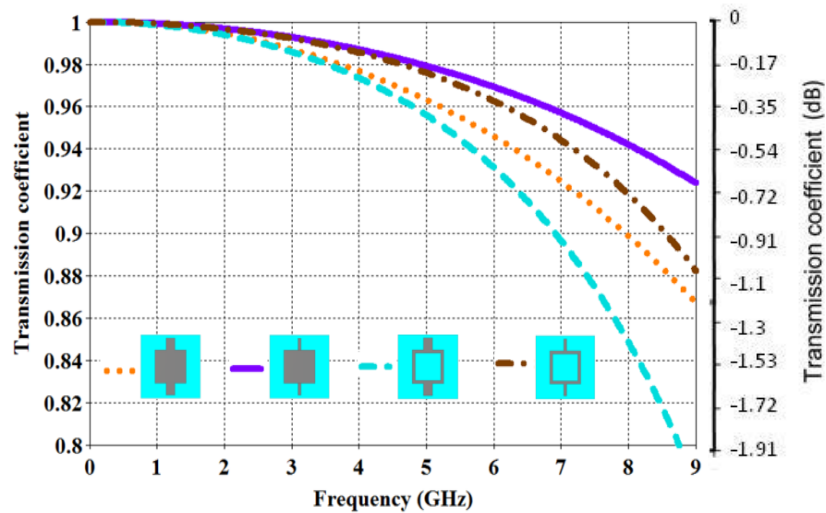
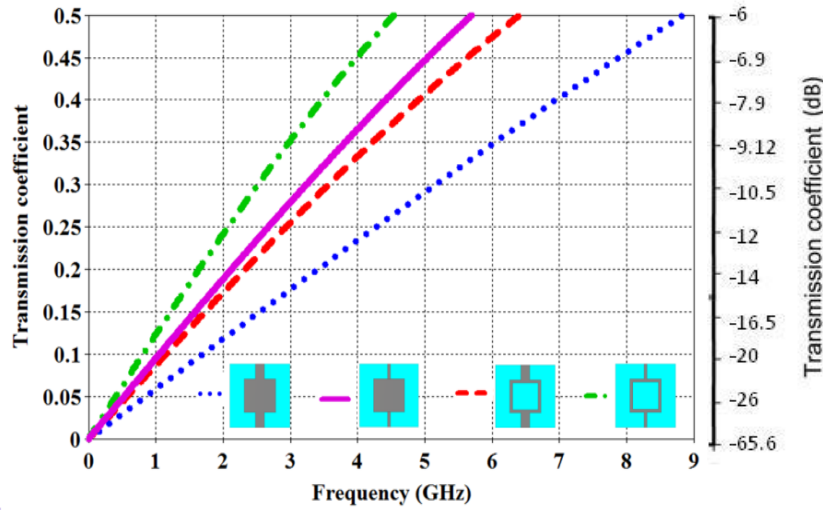


Figure 3-12 Square FSS transmission coefficient in the transparent state at  $f1$ .



**Figure 3-13 Square FSS transmission coefficient in the reflective state at  $f_1$ .**

### 3.2.3 Circular switchable FSS unit-cell

In this FSS design, the number of active elements required to switch the proposed ring FSS is reduced by 75% compared to other FSS designs [55-57]. The influence of integrating less active elements to the unit cell design on the overall performance in terms of cost and switchable frequency band are discussed in Section 2.5.2. The proposed ring unit cell design with less active elements is presented for the first time in literature.

Fig. 3-14 shows the designed switchable FSS unit cells that include loop rings and circular solid interior unit cells. The radius of the unit cells is equal to 2.625 mm. This radius is chosen to be compatible with the other proposed FSS unit cells.

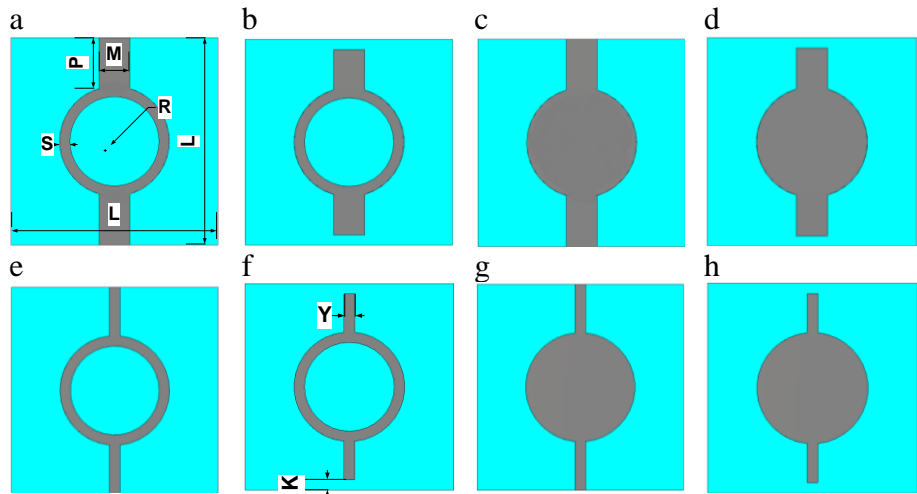


**Figure 3-14 Ring FSS unit cells. Dimensions:  $M=1.5$ ,  $L=10$ ,  $Y=0.5$ ,  $K=0.5$ ,  $P=2.375$ ,  $S=0.5$ ,  $R=2.625$ . (mm)**

### 3.2.3.1 Circular unit cells results for the resonance frequency $f_2$

Fig. 3-15 shows the transmission coefficient in the reflective and transparent state for each proposed unit cell. Fig. 3-16 shows the transmission response of the unit cells in the reflective state. The unit cell in Fig. 3-14d provides the widest bandwidth, while the unit cell in Fig. 3-14f provides the narrowest bandwidth and the highest reflected power. The unit cell in Fig. 3-14b has the lower resonance frequency while unit cell in Fig. 3-14h has the highest resonance frequency and the lowest reflected power. Fig. 3-17 shows the transmission coefficient in the transparent state. As noticed from the graph, the unit cells with thin connecting lines have the highest transmitted power as compared to the unit cells with thick connecting lines.

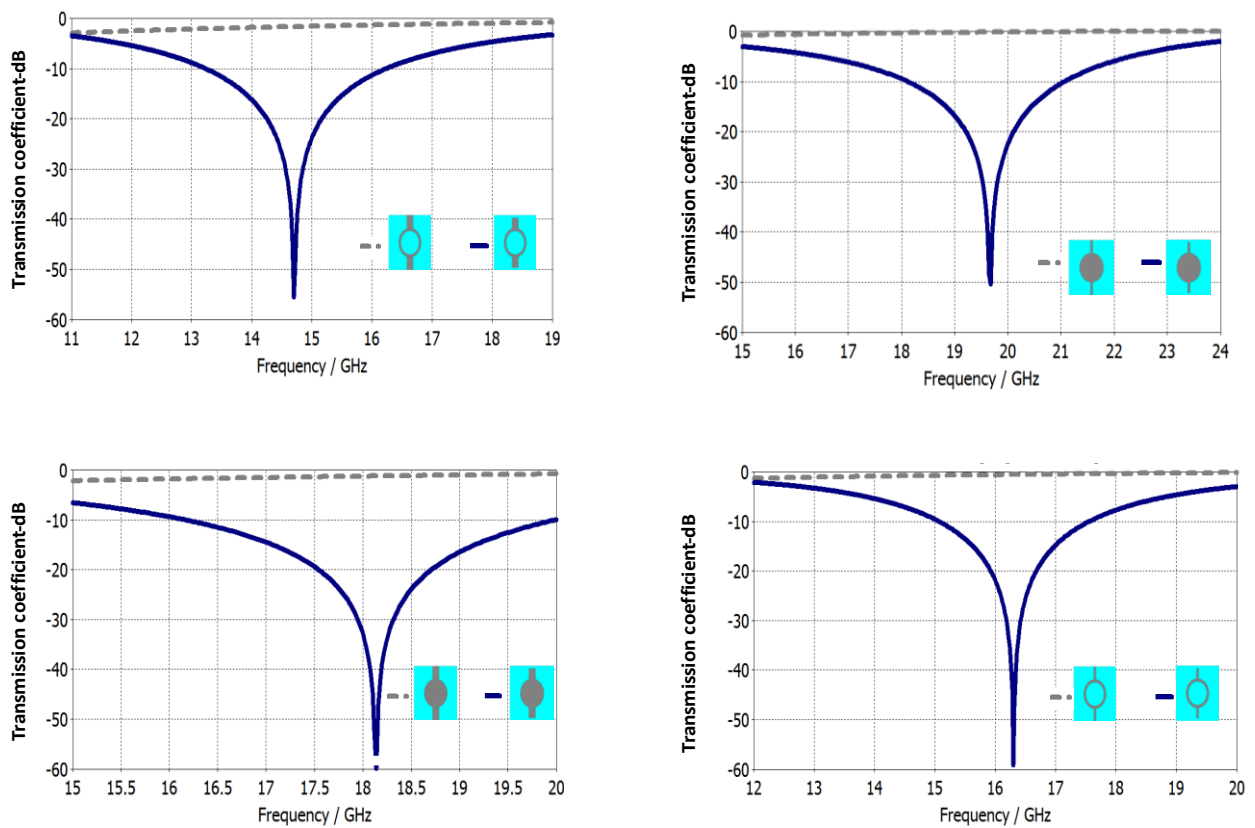


**Figure 3-15 Circular FSS transmission coefficient in the transparent and reflective state at f2.**

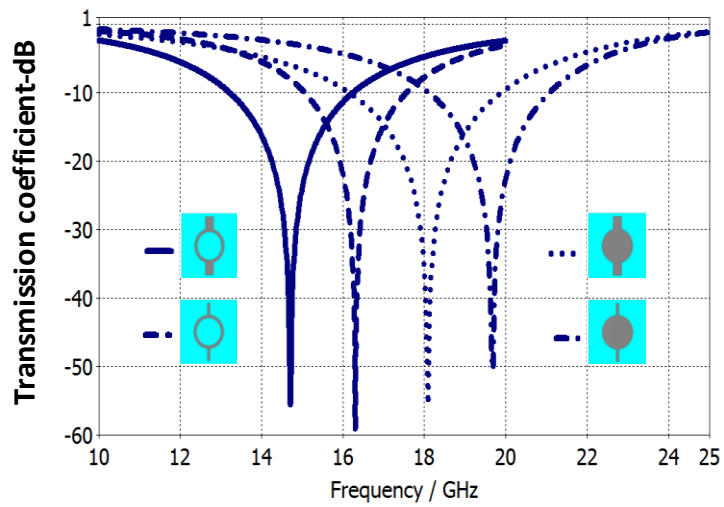


**Figure 3-16 Circular FSS transmission coefficient in the reflective state at f2.**

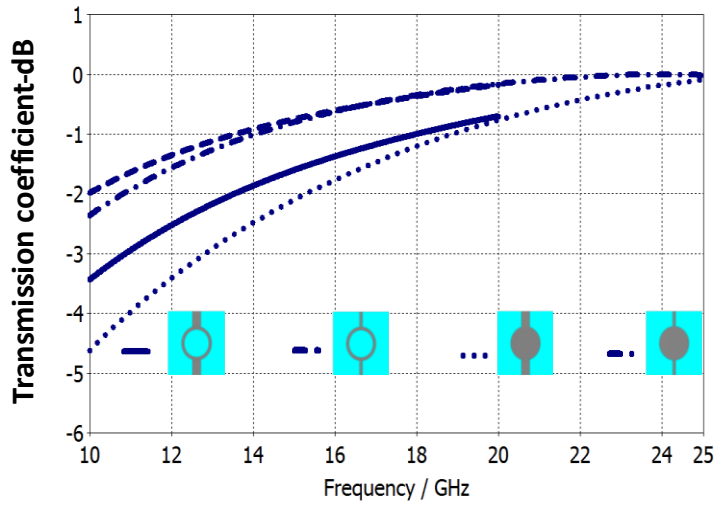


**Figure 3-17 Circular FSS transmission coefficient in the transparent state at  $f_2$ .**

### 3.2.3.2 Circular unit cells results for the non-resonance frequency band $f_1$

Fig. 3-18 shows the transmission coefficient in the transparent state for the first non-resonance frequency band  $f_1$ , unit cell in Fig 3-14h has the widest bandwidth, while unit cell in Fig 3-14b has the narrowest bandwidth. Fig. 3-19 shows the transmission coefficient in the reflective state, unit cell in Fig 3-14c has the widest bandwidth, while unit cell in Fig. 3-14e has the narrowest bandwidth.

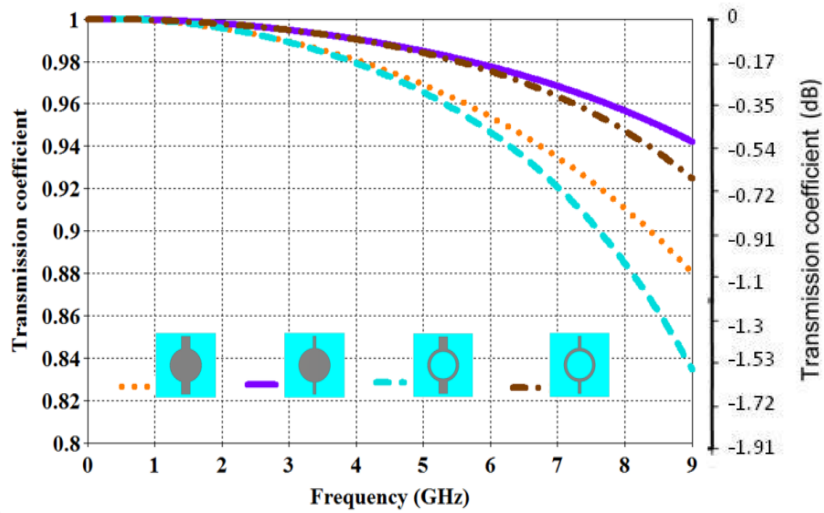


**Figure 3-18 Circular FSS transmission coefficient in the transparent state at  $f_1$ .**

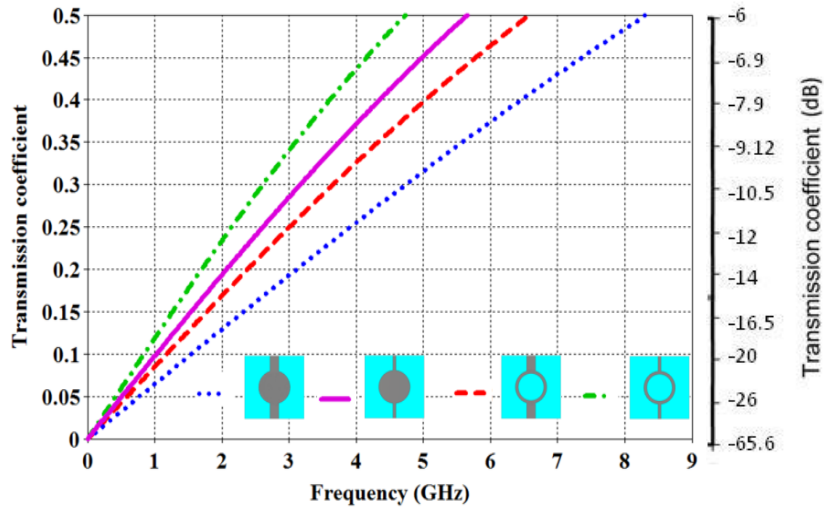


**Figure 3-19 Circular FSS transmission coefficient in the reflective state at  $f_1$ .**

### 3.2.4 Triangle switchable FSS unit-cell

In this section the switchable FSS unit cells is designed in a triangle shape as shown in Fig. 3-20. The proposed FSS unit cells are equilateral triangles with a side length of 5.25mm. The triangle dimensions are compatible with the other unit cells presented in this chapter.

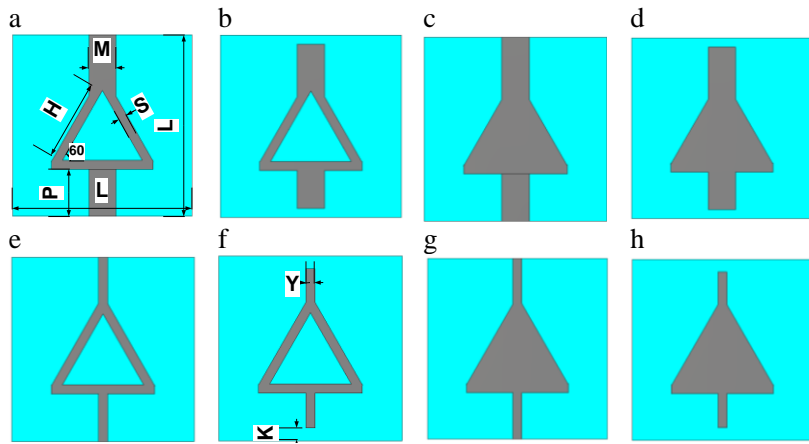


**Figure 3-20 Triangle FSS unit cells. Dimensions :  $M = 1.5$ ,  $L = 10$ ,  $Y = 0.5$ ,  $K = 0.5$ ,  $P = 2.375$ ,  $S = 0.5$ ,  $H = 5.25$  (mm).**

### 3.2.4.1 Triangular unit cells results for the resonance frequency $f_2$

Fig. 3-21 shows the transmission coefficient for each triangular unit cell shown in Fig. 3-20. Fig. 3-22 shows the transmission coefficient in the reflective state. The unit cell in Fig. 3-20d occupies the widest bandwidth, while the unit cell in Fig. 3-20f has the narrowest bandwidth. Fig. 3-23 shows the transmission coefficient in the transparent state. The unit cells with the thin connecting lines have the highest power transmitted, while power is less transmitted in the unit cells with thick lines.

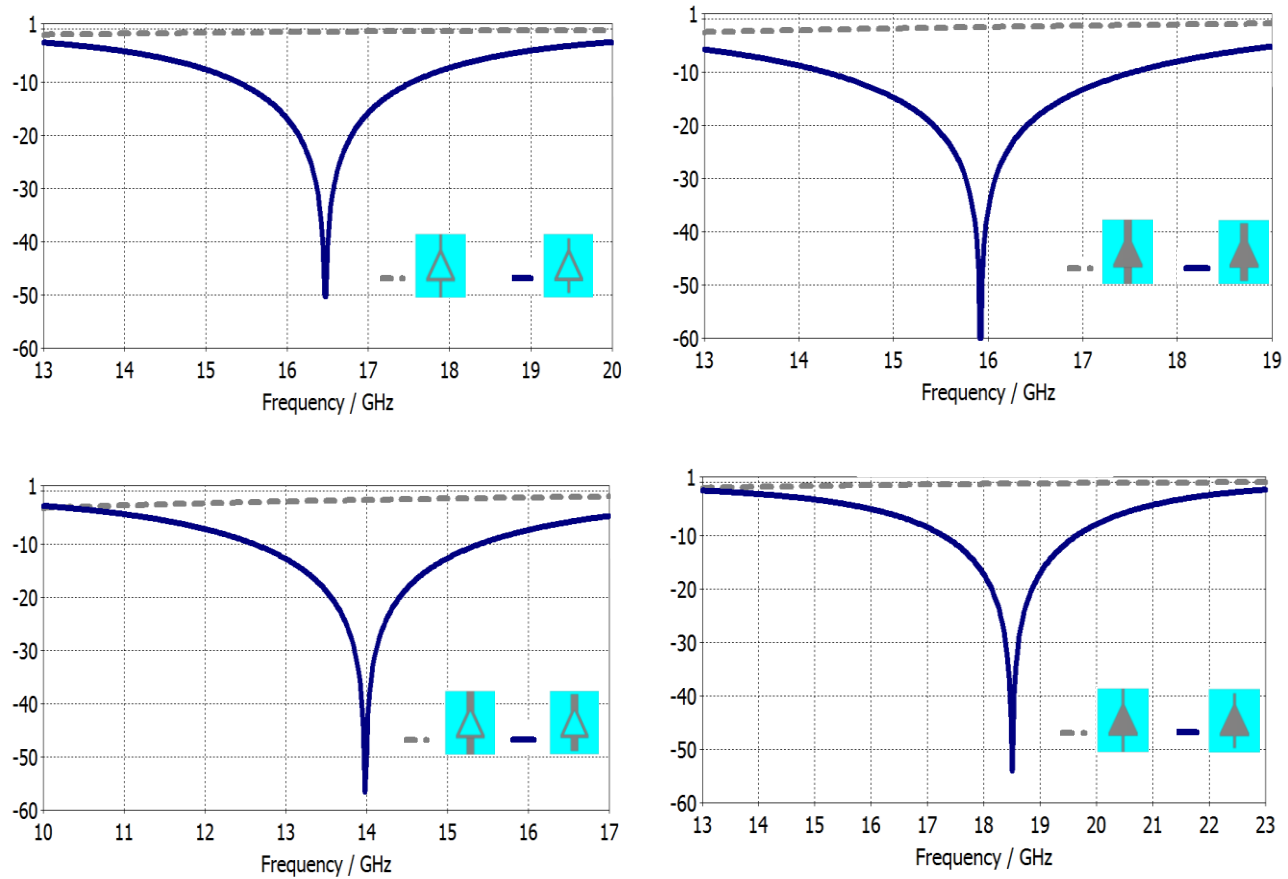


**Figure 3-21** Triangular FSS transmission coefficient in the transparent and reflective state at  $f_2$ .

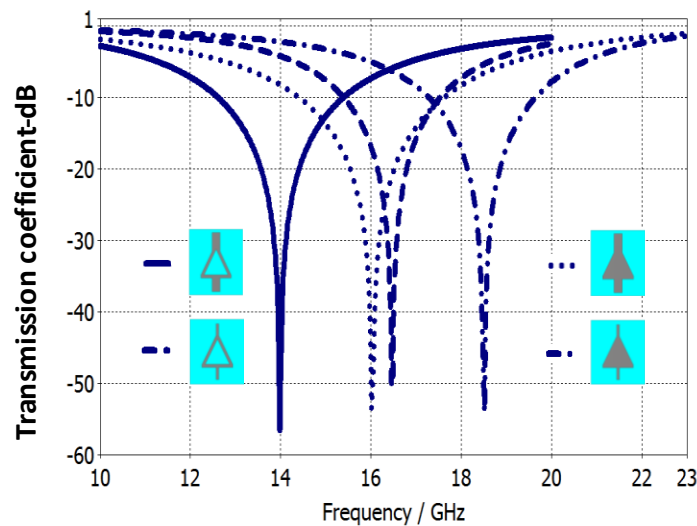


**Figure 3-22** Triangle FSS transmission coefficient in the reflective state at  $f_2$ .

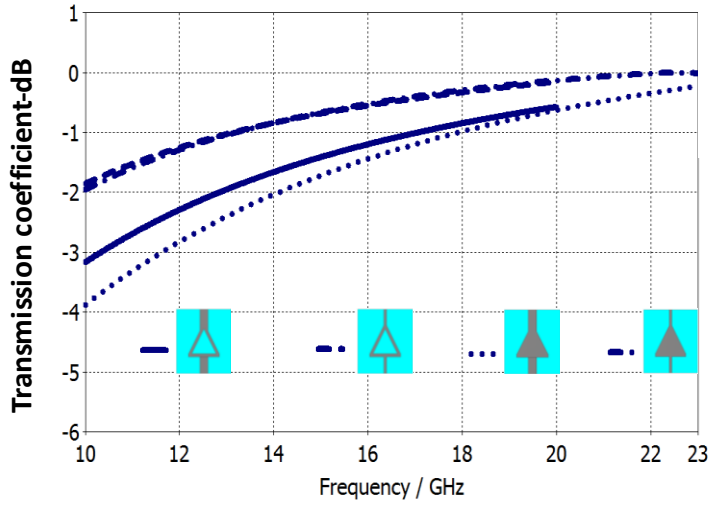


**Figure 3-23 Triangle FSS transmission coefficient in the transparent state at  $f_2$ .**

### 3.2.4.2 Triangular unit cells results for the non-resonance frequency band $f1$

Fig. 3-24 and Fig. 3-25 show the transmission coefficient for the non-resonance frequency band in the transparent and reflected state, respectively. It is obvious from the transparent curves that unit cell in Fig. 3-20h has the widest transparent bandwidth, while unit cell Fig. 3-20b has the narrowest bandwidth. As for the reflective curves, unit cell in Fig. 3-20c has the widest reflective bandwidth, while unit cell in Fig. 3-20e has the narrowest bandwidth.

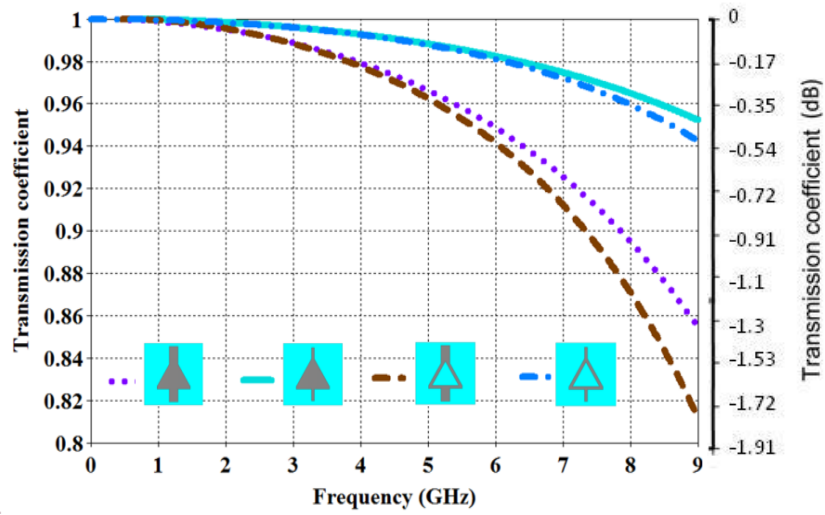


**Figure 3-24 Triangle FSS transmission coefficient in the transparent state at  $f_1$ .**

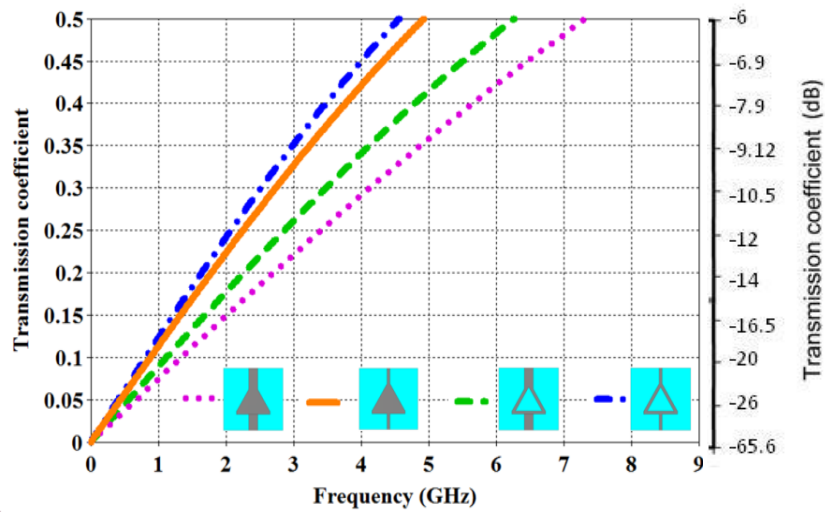


**Figure 3-25 Triangle FSS transmission coefficient in the reflective state at  $f_1$ .**

### 3.3 FSS structures comparison

Figs. 3-26 and 3-27 show the transmission coefficient of the unit cells proposed in this chapter at the first non-resonance frequency band. These two graphs show each unit cell performance as compared to the other presented structures in transparent and reflective states, respectively. The transparent curves show that the unit cell with the widest transparent bandwidth is in Fig. 3-20h, while the unit cell in Fig. 3-8b occupies the least transparent bandwidth. The reflective curves show that unit cell in Fig. 3-8c occupies the widest reflective bandwidth, while the unit cell in Fig. 3-5c occupies the least bandwidth. It could be concluded that the solid interior with thin connection lines has the largest transparent bandwidth, while the solid interior unit cells with thick connection line have the largest reflected bandwidth among the structures presented.

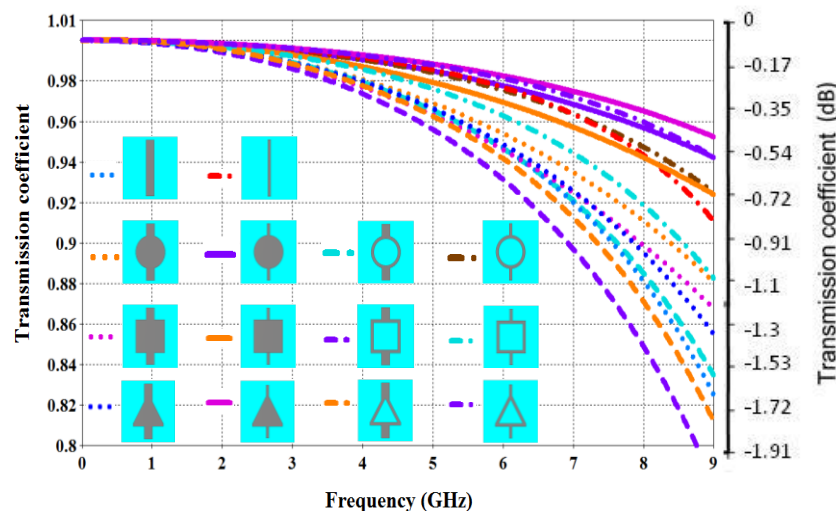


**Figure 3-26 FSS structures transmission coefficient in the transparent state at f1.**

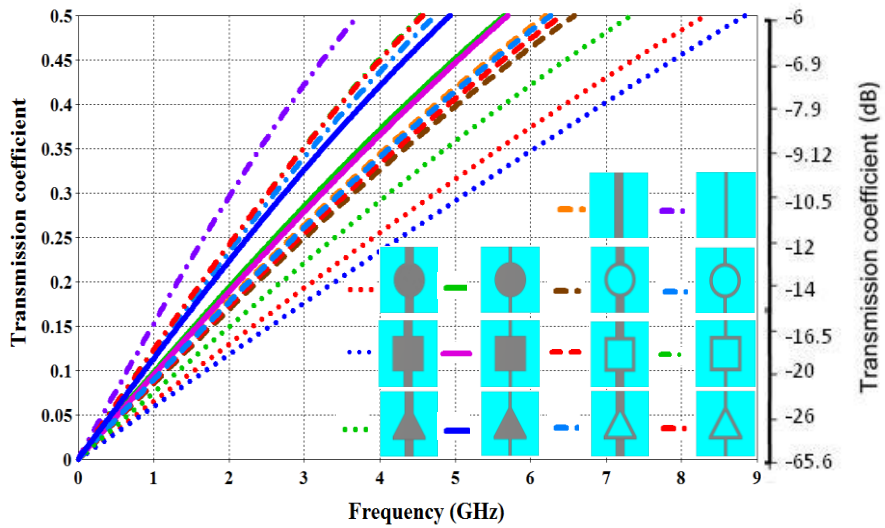


**Figure 3-27 FSS structures transmission coefficient in the reflective state at f1.**

After presenting the results for the proposed FSS unit cells in both  $f1$  and  $f2$  operating frequency bands. Table 3-1 shows the comparison between the different geometric structures presented in this chapter and gives a reference guide to select the suitable FSS design for a specific application. The minimum threshold considered for the results is 90% power transmission for the transparent state and 90% power reflection for the reflective state. These percentages are selected because they are efficient for most industrial applications.

As mentioned, the compared FSS unit cells have the same substrate material, the same unit cell dimensions and similar unit cell element dimensions. Also, the connecting transmission line dimensions are similar, as shown in Fig. 3-28. The variable part is only the shape of the FSS unit cell.

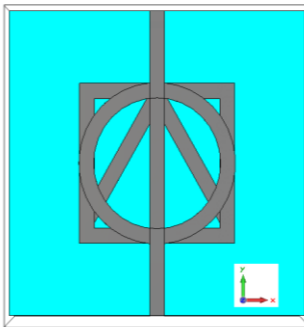


**Figure 3-28 Proposed FSS unit cells**

In table 3-1, the first column presents the FSS design and identifies it by a number so it could be simply mentioned. The second column lists the resonance frequency for the reflective state for each unit cell at  $f_2$ . The third column lists the resonance frequency for the transparent state with maximum power. The fourth column gives the difference between the resonance frequency in the transparent and reflective state. This difference is desired to be small for many applications as for example in our intended antenna application, and the maximum transmitted power is preferred to be correspondent to the maximum reflected power. The fifth column shows the bandwidth of the reflective state where the threshold is minimum 90% power reflected from the incident power. The results for the non-resonance band  $f_1$  are listed beginning from column six. In this column the frequency bandwidth is listed for the transparent state when minimum 90% of the incident power is transmitted. In the seventh column the corresponding level of the reflective state transmission coefficient is provided. Column eight presents the frequency bandwidth for 90% reflected power in the reflective state, and column nine shows the corresponding transmission coefficient in the transparent state.

For further clarification to Table 3-1, unit cell 3 is taken as an example. In unit cell 3, the reflective resonance frequency is at 18.14 GHz and the transparent maximum is at 27.16 GHz. 9.02 GHz is the shift between the maximum transparent and the maximum reflected frequencies. The bandwidth of the 90% reflected power is 3.8 GHz. For the non-resonance band results  $f_1$ , the 90% power transmitted bandwidth in the transparent state is 6.28 GHz and the corresponding transmission coefficient for the reflective state at 6.28 GHz is 0.39. Likewise, in the reflective state the bandwidth of 90% power

reflected is 5 GHz and the corresponding transparent transmission coefficient at 5 GHz is 0.969. According to Table 3-1, the largest bandwidth performance for the transparent in the  $f1$  frequency band occurs in unit cell 12, with a bandwidth of 9.26 GHz. Unit cell 7 has the largest bandwidth that is around 5.46 GHz in the reflective state. Although the mentioned unit cells have high bandwidths they do not necessarily have a similar high bandwidth in the corresponding switchable state. Important to point out that the bandwidths in column five for the resonance frequency band  $f2$  are less than the bandwidths in column six and eight that are for the non-resonance frequency  $f1$ . As a conclusion, the unit cell bandwidth at the non-resonance band  $f1$  is more than its bandwidth at the resonance frequency band  $f2$ . The other important conclusion is shown in column four where the transparent and reflected resonance frequencies at  $f2$  are not compatible for the two states. On the contrary, the switchable frequency at  $f1$  band is nearly compatible for both states as shown in column six and eight.

### 3.4 Conclusion

In this chapter, a theoretical investigation has been made between different FSS shapes. The switchable FSS design selection depends on the intended application. Results have shown that the unit cells with the solid interior and thick connecting lines have the largest bandwidth in the non-resonance frequency band  $f1$ , while the loop shaped unit cells with thin connecting lines have the least bandwidth. When comparing between similar FSS types in  $f1$ , for example, if we have taken the solid interior with thick connecting lines. In this case the square FSS will occupy the largest bandwidth and afterwards comes the circular and then the triangular FSS bandwidths. As noticed from the achieved results, the unit cells with the highest bandwidth in  $f2$  do not necessarily have the maximum transmitted power in the transparent state. Each unit cell has specific characteristics in terms of bandwidth beside the transmitted and reflected power. This diversity shows the importance of presenting different shaped switchable FSS unit cells. This comparative study is important for selecting the suitable switchable FSS characteristics for industrial applications.

**Table 3-1 Switchable FSS unit cells comparison**

Frequency Selective surface	Reflected Resonance Fr- GHz	Transparent Resonance Ft – GHz	Ft-Fr GHz	90%-GHz resonance Bandwidth	90% -GHz transmitted BW in f1	Corresponding Reflective S21	90% -GHz reflected BW in f1	Corresponding Transparent S21
1	13.96	28.65	14.69	2.56	5.9	0.48	3.66	0.984
2	13.62	28.29	14.67	1.58	7.78	0.783	2.16	0.998
3	18.14	27.16	9.02	3.8	6.28	0.39	5	0.969
4	19.88	24.06	4.18	2.94	8.6	0.681	3.36	0.993
5	14.7	24.96	10.26	3	5.92	0.459	3.9	0.98
6	16.3	22.53	6.23	2.08	7.88	0.706	2.76	0.995
7	19.2	23.58	4.38	4.32	5.82	0.337	5.46	0.956
8	20.61	19.92	-0.69	3.39	7.6	0.63	3.44	0.99
9	13.9	21.875	7.975	3.02	5.3	0.427	3.78	0.977
10	15.18	19.075	3.895	2.64	6.74	0.662	2.68	0.994
11	15.92	24.57	8.65	3.22	5.96	0.419	4.4	0.975
12	18.62	22.62	4	2.37	9.26	0.761	2.94	0.996
13	13.98	24.06	10.08	2.74	5.72	0.464	3.72	0.981
14	16.48	22.14	5.66	2.14	8.64	0.755	2.7	0.997

## **4 CHAPTER FOUR: RECONFIGURABLE RADIATION PATTERN ANTENNA (ONE)**

### **4.1 Introduction**

Reconfigurable antennas are important in communication systems evolution, due to their ability to change their characteristics as a function of time [60]. Reconfigurable antennas can be classified according to their functionality into: polarization, frequency, impedance bandwidth, and radiation pattern reconfiguration [61]. These functions can be achieved by specific mechanisms like switching, structural modifications and material tuning [62]. Pattern reconfiguration antennas can be used to provide internet services in different transportations. Communication between the satellite and a moving transportation object is done by using reconfigurable antennas with switchable FSSs. Kymeta is one of the leading companies in this field, they manufacture reconfigurable antennas using metamaterials for transportation such as airplanes and trains. This company was established by Bill Gates with a budget of one million US dollars.

The aim of the thesis is to design a pattern reconfigurable antenna by using FSS. Switchable FSSs could be integrated to an antenna design to make the antenna radiation blocked in one side and allow it to radiate in the desired direction. This could be done by several methods depending on the antenna type. If the antenna is planar then the FSS could be implemented on the antenna substrate or it could be added at any location which will influence the antenna radiation pattern and achieve the desired objectives. In this thesis, the radiating source antenna of interest is an omni-directional antenna which radiates around the elevation plane. The FSS is integrated as a cylinder around the central source antenna. This integration is done to make the antenna directive instead of omni-directional and to steer it along the elevation plane. Many designs are available in literature with this configuration. The proposed antennas are distinguished by their enhancement in bandwidth and in other aspects such as size and number of steering positions.

## 4.2 Reconfigurable radiation pattern antenna application

The proposed FSSs discussed in the earlier chapter are exploited in an important industrial application. A pattern reconfigurable antenna is presented as an application for the proposed FSSs to illustrate their impact on the antenna characteristics. This application is chosen because the designed switchable FSS unit cell has preferable characteristics for enhancing the antenna performance. Two pattern reconfigurable antennas are designed with a central dipole acting as the radiating source and a cylindrical shield composed of switchable FSSs. The first antenna (antenna number one) has switchable FSS operating at the resonance frequency  $f_2$ . While, the second antenna presented in the next chapter (antenna number two) has the switchable FSSs operating at the non-resonance frequency band  $f_1$ . The designed antennas have a reconfigurable pattern across the whole azimuth plane. In this chapter, the design of a reconfigurable antenna with switchable FSS shield working in the resonance frequency is presented. The FSS unit cell design is studied by the transparent and reflective state transmission coefficient. In addition, the antenna experimental and simulated achieved results are discussed and compared with other designs to clarify the enhanced performance of the proposed antenna.

## 4.3 FSS unit-cell design at $f_2$

The pattern reconfigurable antenna performance is modeled by the design of a switchable FSS unit cell. The switchable FSS unit cell has to meet several requirements to fulfill the desired antenna design. The ideal switchable FSS has maximum power reflected in the reflective state and the maximum power passing through the FSS in the transparent state. Both maximums should lie in the same frequency band. This is because the reflection versus transparency bandwidth of the switchable FSS unit cell influences the antenna operating frequency bandwidth.

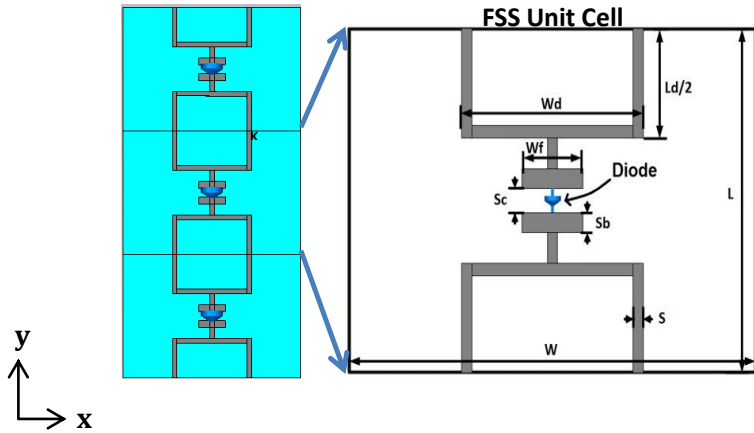


**Figure 4-1 FSS unit cell. Dimensions in millimetres:**  $W=18.7$ ,  $L=14$ ,  $W_d=8.9$ ,  $K=3$ ,  $S_c=1$ ,  $L_d=8.9$ ,  $S_b=0.8$ ,  $S=0.5$ ,  $W_f=3$

Fig. 4-1 shows the dimensions of the proposed FSS unit cell and the PIN diode location that switches the unit cell. The FSS unit cell is designed using a square shaped loop with gaps between the successive unit cells to solder the PIN diodes, as shown in Fig. 4-1. The FSS unit cell is designed on the Rogers substrate R5800 with relative permittivity of 2.2 and thickness of 3.18 mm. Many substrates are examined, and the chosen substrate gave the best results. But the obstacle of this substrate is its solid inflexible properties that make it difficult to perform a cylinder due to its thickness, so the antenna had a nonagon shape instead of a cylindrical shape.

This FSS unit cell operates as a reflective surface when it has a gap and operates as a transparent surface when its gap is close. When the square loops are connected, the resonance frequency is shifted to a higher frequency, making the FSS switch to the transparent state at 3.87 GHz. This is detailed in chapter two, Section 2-4. Switching is done in an automatic manner by adding a (GMP4201) PIN diode [63] in the gap location. When the diode is switched ON, the FSS acts as a transparent surface. Likewise, it acts as a reflective surface when the diode is switched OFF. Each dimension ( $W_d$ ,  $L_d$ ,  $s$ , etc.) has its effect on the switchable FSS unit cell performance, especially on the frequency bandwidth. Figs. 4-2 and 4-3 show the influence of changing the switchable FSS dimensions ( $L_d$ ) and ( $W_d$ ) on the bandwidth. The

proposed design is on the graph left side (A) and the modified dimensions are on the right side (B) and (C). The final switchable FSS design dimensions are listed in Fig.4-1. They are achieved after an extensive parametric study accompanied with optimizations done on the FSS unit cell to achieve the desired bandwidth at the desired center frequency. Curves in Fig. 4-4 show the transmission coefficient of the final switchable FSS unit cell design for the ON and OFF PIN diode switching.

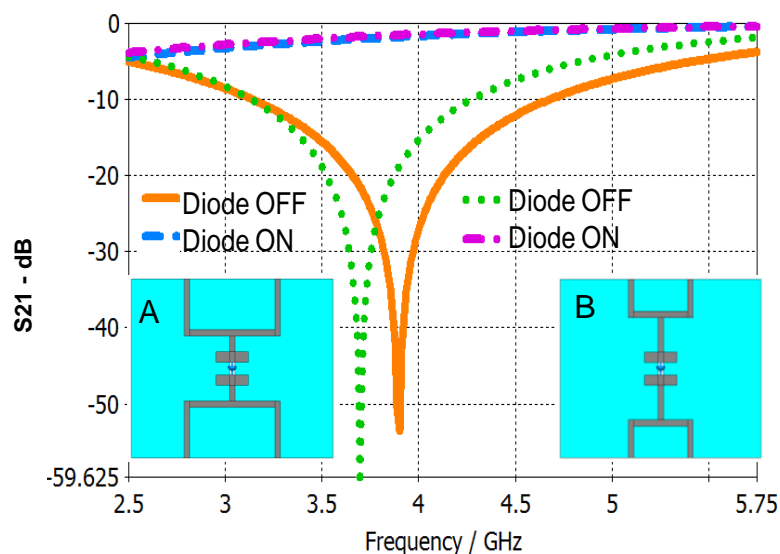


**Figure 4-2 FSS transmission coefficient. Dimensions changed in (B):  $W_d=6$ ,  $L_d=6$  mm**

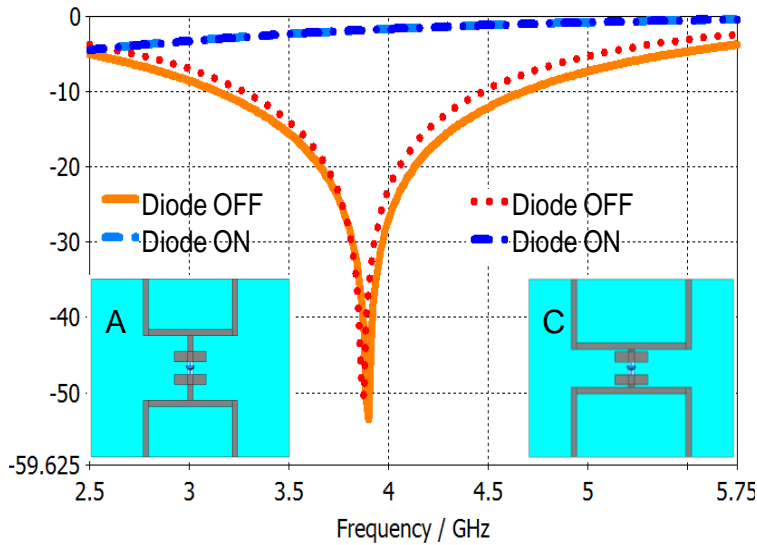


**Figure 4-3** FSS transmission coefficient. Dimensions changed in (C):  $W_d=11$ ,  $L_d=11$  mm

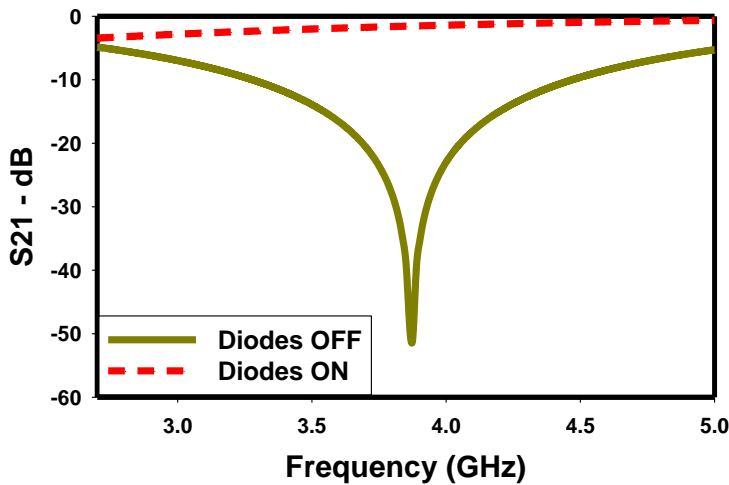


**Figure 4-4** Simulated transmission coefficient of the proposed FSS unit cell. © 2016 IEEE

In this design, the PIN diode is modeled in the simulations using its equivalent lumped elements RLC circuit. When the diode is switched ON in the forward biased, the equivalent model is a series of inductance and resistance  $L=0.5$  nH,  $R=2.3$  Ohms. The PIN diode is modeled as a series of parasitic capacitance and inductance  $C=0.18$ pF,  $L=0.5$ nH when it is switched OFF in the reverse biased. Computer Simulation Technology (CST) Microwave Studio simulator is used to simulate the proposed FSS [64]. The FSS unit cell is simulated by the full Floquet mode which models the FSS as

an infinite array. In simulations, the impinging electromagnetic waves propagate in the Z-direction and are normal to the X-Y plane also; the electric part lies in the Y- direction.

Figs. 4-5 and 4-6 show the FSS electric field distribution in the central Y-Z plane at 3.6 GHz. The electric waves flow from left to right hand side. The two vertical black lines in the center of the electric field distribution are the boundaries of the 3.18 mm substrate. Clear, that the scale bar presents the lowest electric field density in dark blue, while the dark red presents the highest electric field density. Fig. 4-5 shows the FSS unit cell electric field distribution in the reflective state when the diode is switched OFF. As noticed from the figure, the electric field distribution shows high concentration around the diode location, then it decays rapidly, resulting in weak penetration through the FSS unit cell. In a similar manner, Fig. 4-6 shows the FSS unit cell electric field distribution in the transparent state at 3.6 GHz. Here, the diode is switched ON and the FSS unit cells are connected via the diodes. Clear from the figure that the electric field penetrates through the FSS unit cell with high and uniform density at the final edge.

It can be noticed from these figures that the left side ( $Z<0$ ), where the electromagnetic waves are generated is less in the transparent state than in the reflective state in spite that they have the same amount. This is because the electromagnetic wave in the reflective state is reflected towards the generated wave side and is added partially to the emitted wave, while in the transparent state most of the electromagnetic wave penetrates through the unit cell to the right side ( $Z>0$ ).

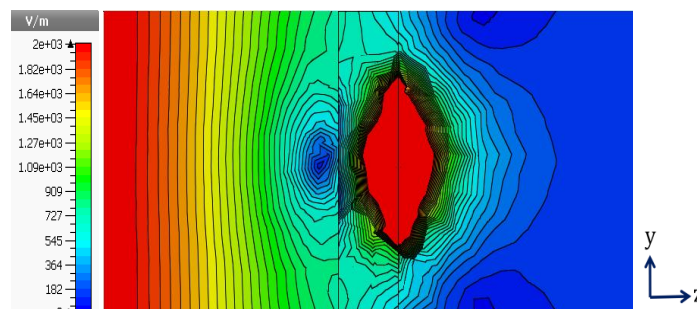


**Figure 4-5 Y-Z plane, FSS electric field distribution in the reflective state. © 2016 IEEE**

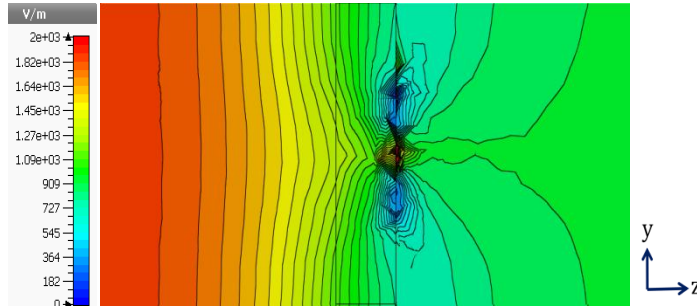


**Figure 4-6 Y-Z plane, FSS electric field distribution in the transparent state. © 2016 IEEE**

#### 4.4 Nonagon reconfigurable pattern antenna design

A nonagon reconfigurable pattern antenna with two main parts is designed. The first part is a radiating source that is a simple dipole made of two metal rods and its center frequency is around 3.67GHz. The second part is the switchable FSS unit cells distributed across a nonagon shape which surrounds the radiating source. The reconfigurable antenna is composed of 9 panels, and each panel includes 11 unit cells.

Panels are assembled by using three parallel lines of scotch foam tape in the inner side of the nonagon. The scotch foam tape is flexible, which allows forming a nonagon. The antenna is fixed on a separate base made from foam material and has a place to fit in the nonagon from its bottom side. An extra 19.7 mm is added to the overall circumference for spacing between the panels.

DC feed lines are implemented on the top and bottom edge of the nonagon to feed the PIN diodes in each panel. In addition, a  $5\text{ K}\Omega$  resistor is added in front of every series of FSS in each panel to prevent the diodes from high biasing currents and to guarantee equal current for each diode. The top and bottom sides of the nonagon are closed with two plates of metal in the inner side. They are added to increase the gain and prevent from any power loss through these regions.

The antenna dimensions are chosen according to the study reported in [34], which models a corner reflector antenna, a semi cylindrical reflector antenna and a cylindrical FSS antenna. These models have been compared in terms of matching, realized gain and radiation pattern to conclude a design guideline for cylindrical pattern

reconfigurable antennas. After calculating the proposed antenna, the dimensions are optimized to compromise between a suitable gain, matching bandwidth and directive radiation pattern. The antenna radius is  $0.355 \lambda$ , where  $\lambda$  is the free-space wavelength. This radius gives the preferred results in terms of gain and matching. The design radius lies within the range recommended in [34] which is between  $0.25 \lambda$  and  $0.4 \lambda$ . Fig. 4-7 shows the proposed antenna with total length of 170 mm and radius of  $R = 30$  mm. It might come to mind why the distance is different from a Yagi-Uda antenna that is  $0.1 \lambda - 0.25 \lambda$ . Actually, here the reflective surface comprises 5 panels around the radiating source forming a half cylindrical shape, and this shape influences the electromagnetic wave response in a different manner.

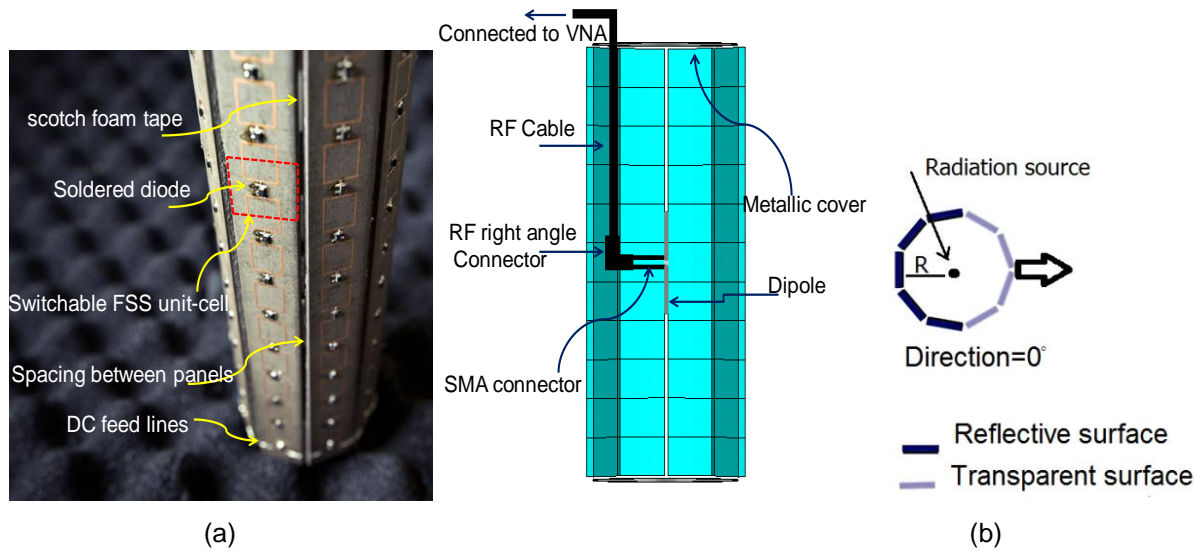


**Figure 4-7 Proposed reconfigurable antenna, total length is 170mm and radius is  $R=30\text{mm}$ .** (a) photo of the antenna. (b) The dipole feed inside the antenna.

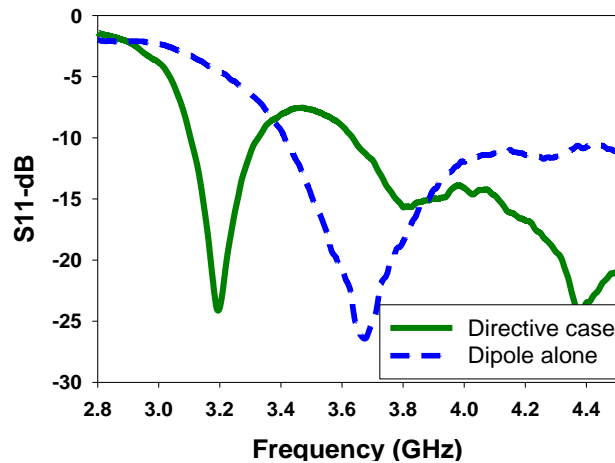
The antenna has four panels in the transparent state and five panels in the reflective state at each reconfigurable beam steering position. The nonagon pattern-reconfigurable antenna beam direction is steered in an automatic manner by switching the active elements in the FSS unit cells surrounding the radiating source. Fig. 4-7 (b) illustrates the dipole and its feed inside the nonagon and shows the pattern-

reconfigurable antenna from the inside with its four transparent panels. An RF cable is placed inside the nonagon in a vertical manner and is connected to a right angle RF connector then connected to an SMA connector to feed the central dipole. With configuration, the antenna can cover 9 steering angle positions through the full 360° azimuth rotation angle.

## 4.5 Antenna measurements and results

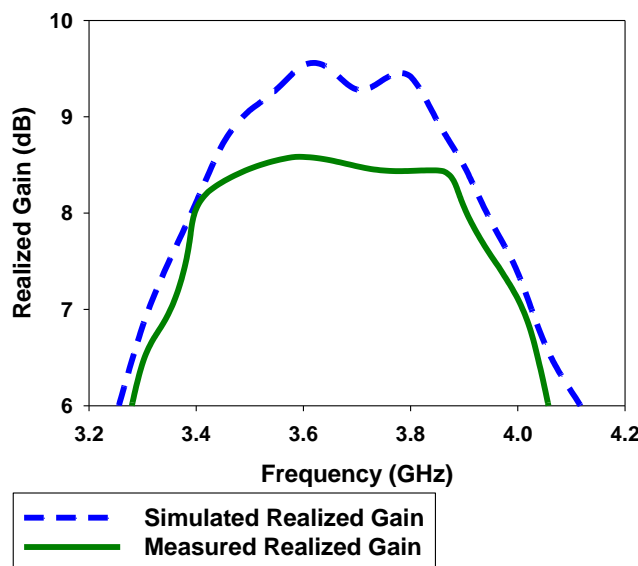
Fig. 4-8 shows the measured reflection coefficient of the reconfigurable pattern antenna compared with the reflection coefficient of the omni-directional dipole alone without the FSS shield. In the directive case, the antenna achieves a wide matching frequency bandwidth of more than 1.4 GHz by accepting the minimum transmitted power to be 85% from the incident power at 3.45 GHz. Results show a significant improvement in matching bandwidth due to the influence of the FSS on the radiating source performance. In the fabricated dipole, no matching is considered so already a mismatch is expected. This is due to the limited space inside the cylinder besides the difficulty of inserting the dipole within a proper position inside the cylinder.

Fig. 4-9 shows the measured and simulated realized gain of the proposed pattern reconfigurable antenna. A gain comparison method is used in the anechoic chamber for the measurements. The difference between the measured and simulated results is due to the slight mismatch that exists in the measured S11 curve and affects the realized gain. The graph shows that the measured realized gain has an approximate flat performance across 500 MHz bandwidth with a maximum of 8.6 dBi.



**Figure 4-8 Measured reflection coefficient of the antenna and dipole. © 2016 IEEE**

The gain and matching bandwidths are not proportional to one another due to the influence of the switchable FSS on the antenna performance. The higher the power transformed in the FSS transparent state, the higher the antenna gain. It is worthwhile to point out that about 95%-100% of the incident power is reflected from the reflective panels in the antenna and adds partially to the waves emitted from the dipole toward the transparent panels, as illustrated in Fig. 4-5.



**Figure 4-9 Simulated and measured realized gain of the proposed antenna. © 2016 IEEE**

The gain presented in Fig 4-9 is the realized gain. The realized gain takes into account the losses of the antenna due to the impedance mismatching as proven in the following intrinsic gain equation:

$$G_{\text{intrinsic}} = \frac{G_{\text{realized}}}{1 - |S_{11}|^2} \quad (1)$$

If the antenna matching is ideal with a dip in the S11 curve, it is expected to have a peak in the realized gain. But a slight mismatch occurs in the S11 curve. This mismatch allows minimum 85% of the incident power to be transmitted. Therefore, according to Equation (1), the realized gain flatness is due to the S11 effect. Hence, it should be expected to have no flatness if the gain is unrealized. In the simulations, the dipole input port is considered an ideal matched discrete waveguide port; as a result a peak appears in the simulated realized gain.

## 4.6 Matching and realized gain bandwidth relation

Unlike other antennas, this antenna has two main parts, the radiation source that is the central dipole and the FSS shield which controls the dipole radiation. The matching and gain in a conventional antenna depend only on the antenna components, but in our case they depend on the source antenna and FSS.

The reconfigurable antenna matching is the matching of the central dipole affected by the FSS shield. The antenna gain depends on the transparency and reflectivity of the FSS surrounding the dipole, and on the radiation source gain. For example, if the FSS transparency and reflectivity are changed, then the antenna gain is influenced. If there were no FSS then the matching and gain would be related together in the traditional way known, but adding the cylindrical FSS arises another justification to relate them together.

To further illustrate the relation between the matching and realized gain bandwidth, results from three references having the same antenna type are presented to compare

between the two bandwidths. The following figure captions are taken as in the reference and the reference number is attached to the figure caption. In the following curves, the yellow shade on the S11 curve shows the gain bandwidth of the antenna.

1- Reference 1-[54]

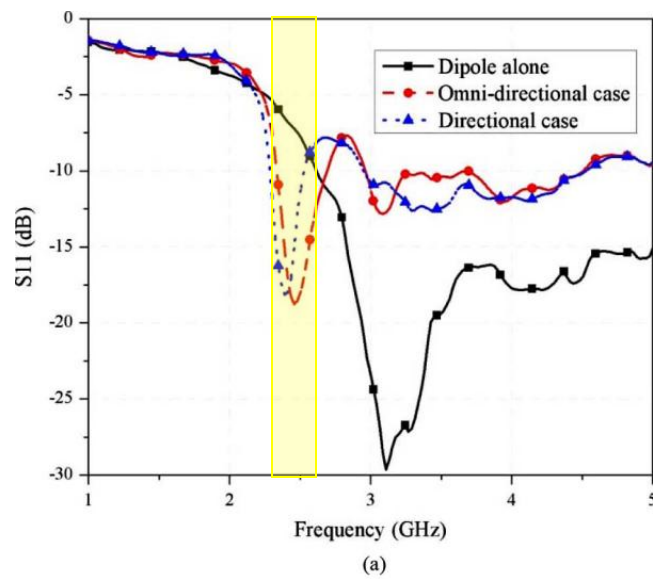
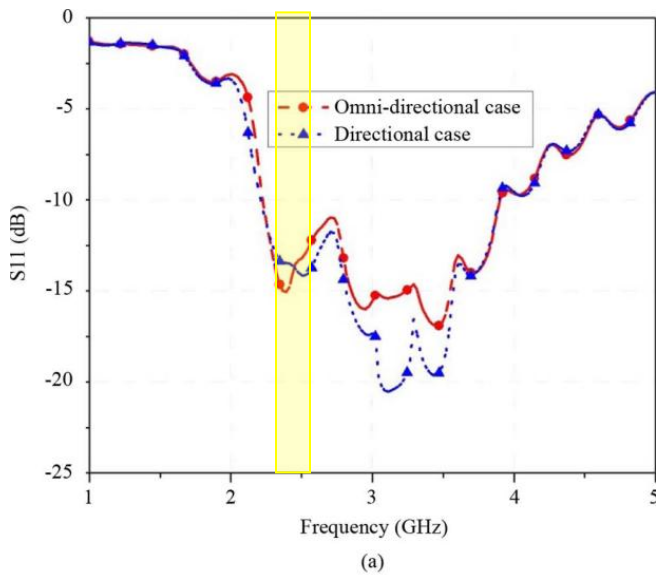


**Figure 4-10** Measured results for Antenna-I (a) Measured reflection coefficient [54]-page 2235.

© 2010 IEEE



(a)

**Figure 4-11 Measured results for Antenna-II: (a) Measured reflection coefficient [54]-page 2235.**

© 2010 IEEE

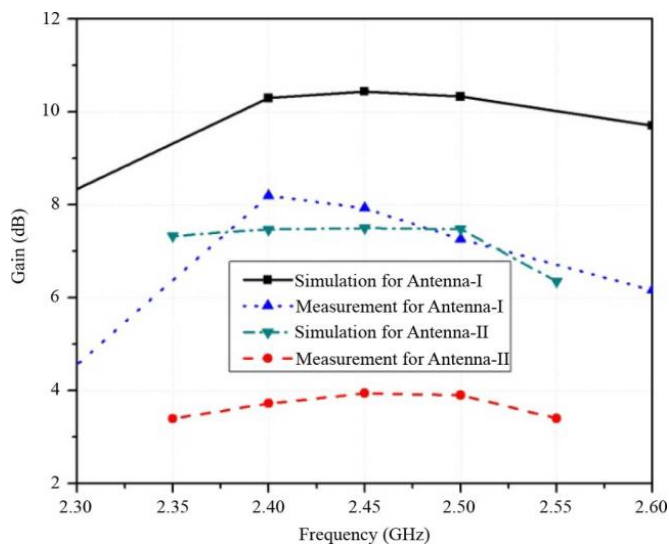


**Figure 4-12 Measured gains for Antenna-I and II compared to the simulation. [54] -page 2236.**

© 2010 IEEE

2- Reference 2-[34]

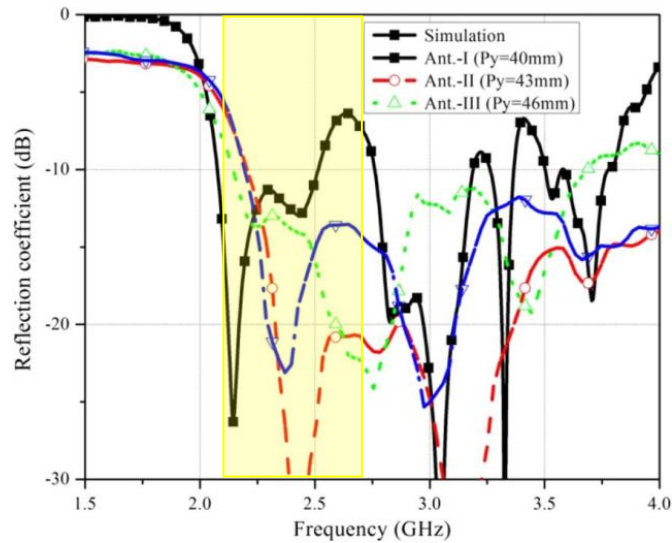


**Figure 4-13** Measured reflection coefficients of the three fabricated antenna prototypes compared to the simulated one. [34]-page 672. © 2013 IEEE

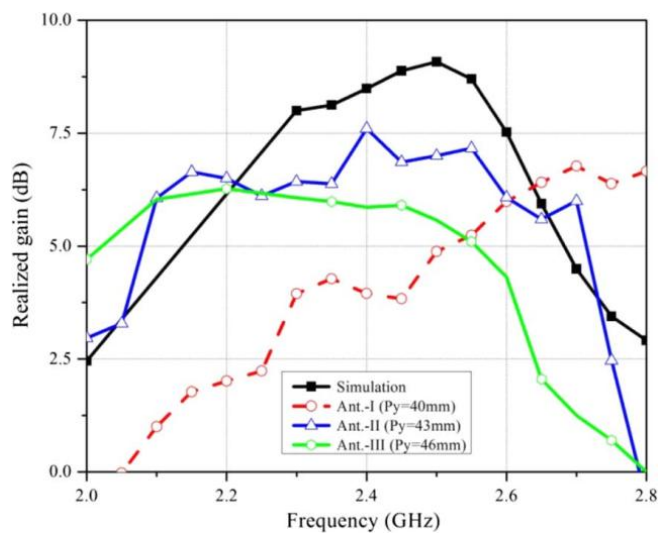


**Figure 4-14** Measured realized gains of the three fabricated antenna prototypes compared to the simulated one. [34]-page 672. © 2013 IEEE

3- Reference 3-[65]

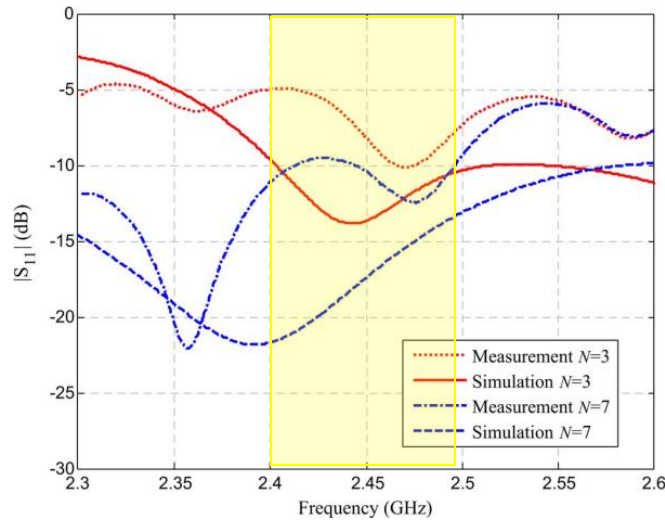


Figure 4-15 Simulation and measurement results of  $S_{11}$ . [65] - page 171. © 2015 IEEE

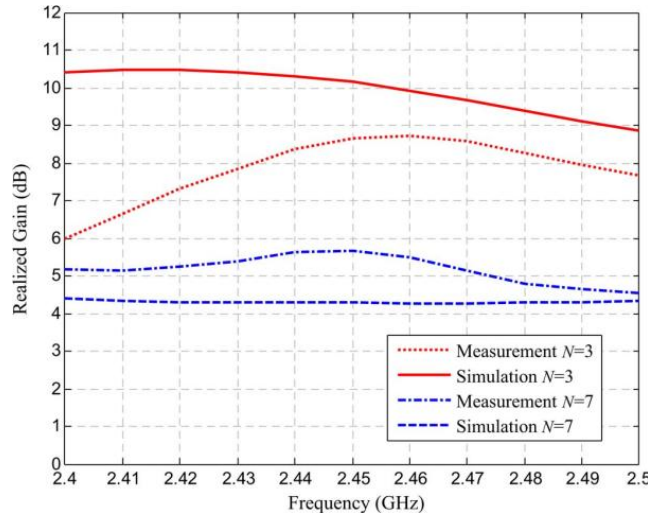


Figure 4-16 Simulation and measurement results: realized gain in H-plane. [65] - page 172. © 2015 IEEE

From the earlier curves it could be noticed that the gain band is not in the same band of the preferred matching. The yellow shade shows the gain band on the reflection coefficient curve to show the difference between the two bands. As discussed earlier, this shift is due to the impact of the switchable FSS characteristics on the antenna performance.

## 4.7 Radiation pattern measurements

Fig. 4-17 and Fig. 4-19 show the H- and E-plane radiation patterns, respectively with maximum scale of 8.6dB. The antenna has its best performance within the frequency band of 3.4 to 3.7 GHz or across 300 MHz, where the back-lobe levels are acceptable in the H- and E-plane patterns. The half power beam-width in the H-plane is  $34^\circ$ , while  $27^\circ$  in the E-plane. The narrow beam in the H-plane adds an angular resolution enhancement to the antenna. The proposed antenna azimuth beam-width is less than those reported in [34, 54, 65].

As observed from the graphs, an asymmetry is noticed in the H-plane radiation pattern. This is due to the interaction which occurs in the region around the central dipole feed shown in Fig. 4-7 (b). In addition a slight asymmetry occurs in the E-plane radiation pattern, due to the misalignment in the implemented dipole.

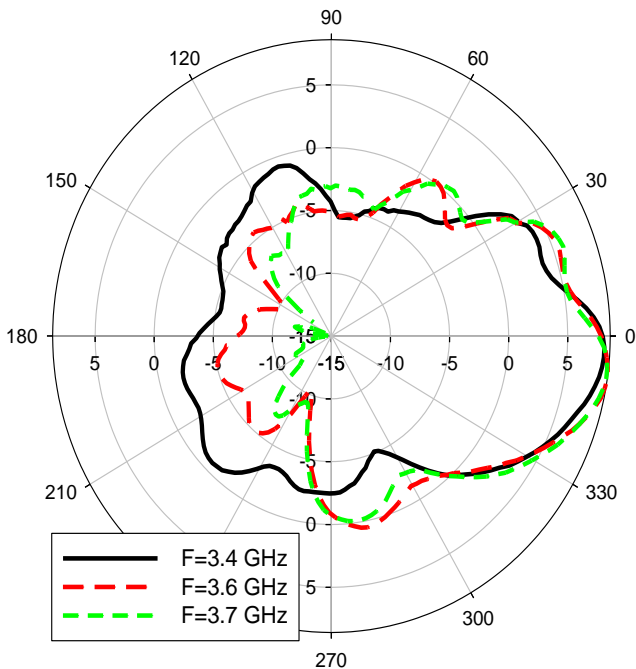
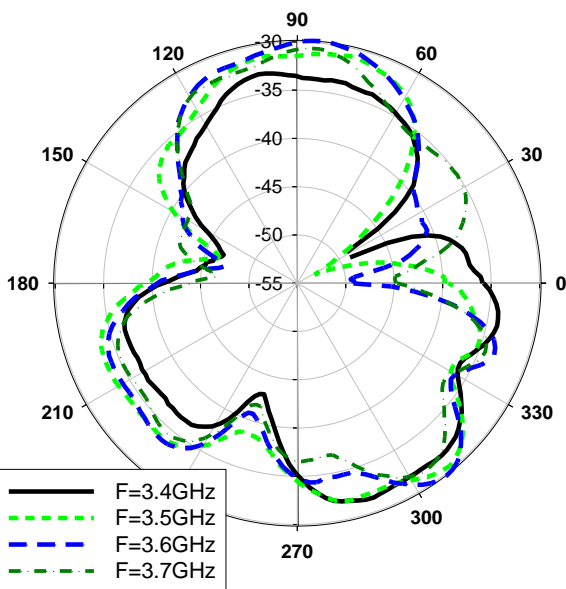
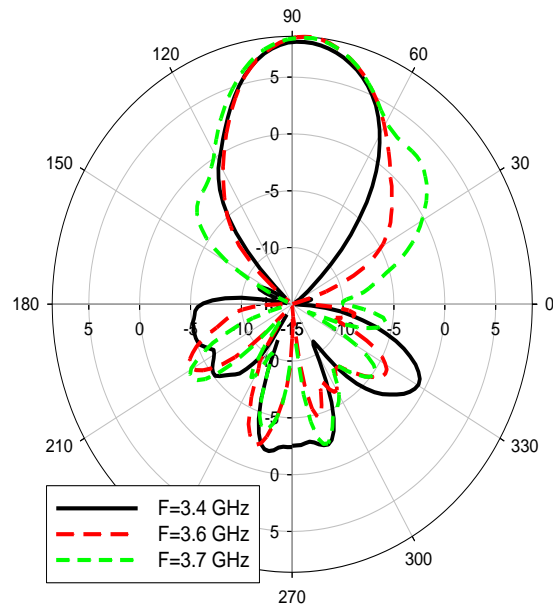


Figure 4-17 Measured H-plane pattern, co-polar, through 300MHz. © 2016 IEEE



**Figure 4-18** Measured H-plane pattern, cross-polar. © 2016 IEEE



**Figure 4-19** Measured E-plane radiation pattern, through 300MHz. © 2016 IEEE

Two important parameters are responsible for the overall antenna bandwidth. The first main parameter that identifies the antenna pattern bandwidth is the central omnidirectional antenna bandwidth. The second main parameter is the switchable FSS

shield bandwidth. The FSS will act as a filter that allows only some frequencies radiated from the central source to pass through the shield in fixed percentages. Hence, the FSS bandwidth should be larger than the source bandwidth to allow penetration of the source frequencies. Most of these frequencies will pass through the FSS shield only if the FSS bandwidth is more than the central source bandwidth. If the FSS bandwidth is less than the source bandwidth, then the reconfigurable antenna bandwidth is limited to the FSS transparent state bandwidth. This is because the FSS will not allow penetration of the source frequencies that lie outside the FSS transparency frequency band. The last effective parameters are the dimensions of the cylinder, its height and radius. They influence the impedance matching and gain in an opposite manner. The radius and height should be compromised to get the desired performance of the reconfigurable antenna. In the proposed designed antenna, Fig. 4-4 and Fig. 4-8 show that the bandwidth of the FSS is larger than the radiating source bandwidth therefore, a bandwidth enhancement is achieved.

**Table 4-1 Comparison of the antennas**

Comparison	Proposed antenna	Antenna in [65]	Antenna in [31]
Fractional Bandwidth	8.45%	4.08%	4.49%
3-dB Beam-width	34°	47°	77°
Center Frequency-GHz	3.55	2.45	1.78

Based on the achieved results, the current antenna design provides more bandwidth compared to other work [65, 31]. Table 4-1 shows the comparison between the proposed antenna and the antenna designs in [65, 31] in terms of beam-width and frequency bandwidth which provides an effective radiation pattern. From this comparison, it can be concluded that the proposed antenna covers more fractional bandwidth compared to the other designs. In addition, it provides a narrower beam, which means more directivity in the H-plane. This antenna could be considered for several utilizations as shown in Fig. 4-20, that provides the US spectrum updated in 23

April 2015.

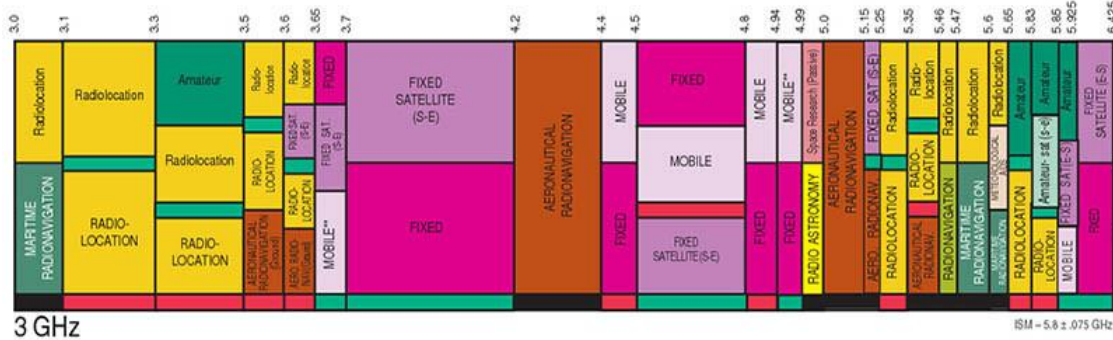


Figure 4-20 United States frequency spectrum.

## 4.8 Reconfigurable antenna bandwidth

In this section, the limitation of the radiation bandwidth and the justification for the bandwidth increase are further illustrated. There are different definitions of bandwidth standards. Fundamentally, a bandwidth of an antenna refers to the band of frequencies within which the antenna operates in the required performance and characteristics [66-68]. The author considered the radiation pattern bandwidth because it is the most limited bandwidth in this antenna. This is due to the undesired lobes which appear in the E-plane in some frequencies. These frequencies could not be considered within the antenna operating frequency band; therefore, they will limit the operational bandwidth of the antenna. The bandwidth listed in the Table 4-1 is the bandwidth where the best radiation pattern occurs.

The following discussion shows the limitation of the radiation pattern bandwidth and the justification of the antenna bandwidth increase. For further illustration, results from other reference are presented to compare the bandwidth:

- In the proposed antenna, the FSS bandwidth is more than the antenna source bandwidth. As a result, most of the source frequencies could penetrate through the

FSS shield. Fig. 4-21 and Fig. 4-22 show the radiation pattern for the E and H-plane, respectively, with adding the frequency 3.8GHz that is not considered in the earlier figures. It can be noticed that the E-plane at 3.8GHz has undesired high gain lobes (shown in blue circles). Because of these undesired lobes, this frequency is not selected to be an operating frequency.

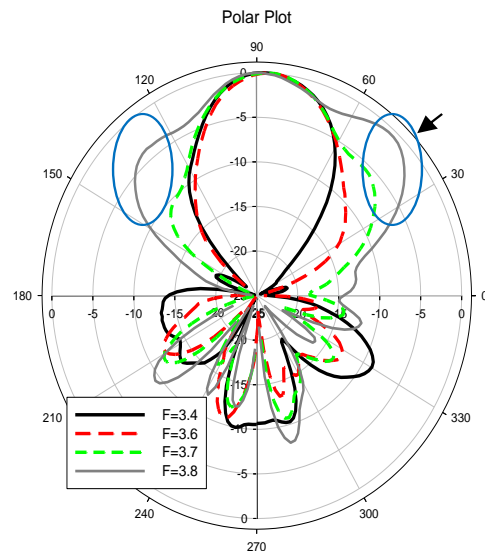


**Figure 4-21 Measured radiation pattern E-plane**

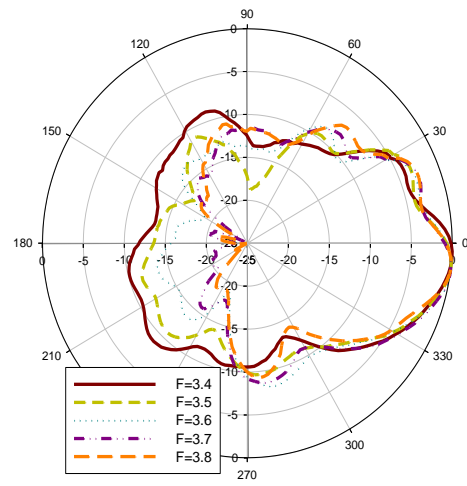


**Figure 4-22 Measured radiation pattern H-plane**

- In reference [65], the central source is a monopole with a bandwidth of 2.4-2.5 GHz and the FSS band is shown in Figure 4-23. The transparent state bandwidth is more than the source bandwidth. Hence, the reconfigurable antenna transmitted the source frequencies 2.4-2.5GHz in both models presented N=3 and N=7, as shown in Fig. 4-24, Fig. 4-24, respectively. The reconfigurable antenna radiation pattern bandwidth is limited by the least bandwidth that is the radiating source bandwidth. It can be noticed in this antenna that the E-plane has undesired side lobes in both presented models with high gain at 2.4GHz, as shown below in the green circles.

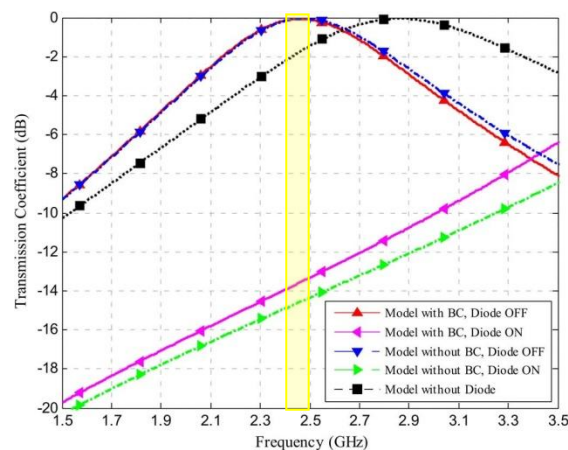


**Figure 4-23 FSS unit cell Transmission coefficient [65]. © 2015 IEEE**

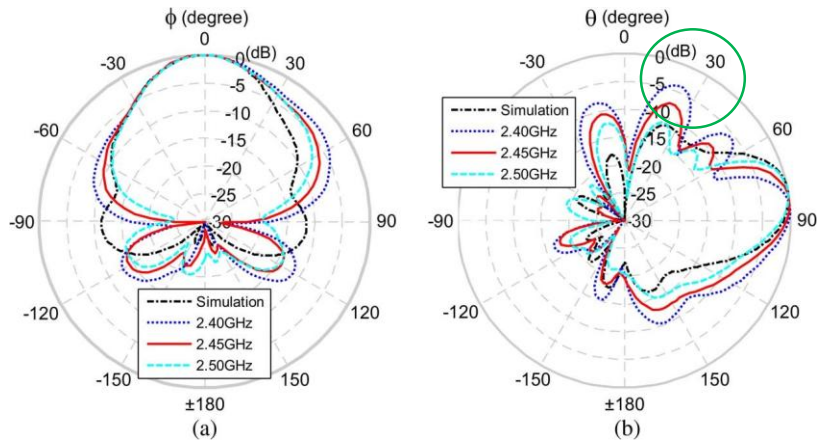


**Figure 4-24 Measured radiation pattern N=3 (a) H-Plane (b) E-plane [65]. © 2015 IEEE**

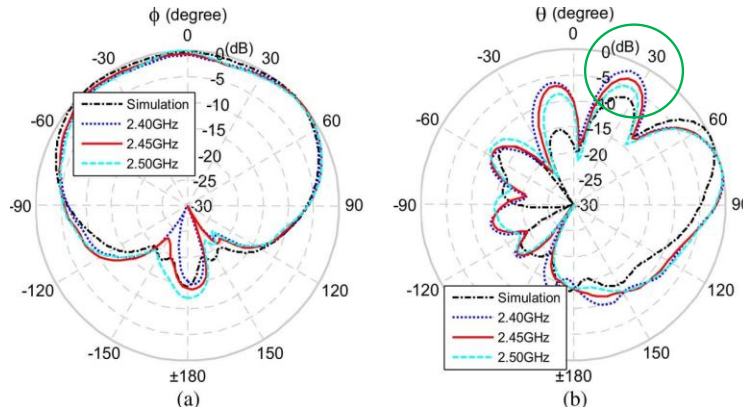


**Figure 4-25 Measured radiation pattern in N=7 (a) H-Plane (b) E-plane [65]. © 2015 IEEE**

- Reference [31] has a narrow FSS band compared to the central source antenna, as shown in Fig. 4-26. As a result, the reconfigurable antenna radiation pattern bandwidth is limited by the least bandwidth that is the FSS transparent state bandwidth. Fig. 4-27 shows the E-plane from 1.74-1.82 GHz.

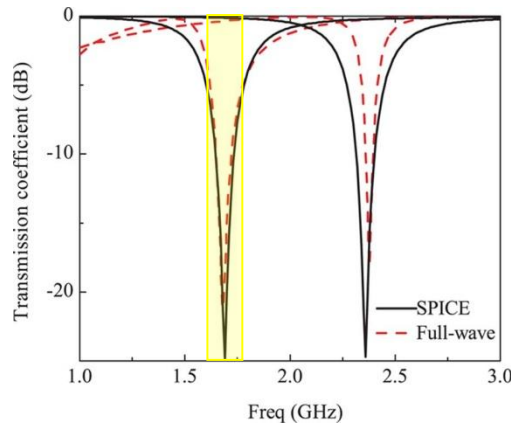


**Figure 4-26 FSS unit cell Transmission coefficient [31]. © 2013 IEEE**

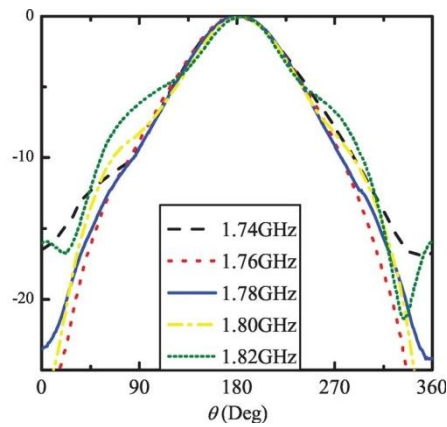


**Figure 4-27 Measured radiation pattern E-plane [31]. © 2013 IEEE**

Both references [65] and [31] have the same idea that is designing a pattern reconfigurable antenna by a central radiating source surrounded by a cylindrical FSS shield. In spite the differences in the central radiating source and the FSS unit cells, the three compared antennas have the same reconfigurable mechanism and a central omni-directional radiating source. The bandwidth considered in the comparison with these references is the radiation pattern bandwidth. As for reference [65], the central

source, monopole, operating bandwidth is limited between 2.4-2.5 GHz (100MHz) hence, it is not expected to have any other frequencies radiated from the reconfigurable antenna outside this range. The FSS acts only as a filter for the electromagnetic waves therefore no new frequencies are generated.

Reference [31] is comparable in spite of using varactors to switch the unit cells. This only represents a different switching method for the FSS transparent and reflective state in the reconfigurable antenna. There are different reconfigurable functionalities in this design, but the comparison is made with the 5-5 mode at Fig. 18 (as numbered in reference [31]), that has the same functionality as in the proposed antenna. Table 4-1 shows the bandwidth enhancement of the proposed antenna compared with other work in literature. The fractional bandwidth achieved is 8.45% that is more than the other compared antennas.

## 4.9 Conclusion

In this chapter, a pattern reconfigurable antenna based on a switchable frequency selective surface working in the  $f_2$  has been presented. Basically, the structure is a nonagon FSS structure centered by a simple radiating dipole. The obtained results have shown that the proposed FSS antenna could sweep its radiation pattern over the entire azimuth plane angles with a step of  $40^\circ$ . The antenna is distinguished by its wide operational bandwidth and narrow beam-width. The fractional bandwidth has been proven to be 8.45%. The antenna has stable radiation pattern across a frequency band of 300MHz with suitable front-to-back ratio. With these features, the proposed reconfigurable radiation pattern antenna presents a cheap alternative in communication system applications.

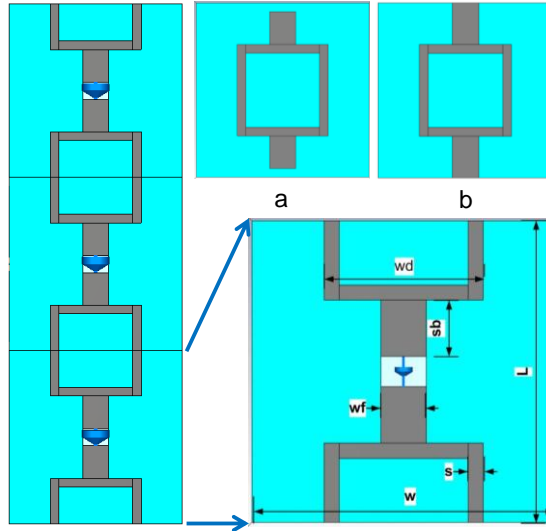
## 5 CHAPTER FIVE: RECONFIGURABLE RADIATION PATTERN ANTENNA (TWO)

### 5.1 Introduction

After presenting a reconfigurable antenna with an FSS shield in the  $f_2$  band, a cylindrical pattern reconfigurable antenna that utilises the  $f_1$  band is presented in this chapter for the first time in literature. These two antennas are presented to show the impact of the switchable FSS on the antenna performance when designed in the frequency bands  $f_1$  and  $f_2$  as illustrated in chapter three.

### 5.2 FSS unit-cell design at $f_1$

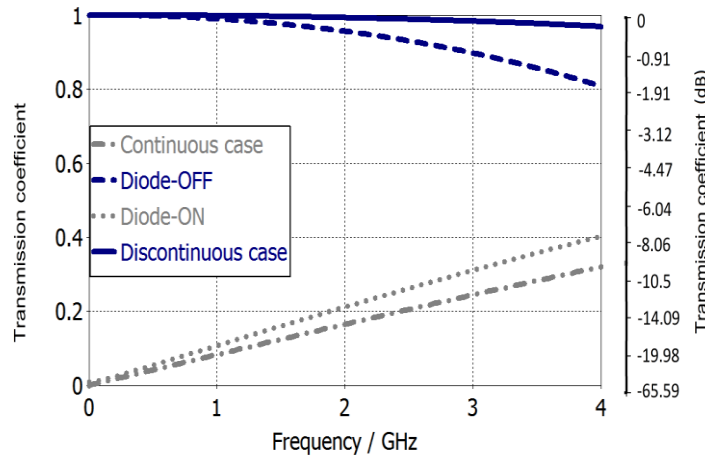
The FSS unit cell used in this antenna design is shown in Fig. 5-1. This unit cell is used to construct a cylindrical FSS around a central radiating source to operate as a beam sweeping antenna controlled by switching the FSS. If the FSS unit cells are connected as in Fig. 5-1b, they perform as a reflective surface. If a gap exists between the successive unit cells, as shown in Fig. 5-1a, they will act as a transparent surface. Integrating the PIN diode (GMP4202) [63] into the gap will enable the unit cell to switch electronically between the reflective and transparent states. When the PIN diode is switched OFF, the FSS is a transparent surface, and when the PIN diode is switched ON, it is a reflective surface.



**Figure 5-1 Proposed FSS unit cell structure. (a) Transparent state. (b) Reflective state.**

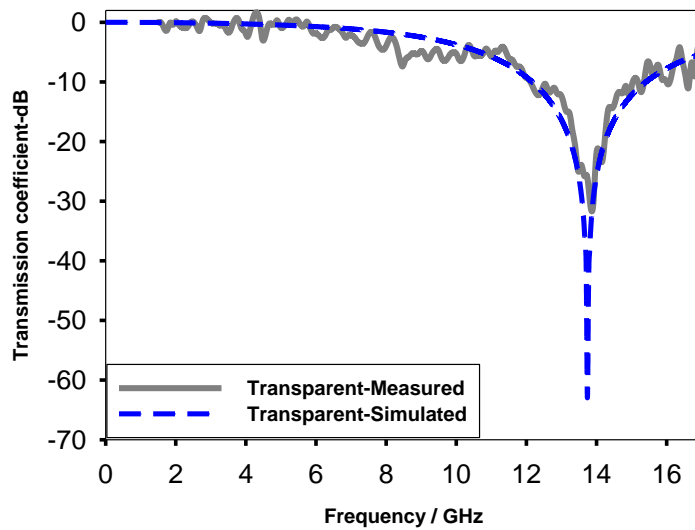
Fig. 5-2 compares the transmission coefficient of the FSS unit cells for the cases when the PIN diodes are integrated in the ON and OFF states and when no diodes are integrated to the unit cell. The figure shows an additional decibel scale to ease comparison with other unit cells in literature. In fact, in simulation the PIN diode is modelled by its equivalent lumped element circuit. When the diode is switched ON in the forward bias, the equivalent model is a resistor  $R=1.80 \Omega$ . When the diode is switched OFF in the reverse bias, it is modelled in simulation as a series connection of the parasitic capacitance and inductance [54] with  $C=0.07 \text{ pF}$  and  $L=0.5 \text{ nH}$ . Note that when the PIN diodes are integrated to the FSS, the power is decreased in both the transparent and reflective states due to the PIN diodes degrading influence. The transparent state is influenced more by this degradation than the reflective state because of the PIN diode characteristics. This could be improved by choosing high quality PIN diodes with better performance. If working in the  $f_2$  band, the reflective state would be affected more than the transparent state because it has a reciprocal performance. It is observed from Fig. 5-2 that the FSS bandwidth is decreased when integrating the diodes to the unit cell. Diodes with high specifications and suitable packaging style could be expensive, especially if 160 diodes are needed, as in our case. However, the chosen PIN diode is suitable for our antenna design because the antenna performs at a maximum frequency of 2.4 GHz. At this frequency band, the

minimum transmitted power is about 88% of the incident power when the PIN diode is switched OFF, while a maximum power of about 93% is reflected when the PIN diode is switched ON. These percentages are sufficient for the demand of the proposed cylindrical pattern reconfigurable antenna design.



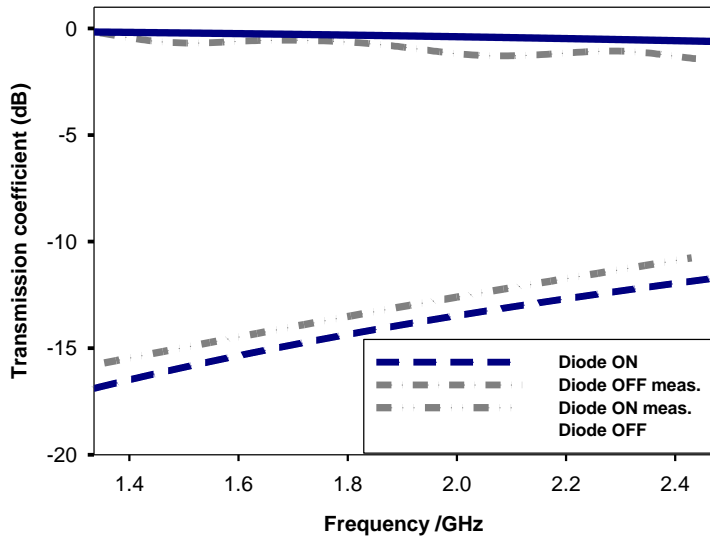
**Figure 5-2 FSS transmission coefficients for reflective and transparent states, with and without integrated PIN diodes.**

Fig. 5-3 shows the simulated and measured transmission coefficient for the switchable FSS in the transparent state. The prototype has gaps as shown in Fig. 5-1a, without the diodes connected. A measurement setup composed of two horn antennas on each side where the FSS prototype is set between the two horns. The size of the prototype is 16X10 unit cells. Substrate used for implementation is a flexible RO3003. The switchable FSS is implemented with gaps so that the PIN diodes could be soldered in them later for the antenna prototype. The gap length is designed to be 1 mm so it is compatible with the PIN diode size.



**Figure 5-3 Measured and simulated transmission coefficients for the transparent state.**

After soldering the PIN diodes, experimental measurements are carried out. Fig. 5-4 shows the transmission coefficient for the FSS transparent and reflective states. Two horizontal DC feed lines are added at the top and bottom of the FSS to feed the diodes. A high-value  $5\text{ k}\Omega$  resistor is mounted before each series of diodes on each panel to protect the diodes from high-biasing currents and to make sure that the same current flows in each panel. The figure shows the transmission coefficient of the FSS unit cell when the PIN diode states are ON and OFF. Measurements are done inside the anechoic chamber and show good correlation with simulated results. The reflective state result shows a difference of about 1dB. Improved results could be achieved when using a larger prototype so it could seize most the power generated by the horn antennas.



**Figure 5-4 FSS measured and simulated transmission coefficients in the reflective and transparent states with diodes.**

Fig. 5-5a and b show the electric field distribution for the transparent and reflective states at 2.25 GHz in the central Y-Z plane for the proposed FSS with integrated diodes, as shown in Fig. 5-1. The vertical black line in the centre represents the 0.13 mm thick substrate. The periodic boundary conditions sustain the electromagnetic wave generated from the left side ( $Z < 0$ ) to be absorbed at the right side ( $Z > 0$ ). Both graphs have the similar generated waves at ( $Z < 0$ ) side. Fig. 5-5a shows the Y-Z plane electric field distribution of the FSS unit cell when the diode is switched OFF. The majority of the incident wave penetrates through the unit cell in the red region shown at the diode location. In parallel, the electric field propagates weakly through the upper and lower sides and through the loop square. Likewise, Fig. 5-5b shows the electric field distribution for the reflective state when the diode is switched ON. In this state, the unit cell reflects a large part of the incident electric field towards the direction ( $Z < 0$ ). From the scale bar, the lowest electric field density is presented in dark blue, whereas the dark red colour represents the highest electric field density. It can be observed that there is a difference in the scale bars between the maximums for the transparent and

the reflective electric field distribution figures. These scales are chosen to show the maximum level in both states. In Fig. 5-5a, the maximum appears in the generated wave side ( $Z<0$ ) and in the diode location. This value decreases as the wave penetrates through the FSS to the other side ( $Z>0$ ). In Fig. 5-5b, the maximum scale is in the generated wave region ( $Z<0$ ). The difference between the two maximums is the amount of the electric field reflected by the FSS towards the left side ( $Z<0$ ) in the reflective state. These figures are presented to show the differences in electric field concentration between the reflective and the transparent states. In particular, to characterize the amount of reflected electric field added to the incident wave at ( $Z<0$ ) side in the reflective state. This amount will influence the antenna performance, as elaborated in the following sections.

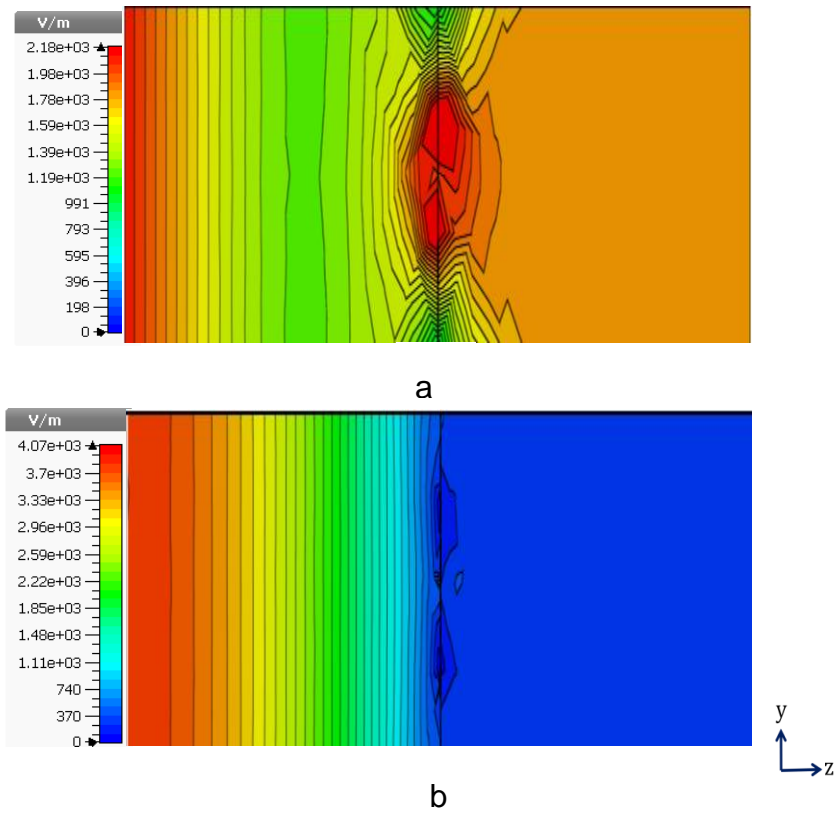


**Figure 5-5** (a) *Electric field distribution for the transparent state in the Y-Z plane.* (b) *Electric field distribution for the reflective state in the Y-Z plane.*

### **5.3 Pattern reconfigurable antenna design and steering mechanism**

In this section, the proposed FSS unit cell with integrated diodes, showed in the earlier section applies to design a cylindrical pattern reconfigurable antenna. The reconfigurable antenna performance is influenced by the characteristics of the FSS unit cell. The *f1* frequency band is chosen for this application for the following reasons:

- a) To offer performance improvement to the pattern reconfigurable antenna, the FSS should show high power reflection in the reflective state and high power transmission in the transparent state. The high power transmission in the FSS means that more power is transmitted in the antenna's transparent side, and thus more antenna gain. The high reflected power in the FSS offers two features. First, it reduces the back-lobe level of the antenna radiation pattern. Second, it increases the gain because the reflected power is reflected towards the antenna's transparent side. It is important to mention that the high power in both the reflective and transparent states should have correspondent frequencies and thus be within the antenna operating frequency band.
- b) The FSS has a wide operating frequency bandwidth with sufficient reflected and transmitted power. This makes it possible for the antenna to transmit the frequencies of the radiating source. The FSS acts as a filter on the central radiating source frequencies. If the FSS transparent bandwidth is more than the central source bandwidth, it will allow the source frequency band to penetrate through the antenna's transparent side. As a result, the antenna can realize a wide operating bandwidth.
- c) The FSS unit cell dimension is reduced, and this leads to a reduction in the antenna size while operating at low frequency bands. Usually reducing the size of the antenna influences its operating parameters negatively. Never the less, the proposed antenna has enhanced parameters along with compact size. Because of the reduced FSS unit cell size, 16 panels could be adapted in the antenna. The antenna can thus work with extra directive functionality and cover a high number of

angle steps in the azimuth plane.

The antenna is designed according to the procedures available in literature, and is optimized to reach the compact size and performance desired. The cylindrical antenna radius  $R = 25.4648$  mm is smaller than other similar antenna designs in literature. This leads to the need to investigate if the planar FSS assumption model is valid for the conformal FSS model used in the antenna design. For this validation, **B** is considered a central point on the planar FSS, and **A** is a point on the left or right edge of the planar FSS that lies on the cylinder as shown in Fig. 5-6. Calculations show that the phase shift between point **A** and **B** is very small and equal to  $1.34^\circ$ . Therefore, the proposed approach with planar FSS could be modeled for the curved FSSs in the cylindrical antenna.

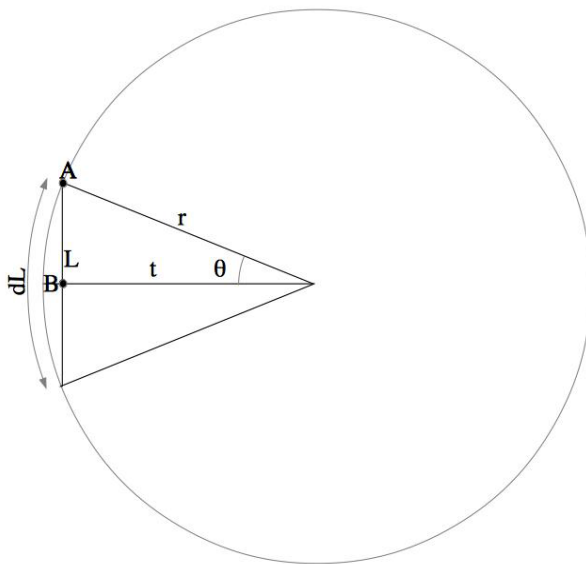


**Figure 5-6** Top view of the realized cylindrical structure.  $dL$  is width of the FSS unit cell,  $\theta=0.1976$  rad = $11.32^\circ$ ,  $t=24.969$  mm,  $r=25.4648$  mm,  $F=2.25$  GHz,  $k_0=47.156$  [1/M],  $\Delta\phi=k_0(r-t)=0.0233$  rad =  $1.34^\circ$  (phase shift between points A and B)

The proposed antenna has a cylindrical shape constructed of FSS unit cells. An omni-directional radiating source is placed at the centre of the cylinder. It is a simple dipole operating around 2.25 GHz. A group of FSS unit cells forming the cylinder consists of 16 panels, and each panel includes 10 FSS unit cells, they totally form 10 rows and 16 columns. The antenna is implemented on a flexible RO3003 substrate with a dielectric constant of 3 and a thickness of 0.13 mm. The total length of the antenna is 110 mm, and its radius is about 25 mm. The top and bottom sides of the cylinder are closed with a circular metallic plate covered with a non-metallic material on the outer side. These two plates are added to prevent from any power loss that might reduce the gain of the antenna. Fig. 5-7 shows than antenna design and the fabricated antenna prototype.

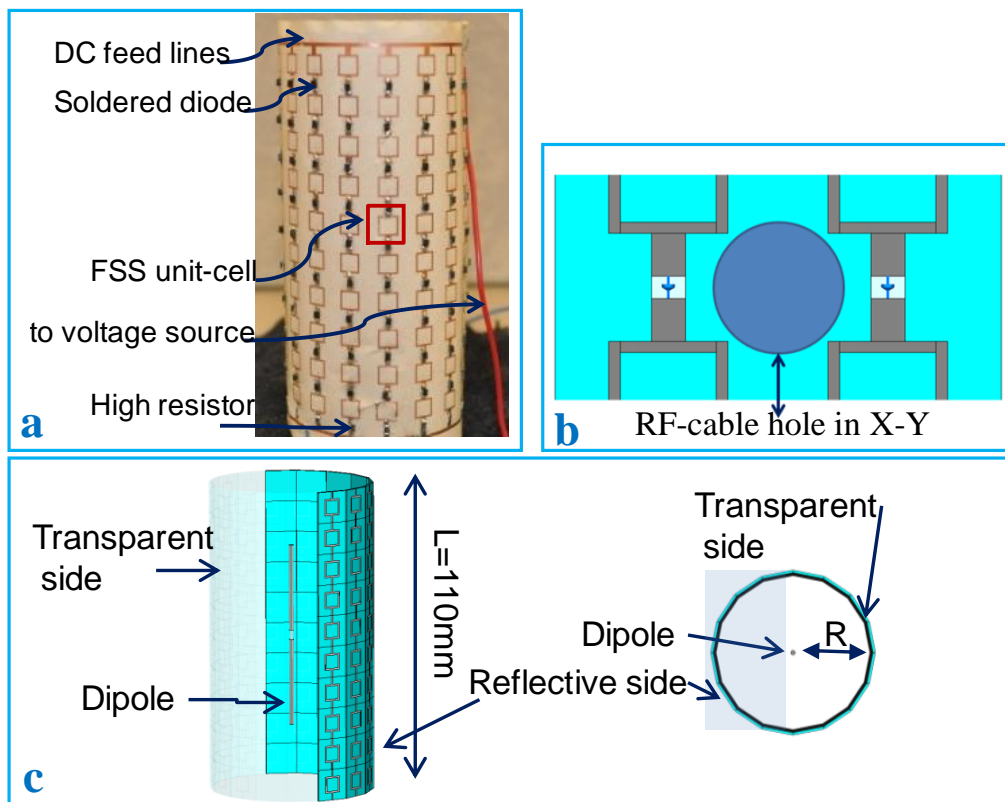


**Figure 5-7 Proposed antenna (a) Photo of the fabricated antenna.(b) The FSS shield hole for the RF-cable entrance.(c) Top and side view antenna design.**

The antenna has eight panels on the transparent side and eight on the reflective side at each reconfigurable beam steering position. Steering the radiation beam is achieved by switching the active elements in the panels to the desired direction. The PIN diodes of eight panels are activated at every step, and the PIN diodes of the other eight panels are deactivated. The proposed antenna covers 16 positions through the entire azimuth rotation with a  $22.5^\circ$  angle step. This small angle step gives the antenna extra functionality to cover more directive positions than other similar antennas proposed in [31, 34, 54, 65] thanks to the small size of the FSS unit cell. Fig 5-8 shows the H-plane reconfigurable radiation pattern when considering only six angle steering positions.

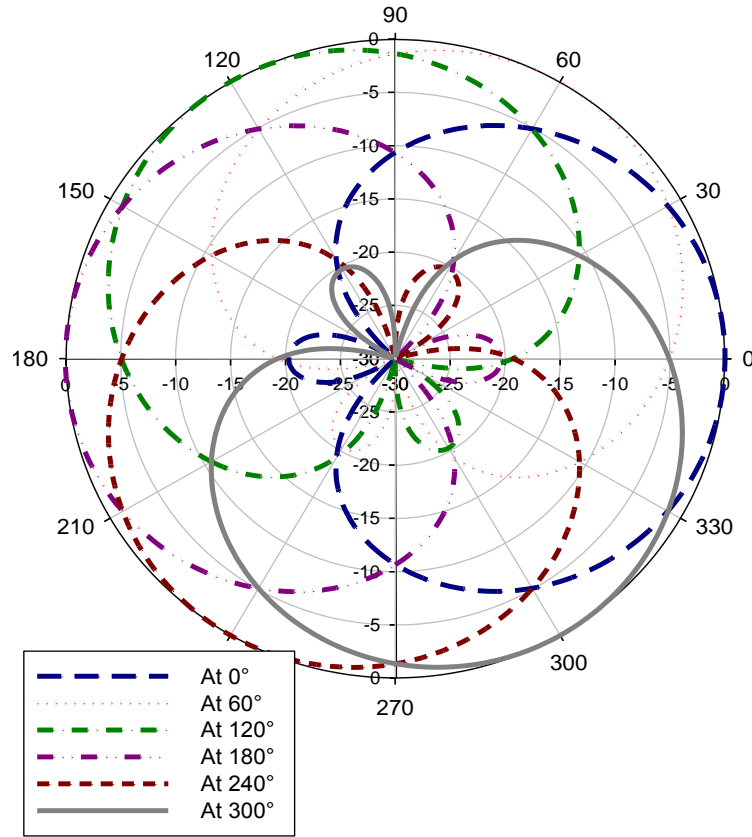


**Figure 5-8 H-plane radiation pattern for six angles**

Fig. 5-9 is drawn to illustrate the proposed antenna beam steering mechanism. The computers shown in the figure present the receivers, which could be any receiving device. The figure shows that the antenna could cover a maximum of 16 different positions, presented as coloured arcs. The width of each arc is related to the proposed antenna half power beam-width, 70°.

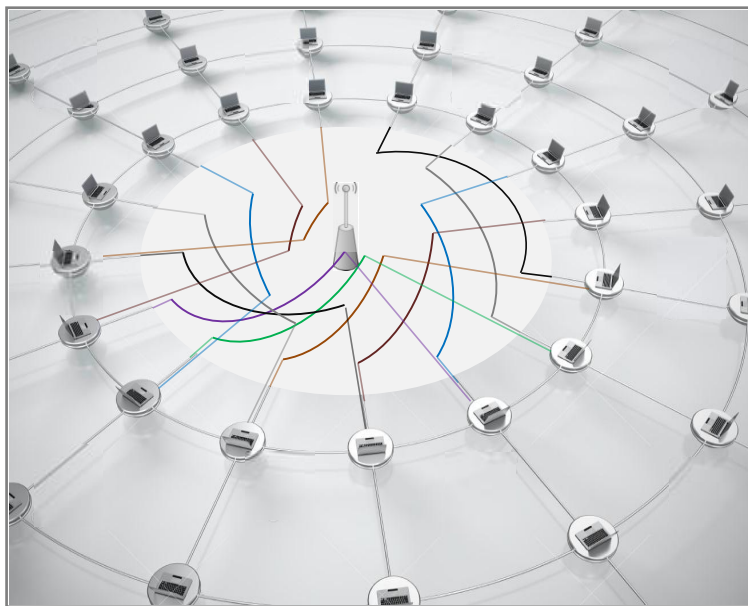


**Figure 5-9 Antenna beam-steering mechanism**

## 5.4 Experimental results and discussion

Fig. 5-10 shows the measured reflection coefficients for the dipole alone and for the pattern reconfigurable antenna with the FSS shield. The antenna is in the directional case when eight panels are reflective and eight other panels are transparent. The antenna is in the omni-directional case when the cylinder diodes are deactivated and the unit cells are in the transparent state. From Fig. 5-10, it can be seen that the antenna in its directive radiation case possesses more bandwidth than the omni-directional and single dipole cases. This is due to the influence of the FSS on the radiating source performance.

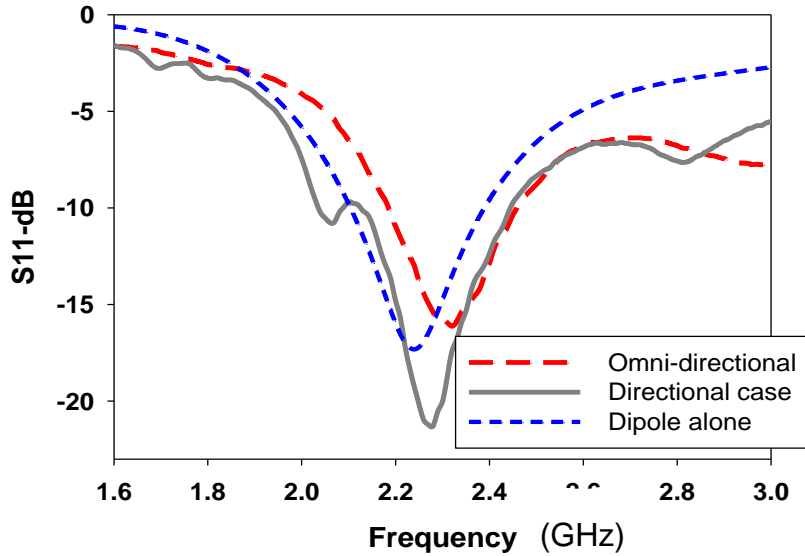


**Figure 5-10 Measured reflection coefficient**

Because of the symmetrical geometry, the antenna has a similar radiation pattern in any direction through the 16 positions it covers. Thus, only one directional position is presented for the radiation pattern graph.

Figs. 5-11 and 5-12 show the measured and simulated results for the H- and E-plane radiation patterns across 2.1 GHz - 2.4 GHz frequency range. As shown in these figures, the back lobe-level is sufficient. In addition, the half-power beam-widths are at a maximum of 70° and 62° in the H- and E-planes, respectively. These beam-widths are nearly correspondent across the frequency range of 2.1 GHz to 2.4 GHz.

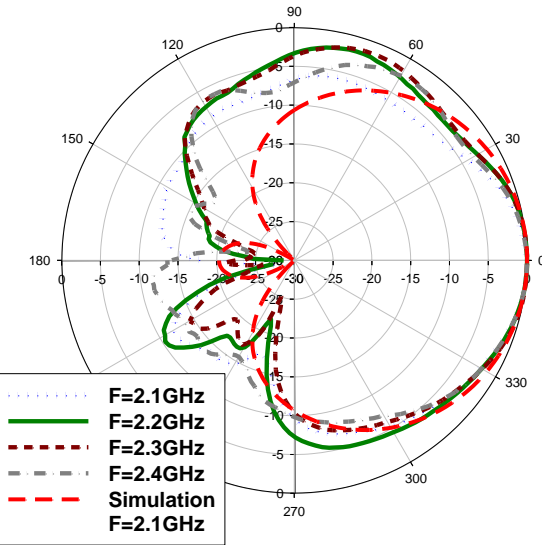


**Figure 5-11 Measured H-plane radiation pattern.**

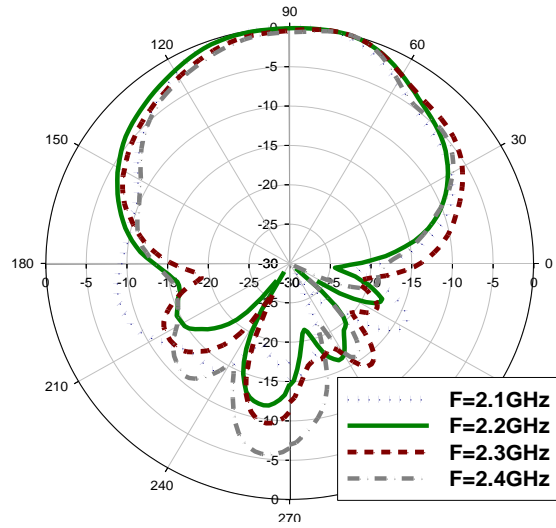


**Figure 5-12 Measured E-plane radiation pattern.**

In general, there is no unique bandwidth definition in literature [66-68]. Therefore, the bandwidth of an antenna refers to the frequencies where the antenna operates within the desired characteristics. In this antenna the most effective bandwidth is the radiation pattern bandwidth. This is because of the undesired lobes which appear at some frequencies. Thus, these undesired frequencies limit the antenna operating bandwidth.

This point has been discussed in details in chapter four, Section 4.8.

Both simulation and experimental radiation pattern results in Fig. 5-11 show a good agreement, except for a slight difference related to the symmetry of the radiation pattern in the H-plane. This asymmetry is due to the feeding required for the central dipole. The dipole inside the FSS cylindrical shield is fed by an SMA connected to an RF-cable. The RF-cable enters the cylinder horizontally through a hole in the FSS at the dipole central position, as shown in Fig. 5-7b. The hole is chosen to be at the middle of four adjusted FSS unit cells to reduce its influence on the unit cells performance. This dipole feed effect is not considered in the simulations.

The maximum gain of the proposed antenna of 9 dBi is considered high for this type of antenna, keeping in mind that a simple low gain dipole antenna is functioning as the radiating element source. This good gain value is a result of the FSS unit cell high transmitted power in the transparent state and is also related to the high power reflected in the reflective state.

## 5.5 Conclusion

In this chapter, a reconfigurable cylindrical beam-steering antenna composed with an FSS structure has been presented. The antenna performance depends on the FSS characteristics. The transmission coefficient of the FSS unit cell operating in  $f_1$  has carefully been studied to determine the desired performance to achieve the required characteristics of the reconfigurable antenna. The antenna directive radiation pattern covers an enhanced frequency range of 2.1-2.3GHz with a suitable back-lobe level in both the H- and E-plane radiation patterns. Moreover, the half power beamwidth is 70° and 62° in the directive H- and E-plane radiation patterns, respectively. Simulated and experimental results have demonstrated the antenna improvement in terms of size, bandwidth and radiation pattern.

## **6 CHAPTER SIX: CONCLUSIONS AND FUTURE WORK**

### **6.1 Introduction**

The importance of this work is attracted from the various FSS applications and the industrial value of these applications in both military and civilian domains. The concept of increasing the bandwidth of both the FSS unit cells and the antenna are substantial for future high-data-rate expansion. The bandwidth enhancement has been discussed for the first time from the view of the FSS bandwidth influence and the view of considering the radiation pattern as the identified bandwidth. This point has thoroughly been discussed to draw attention that the impedance bandwidth and the gain bandwidth are irrelevant in this type of antenna as long as undesired lobes appear in certain frequencies. These lobes limit the antenna operation and could not be acceptable at certain levels where the radiation pattern shape is distorted. These points are investigated for the first time in literature in this thesis and could be discussed more and improved in future.

### **6.2 Conclusions**

In this thesis, two main subjects are investigated. The first one is the design of switchable FSS and the second is the utilization of the switchable FSSs in reconfigurable pattern antennas to enhance the bandwidth. The switchable FSSs are designed to work in both  $f1$  and  $f2$  bands. The difference between the two bands is investigated and the obtained results are compared. The switchable FSS working in the  $f1$  band is used in a reconfigurable antenna design for the first time in this thesis. To show the switchable FSS working band influence on the antenna parameters, two new reconfigurable radiation pattern antennas have been proposed. The first antenna designed, in chapter 4, has a switchable FSS operation at the resonance frequency  $f2$ . And the second antenna presented, in chapter 5, has a switchable FSS operation at the first non-resonance frequency  $f1$ . The results in chapters 4 and 5 show the difference in

both antenna performances.

Table 4-1, shows that the first proposed antenna bandwidth has an improvement of 8.45% over the other antennas in literature that have fractional bandwidth of 4.49% and 4.08% in [31] and [65], respectively. Table 6-1 shows the improvement in the functionality of the second proposed antenna in chapter 5 as compared to the first antenna in chapter 4. The most important enhancement is the increase in the fractional bandwidth by a percentage of 13.33%. This proves that the second antenna has more bandwidth than the antennas presented in literature. From Table 6-1 it can be concluded that the second proposed antenna directional beam is broad as compared to the first antenna that has a more directive beam. In addition, the peak gain in the directional case for the second antenna is 9 dBi. Important to point out, the reduction in the second antenna size has been achieved even though this antenna operates at lower frequency ranges than the first antenna. Another feature of the second antenna is that it could cover more reconfigurable positions in the azimuth plane. The only drawback of the second antenna is that it consumes more power due the additional number of PIN diodes required because of the unit cell small size. According to the results obtained for the first and second antennas, it could be concluded that the performance of this antenna type is related to the design of the switchable FSS used to form the shield around the central radiation source. In particular, the switchable FSS transmitted and reflected power percentages and the joint bandwidth of the two states that show significant impact on the final antenna characteristics and bandwidth.

**Table 6-1 Comparison of the antennas**

Comparison	Antenna one in Ch-4		Antenna two in Ch-5	
Fractional Bandwidth	<b>8.45%</b>		<b>13.33%</b>	
3-dB Beam-width	H	E	H	E
	34°	27°	70°	62°
Center Frequency-GHz	<b>3.55</b>		<b>2.25</b>	
Electrical length & radius	<b>2.01λ X 0.355λ</b>		<b>0.825λ X 0.19λ</b>	
Sweep azimuth angle	<b>40°</b>		<b>22.5°</b>	
Number of directive positions	<b>9</b>		<b>16</b>	
Peak gain (dB)	<b>8.6</b>		<b>9</b>	
Transparent section percentage	<b>44.44%</b>		<b>50%</b>	
Number of PIN diodes	<b>99</b>		<b>160</b>	

### 6.3 Future work

This research domain is one of the most important domains due to several aspects. The topology of 3D cylindrical or conformal antenna in any shape with a central radiating source can provide functionalities that differ from other kinds of antennas. The complex antenna design and implementation make it a challenge for many researchers, therefore only few designed antennas are available in literature. These antennas are higher in gain as compared to planar reconfigurable antennas due to the radiating

source used. In addition beam sweeping could be done easily and controlled remotely due to the active elements used in the switchable FSS. The drawbacks of these antennas are their large size and their limited bandwidth as compared to other reconfigurable antennas. These two issues are investigated in this thesis to improve the antenna and give it a role to be considered in future technological evolution.

According to the concept for increasing the antenna bandwidth proposed in the thesis even more antenna bandwidth could be achieved in future research. This could be done by combining a suitable radiation source antenna with a switchable FSS that has a large joint bandwidth. Investigation is done in this path and work is in progress for designing an antenna with ultra wide bandwidth using wide-band FSS unit cells.

Due to the wide applications of switchable FSS, the designed unit cells proposed in the thesis and the antennas designed within different frequency bands could add more ideas for future researches within the antenna domain.

## 7 CHAPITRE SEVEN: RÉSUMÉ

### 7.1 Motivations

De nombreuses applications militaires et civiles pour les antennes reconfigurables peuvent être citées dans la littérature [1-3]. Par exemple, les communications entre un satellite et un usager en mouvement doit avoir une antenne orientable afin de garder une connexion stable [4]. Les antennes orientables peuvent changer la direction de rayonnement en fonction de la position de l'objet en vue de garder ainsi son suivi. Les antennes reconfigurables peuvent permettre un accès internet haut débit aux usagers dans toutes les catégories de transmission. En outre, la connexion GPS et d'autres types de liens de communications importants pourraient être également établis en utilisant les antennes reconfigurables [5].

Dans un avenir proche, la demande pour le haut débit est grandissante non seulement pour les particuliers et les entreprises, mais aussi pour les utilisateurs mobiles. Cisco Systems estime [6] que: « Environ trois quarts du trafic de données mobiles dans le monde deviendront vidéo d'ici l'an 2019, et que la moyenne des téléphones intelligents vont générer environ 4.0 GB de trafic par mois en 2019 ».

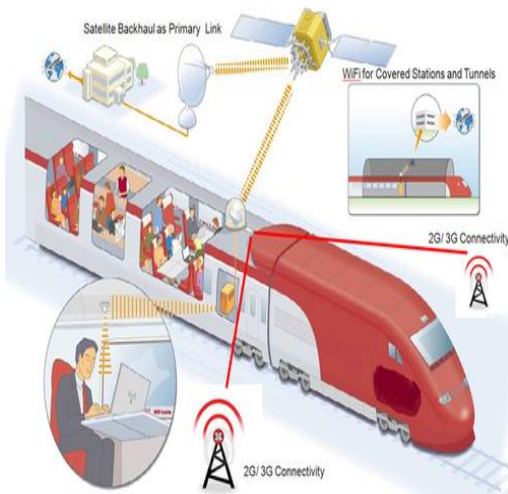


Figure 7-1 Liens de communication en utilisant des antennes reconfigurables [69].

## 7.2 Problème et objectifs de recherche

Les antennes reconfigurables ont été présentes depuis les années 1930 [9], et elles sont devenues encore plus intéressantes pour l'industrie. Elles attirent une grande attention parce que ces antennes fournissent une fonctionnalité supplémentaire et ont des propriétés plus flexibles tout en occupant un plus petit volume physique par rapport aux antennes intelligentes traditionnelles [10].

En général, les antennes reconfigurables sont capables de modifier la fréquence de fonctionnement, la polarisation, la largeur de bande d'impédance et le diagramme de rayonnement d'une manière indépendante pour réussir les opérations requises [5]. Cependant, les développements de ces antennes ont créé des défis importants pour les ingénieurs, pour les concevoir ainsi que les autres parties requises du système. Les surfaces sélectives en fréquence (FSS) sont des éléments importants dans la conception des antennes reconfigurables, en raison de leur impact sur la propagation d'ondes dans les antennes reconfigurables [11-12]. Une surface sélective en fréquence est également connue en tant que surface à haute impédance en raison de sa capacité à supprimer la propagation des ondes de surface à la fréquence de fonctionnement. Cette structure a également la possibilité de réduire l'impact de l'effet de couplage mutuel dans les applications de réseau [13-14].

Les surfaces sélectives en fréquence ont été exploitées dans la conception des antennes reconfigurables pour de nombreuses applications de communication en raison de son effet variable sur le champ électromagnétique [14]. Elles sont composées de structures périodiques ayant une bande interdite [15]. Les ondes électromagnétiques ne peuvent pas se propager à travers cette structure dans la bande interdite. Ce comportement change si un défaut est réalisé concernant la périodicité du matériau. Si la périodicité est brisée, l'onde électromagnétique se propage à travers le défaut [16]. La surface sélective en fréquence est utilisée comme une surface partiellement réfléchissante ou transparente dans de nombreuses structures d'antennes pour améliorer les performances de l'antenne en particulier le gain de l'antenne et le diagramme de rayonnement [17].

L'objectif de ce travail est de présenter de nouvelles cellules unitaires de surface sélective en fréquence commutable aux composants de base des antennes reconfigurables. Le coefficient de transmission de chaque cellule élémentaire proposée est étudié avec soin afin de déterminer la meilleure performance de la cellule unitaire pour obtenir les caractéristiques requises de l'antenne reconfigurable. La conception de la cellule d'unité de surface sélective en fréquence est le composant d'influence principale qui affecte la fonctionnalité du diagramme de rayonnement de balayage de l'antenne reconfigurable.

Les réalisations de la thèse peuvent être résumées comme suit:

1. Quatre différentes sortes de surfaces sélectives en fréquence commutables ont été proposées et leurs paramètres ont été étudiés. Une comparaison est faite en termes de coefficient de transmission et de la bande passante pour les cellules unitaires proposées à la fois dans la bande de fréquence de résonance et de non-résonance. Les caractéristiques des surfaces sélectives en fréquence commutables ont été profondément étudiées pour montrer la différence entre chaque design. Cette étude comparative est très importante pour la sélection des caractéristiques appropriées de surface sélective en fréquence commutable pour une application particulière.
2. La conception et la fabrication d'une antenne reconfigurable basée sur la surface sélective en fréquence commutable ont été effectuées. La surface sélective en fréquence commutable fonctionne à la fréquence de résonance, et l'antenne fonctionne à 3.6 GHz. L'antenne est capable de balayer l'ensemble d'angles d'azimut avec 9 angles différents et a amélioré la bande passante.
3. La conception et la fabrication d'une antenne reconfigurable fonctionnant à 2.1 GHz avec utilisation d'un format plus compact que l'antenne mentionnée précédemment a été faite, ce qui signifie que l'antenne est plus petite, même si elle fonctionne à une fréquence inférieure. Cette situation est rare parce que lors du passage de l'antenne à une fréquence inférieure, sa taille est devrait être plus

grande. L'antenne proposée est capable de balayer l'ensemble d'angles d'azimut de plus de 16 angles différents. La surface sélective en fréquence commutable utilisée dans cette conception de l'antenne fonctionne dans la première bande de fréquence de non-résonance. L'antenne se distingue par sa largeur de bande très large.

### 7.3 Contributions de la thèse

Le travail de cette thèse porte sur le recours aux propriétés significatives des surfaces sélectives en fréquence commutables pour créer une antenne à diagramme de rayonnement reconfigurable et directif. Cette recherche est importante car elle permet de surmonter les problèmes associés aux performances du système de communication par l'intégration de plusieurs fonctions dans un élément unique [18]. Cela permettra de réduire le nombre d'antennes nécessaires et ne pas gaspiller l'espace de plate-forme par des antennes multiples pour chaque fonction.

L'importance du travail dans cette thèse découle des points suivants:

1. L'amélioration les performances de l'antenne reconfigurable et sa fonctionnalité ; deux nouvelles cellules unitaires à surfaces sélectives en fréquences sont proposées dans deux bandes de fréquence différentes. Ces surfaces sélectives en fréquence sont les éléments de base dans la conception des antennes proposées.
2. L'augmentation de la fonctionnalité de l'antenne reconfigurable en termes d'amélioration de la bande passante avec un lobe arrière réduit et des lobes secondaires faibles.
3. La réduction de la taille de l'antenne, en utilisant une surface sélective en fréquence ayant une petite taille. Plusieurs positions directives sont atteintes dans tout le plan d'azimut avec des performances améliorées.

## 7.4 Surfaces sélectives de fréquence

Le domaine de FSS joue un rôle primordial dans la technologie grâce à ses applications diverses. En général, l'idée de FSS est basée sur sa structure qui influence sur l'onde électromagnétique [58]. L'aspect adaptable de FSS permet le contrôle de la propagation des ondes électromagnétiques avec deux façons différentes. Soit il permet la pénétration de la plupart des ondes électromagnétiques dans la structure à l'état transparent ou il réfléchit l'onde incidente dans un état de réflexion [59].

Quatre formes différentes de FSS sont introduites: bande plane, carré, anneau et triangle. Les variantes de FSS adaptables sont similaires en termes de taille, matériel et l'espacement périodique entre les cellules unitaires. Mais elles sont différentes seulement au niveau de la forme et la structure géométrique. Le but de changement de la structure géométrique et de garder la similarité entre les autres paramètres est d'étudier l'impact de la forme sur la performance dans les deux états: transparent et réflexion.

Les variantes de FSS adaptables sont conçues pour fonctionner dans la première bande de fréquence non résonnante ( $f1$ ) et la fréquence de résonance ( $f2$ ). Ces deux bandes de fréquences sont exploitées en raison des caractéristiques suivantes. D'abord, les performances de l'état transparent et de l'état de réflexion atteignent leur maximum à  $f1$ , alors qu'avec  $f2$  la fréquence maximale transmise n'est pas obligatoirement compatible avec la fréquence optimale de réflexion, comme expliqué dans [34]. Deuxièmement, l'état transparent et de réflexion ont une grande largeur de bande commune dans  $f1$  en les comparants avec la fréquence de résonnance  $f2$  où ils ont une bande passante étroite commune son l'étude parue dans [31]. Ces deux points d'intérêts ont prouvés l'importance d'examiner et d'analyser la performance des cellules unitaires dans les deux bandes de fréquences  $f1$  et  $f2$ .

Des formes circulaires intérieures sont appelées souvent en anglais "solid interior circular» sont utilisées dans nos simulations pour clarifier la différence entre  $f1$  et  $f2$ . Fig. 7-2 (a, b) représentent la conception des formes circulaires intérieures dans les deux états transparent et l'état de réflexion. La Fig. 7-3 montre la transmission de coefficient

dans les deux états. Lors de la première bande de fréquence réalisée, la fréquence  $f1$ , les deux états sont approximativement identiques et ont plus de 90% de puissance transmise et réfléchie à travers une bande de fréquence commune qui est égale à 5 GHz. D'autre part, avec la fréquence de résonnance  $f2$ , la fréquence commune peut varier entre 19.8 -21.04 GHz, à travers une bande passante de 1.24 GHz. Dans cette bande de fréquence, la puissance réfléchie est comprise entre 90%-75% et la puissance transmise est supérieure à 83%.

Si la bande utilisée contient au minimum 90% de la puissance réfléchie alors la bande passante est égale à 3.8 GHz et la puissance transmise correspondante doit varier entre 68% - 83%. Le choix d'une bande de  $f2$  dépend fortement de l'application à réaliser. Il existe deux façons différentes pour assurer ce choix, soit-on choisi une grande valeur de la puissance réfléchie avec une haute bande passante, soit on choisi une haute puissance transparente avec une bande étroite.

À la base de ces résultats, nous pourrons conclure que la bande  $f1$  est plus préférable que la bande  $f2$  en termes de pourcentage de puissance élevé et de largeur de bande de fréquence commune dans les deux états transparent et l'état réflexion.

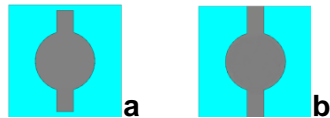


*Figure 7-2 La structure de la cellule FSS proposée.*

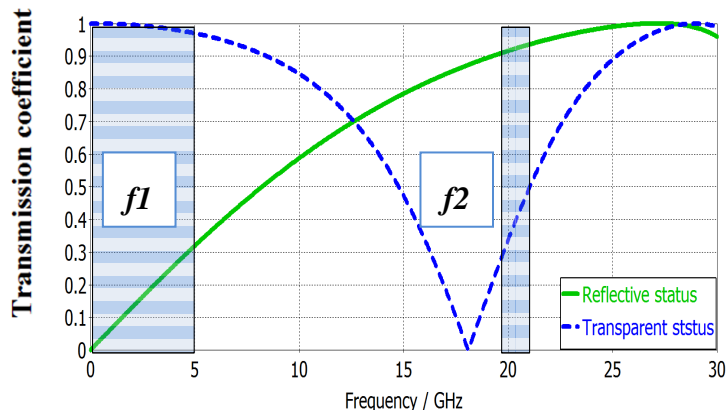


**Figure 7-3 le coefficient de transmission simulé de la cellule FSS, pour  $f_1$  et  $f_2$ .**

## 7.5 Antenne reconfigurable en diagramme de rayonnement

### 7.5.1 Introduction

L'antenne reconfigurable en diagramme de rayonnement est présentée comme une application des surfaces sélectives en fréquence. Cette application est sélectionnée puisque la cellule unitaire des surfaces sélectives en fréquence a des caractéristiques convenables pour améliorer les performances de l'antenne. Deux antennes reconfigurables en diagramme ont été conçues avec un dipôle central utilisé comme une source de rayonnement et une surface cylindrique de surfaces sélectives en fréquence. La première antenne consiste à des surfaces sélectives en fréquence commutées fonctionnant à la fréquence  $f_2$ , tandis que la deuxième antenne présentée a des surfaces sélectives en fréquence commutées fonctionnant dans la bande de fréquence  $f_1$ . Les antennes conçues ont un diagramme reconfigurable à travers tout le plan azimutal. La conception de la cellule unitaire est démontrée par l'état du coefficient de transmission. En plus, les résultats obtenus de la simulation et de l'expérimental ont été présentés, discutés et comparés avec d'autres concepts pour clarifier l'amélioration des performances de l'antenne proposée.

### 7.5.2 Conception de la cellule unitaire FSS à la fréquence $f_2$

L'antenne reconfigurable en diagramme de rayonnement est modélisée par la conception de la cellule unitaire des surfaces sélectives en fréquence commutées. Cette dernière doit répondre à certaines exigences pour effectuer la conception de l'antenne souhaitée. La cellule idéale des surfaces sélectives fréquences commutées devrait avoir la puissance maximale réfléchie dans l'état de réflexion, et la puissance maximale qui traverse les surfaces sélectives en fréquence dans l'état transparente. Les deux maximums doivent se trouver dans la même bande de fréquence. La réflexion par rapport à la bande passante des surfaces sélectives en fréquence dans l'état transparent affecte directement la largeur de bande de fréquence de fonctionnement de l'antenne.

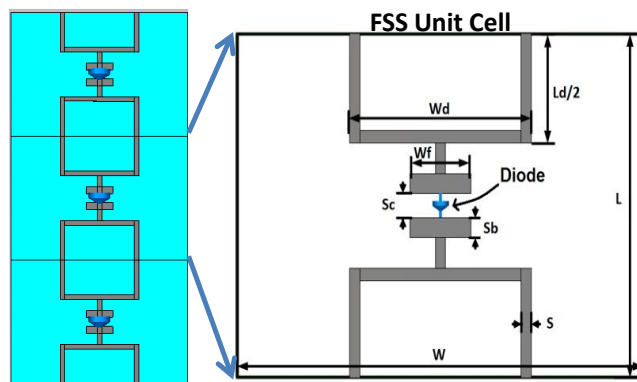


**Figure 7-4 Structure de la cellule unitaire de FSS. Dimensions en millimètre:  $W=18.7$ ,  $L=14$ ,  $W_d=8.9$ ,  $K=3$ ,  $S_c=1$ ,  $L_d=8.9$ ,  $S_b=0.8$ ,  $S=0.5$ ,  $W_f=3$ .**

La Fig. 7-4 montre les dimensions de la cellule unitaire des FSS proposée ainsi que la localisation des diodes PIN qui permettent la commutation de ces cellules. La cellule unitaire FSS est conçue en utilisant une boucle de forme carrée avec des écarts entre les cellules successives pour souder les diodes PIN, comme le montre la Fig. 7-4. Le substrat de la cellule FSS est de type Rogers R5880 avec une permittivité 2.2 et une épaisseur de 3.18 mm. La cellule FSS a deux états pour contrôler le flux de l'incidence de l'onde électromagnétique, soit elle bloque la majeure partie de l'onde électromagnétique de circuler à travers la structure ou elle permet à la majeure partie de l'onde électromagnétique à circuler à travers la structure. Ces deux états sont

appelés réfléchissant et transparent, respectivement. Les états dépendent de la périodicité représentée par l'écart entre les cellules unitaires des surfaces sélectives en fréquence.

La cellule unitaire de FSS fonctionne comme une surface transparente lorsque l'écart est ouvert et comme une surface réfléchissante dans le cas où l'écart est fermé. Lorsque les boucles carrées sont connectées les uns avec les autres, la fréquence de résonance est décalée vers les hautes fréquences, rendant les surfaces sélectives en fréquence à l'état transparent à la fréquence 3.87GHz. Alternativement, la commutation peut se faire de façon automatique en ajoutant des diodes PIN (GMP 4201) [63] à l'emplacement de l'écart. Lorsque la diode est allumée (en conduction, ON), la cellule FSS agit comme une surface transparente. De même, elle agit comme une surface réfléchissante lorsque la diode est éteinte (OFF). Chaque paramètre ( $W_d$ ,  $L_d$ ,  $s$ , etc.) a son effet sur les performances des cellules FSS commutables, en particulier sa largeur de bande de fréquence. La Figure 7-5 présente le coefficient de transmission de la cellule unitaire FSS commutable pour les deux états de la diode PIN ON et OFF.

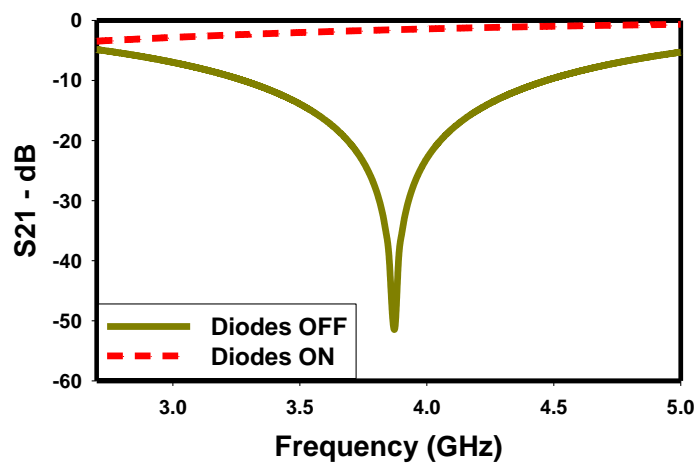


**Figure 7-5 le coefficient de transmission simulé de la cellule FSS**

Dans cette conception, la diode PIN est modélisée dans les simulations à l'aide de ses éléments équivalents de circuit RLC. Lorsque la diode est sous tension en polarisation directe, le modèle équivalent est une série d'une inductance  $L = 0,5 \text{ nH}$  et une

résistance  $R = 2,3 \Omega$ . Lorsque la diode est éteinte dans la polarisation inverse, elle est modélisée sous forme d'une série de capacité parasite  $C = 0.18 \text{ pF}$  et inductance  $L = 0.5 \text{ nH}$ . Le logiciel CST Microwave Studio a été utilisé pour simuler la cellule unitaire FSS [64]. En outre, la cellule unitaire sélective en fréquence est utilisée par le mode Full Floquet qui modélise la structure dans une gamme infinie. Dans cette simulation, l'onde électromagnétique incidente est perpendiculaire au plan X-Y et elle se propage dans la direction Z, et la composante électrique se trouve dans la direction Y.

## 7.6 Antenne reconfigurable de forme ennéagone

L'antenne ennéagone de diagramme de rayonnement reconfigurable comporte deux parties principales. La première partie est une source de rayonnement qui est un dipôle simple constitué de deux tiges métalliques et sa fréquence centrale est de l'ordre de 3.67 GHz. La deuxième partie est les cellules unitaires commutables FSS distribués à travers une forme d'un nonagon qui entoure la source rayonnante. Fondamentalement, le diagramme de rayonnement de l'antenne reconfigurable est composé de 9 panneaux, et chaque panneau comprend 11 cellules unitaires.

Les panneaux sont assemblés à l'aide de trois lignes parallèles de la bande de mousse de scotch dans le côté intérieur de la nonagon. La bande de mousse de scotch est flexible, ce qui permet la formation d'un nonagon. L'antenne est fixée sur une base séparée en matériau en mousse et a une place à tenir dans la nonagon de sa face inférieure. Une distance supplémentaire de 19.7 mm est ajoutée à la circonference globale de l'espacement entre les panneaux.

Les lignes d'alimentation DC sont mises en œuvre sur le bord supérieur et inférieur du nonagon pour alimenter les diodes PIN dans chaque panneau. En outre, une résistance de  $5 \text{ K}\Omega$  est ajoutée devant chaque série de surface sélective en fréquence dans chaque panneau pour prévenir contre les forts courants de polarisation dans les diodes et de garantir la même quantité de courant pour chaque diode. En outre, les côtés supérieur et inférieur du nonagon sont fermés par deux plaques de métal. Ils sont ajoutés pour augmenter le gain et pour empêcher toute perte d'alimentation à travers

ces régions. Les dimensions du cylindre sont choisies en fonction de l'étude présentée dans [34], qui modélise une antenne à un réflecteur, une antenne à réflecteur semi-cylindrique et une antenne de surfaces sélectives en fréquence cylindrique. Ces modèles ont été comparés en termes de correspondance, gain et diagramme de rayonnement. Après le calcul, les dimensions de l'antenne proposée sont optimisées pour un compromis entre un gain approprié, une bande passante et un diagramme de rayonnement directif. Le rayon de l'antenne est de  $0.355 \lambda$ , où  $\lambda$  est la longueur d'onde en espace libre à la fréquence d'opération. La Fig. 6-6 montre l'antenne proposée avec une longueur totale de 170 mm et un rayon  $R = 30\text{mm}$ .

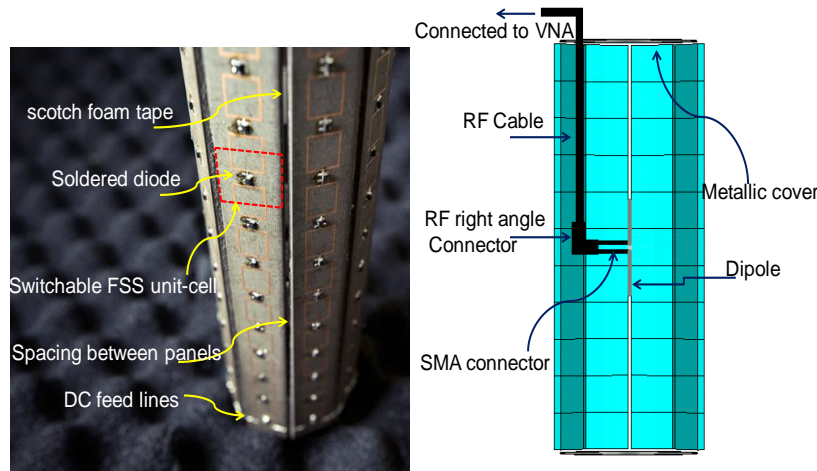


**Figure 7-6 L'antenne reconfigurable proposée, la longueur totale est 170mm et un rayon  $R=30\text{mm}$ .**  
**(a) la photo de l'antenne. (b) le dipôle d'alimentation à l'intérieur de l'antenne.**

L'antenne a quatre panneaux dans l'état transparent et cinq panneaux dans l'état de réflexion à chaque position d'orientation de faisceau reconfigurable. La direction du faisceau de l'antenne reconfigurable ennéagone est pilotée de façon automatique par commutation des éléments actifs dans la surface sélective en fréquence entourant la source de rayonnement. La Fig. 7-6 (b) illustre le dipôle et son alimentation à l'intérieur du nonagon et montre l'antenne reconfigurable de l'intérieur avec ses quatre panneaux transparents. Un câble RF placé à l'intérieur du nonagon d'une manière verticale est relié à un connecteur RF à angle droit qui est relié à un connecteur SMA pour alimenter le dipôle central. Avec cette configuration, l'antenne peut couvrir 9 positions d'angle d'orientation, ce qui complète une plage de 360 ° en azimut.

### 7.6.1 Fabrication et résultats de mesure

La Fig. 7-7 représente le coefficient de réflexion mesuré de l'antenne reconfigurable par rapport au coefficient réflexion du dipôle omnidirectionnelle seul sans le bouclier de surfaces sélectives en fréquence. Dans le cas où l'antenne est directive, l'antenne permet d'obtenir une large bande passante correspondante au plus de 1.4 GHz en acceptant la puissance minimale transmise à 85% de la puissance incidente à la fréquence 3.45 GHz. Les résultats montrent une amélioration significative en termes de largeur de bande d'adaptation due à l'influence de la surface sélective de fréquence sur la performance de la source de rayonnement.

La Fig. 7.8 montre le gain mesuré et simulé de l'antenne reconfigurable du modèle proposé. Le procédé de comparaison de gain est utilisé dans la chambre anéchoïque pour les mesures. La différence entre les résultats mesurés et simulés est due au léger décalage qui existe dans la courbe S11 mesurée et affecte le gain réalisé. Le graphique montre que le gain mesuré a une performance plate approximative dans la bande passante de 500 MHz avec un maximum de 8.6 dBi.

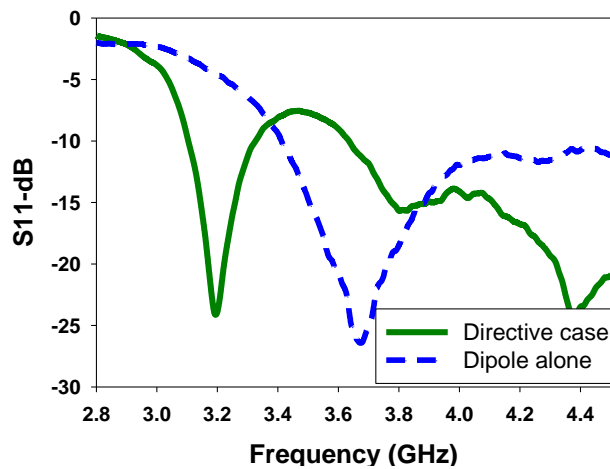


Figure 7-7 Le coefficient de réflexion mesuré de l'antenne et du dipôle.

Le gain et les largeurs de bande correspondants ne sont pas proportionnelles les uns

aux autres en raison de la présence du troisième paramètre, la surface sélective en fréquence commutable. Plus la puissance est transformée à l'état transparent, plus le gain de l'antenne est augmenté. Il est important de souligner qu'environ 95% à 100% de la puissance incidente est réfléchie par les panneaux réfléchissants à l'antenne et ajoutés partiellement aux ondes émises directement à partir du dipôle dans la direction des panneaux transparents.

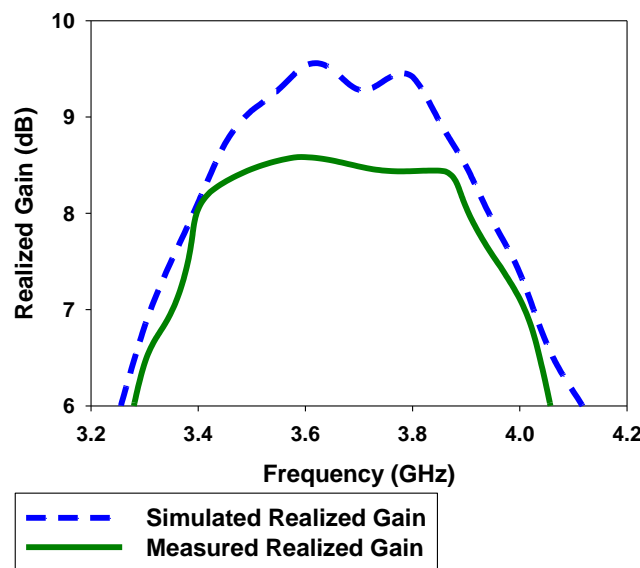


Figure 7-8 Le gain simulé et mesuré de l'antenne proposée

### 7.6.2 Diagrammes de rayonnement mesurés

Les Figs 7-10, 7-12 montrent les diagrammes de rayonnement dans les plans H et E, respectivement, avec une échelle maximale de 8.6 dB. L'antenne a sa meilleure performance dans la bande de fréquence de 3.4 à 3.7 GHz, une largeur de bande de 300 MHz, où les niveaux de lobe arrière sont acceptables pour les deux plans H et E. En outre, la largeur du faisceau à demi-puissance dans le plan H est de 34 ° alors qu'elle est de 27 ° dans le plan E. Le faisceau étroit dans le plan H ajoute une amélioration de résolution angulaire de l'antenne. La largeur du faisceau de l'antenne proposée est inférieure à celles rapportées dans [34, 54, 65].

Comme on peut l'observer à partir des graphiques, l'asymétrie est remarquée dans le

diagramme de rayonnement dans le plan H. Cela est dû à l'interaction qui se produit dans la région autour de la source primaire, le dipôle central représenté sur la Fig. 7-6 (b). Aussi, il y a une légère asymétrie apparaît dans le diagramme de rayonnement dans le plan E, cela est dû à un défaut d'alignement dans la mise en œuvre du dipôle.

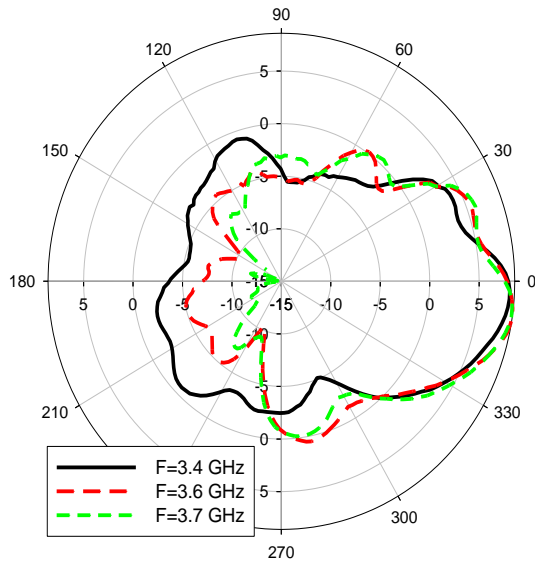


**Figure 7-9 Diagramme de rayonnement co-pol mesuré dans le plan H à travers la bande 300MHz**

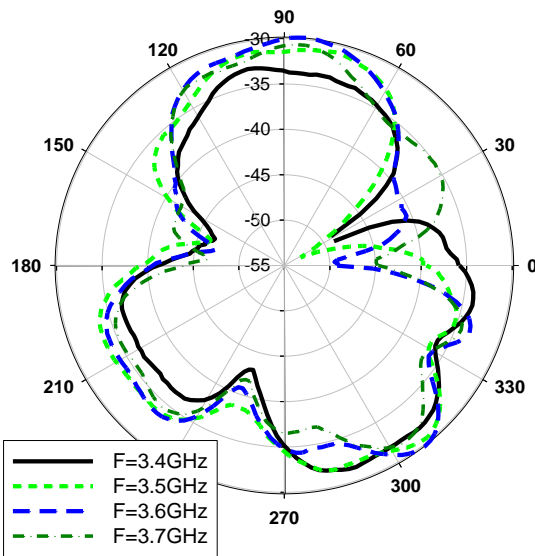


**Figure 7-10 Diagramme de rayonnement cross-pol mesuré dans le plan H à travers la bande 300MHz.**

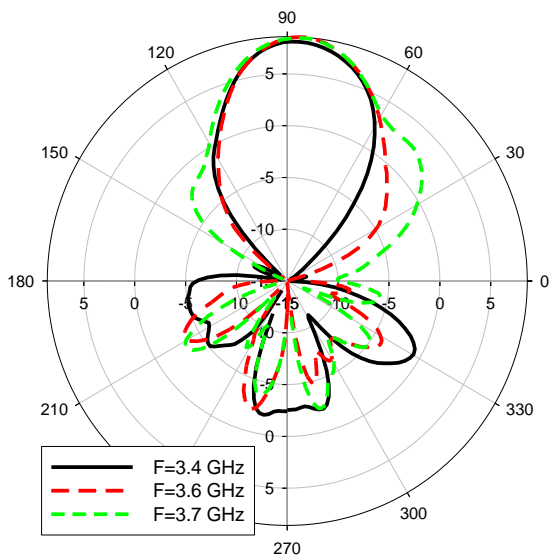


**Figure 7-11 Diagrammes de rayonnement mesurés à travers la bande 300MHz**

Le principal paramètre qui identifie la bande passante du diagramme de l'antenne est la largeur de bande centrale de l'antenne omnidirectionnelle. Le deuxième paramètre principal est la fréquence commutable bande passante de protection de surface sélective. La surface sélective en fréquence agira comme un filtre qui permet seulement certaines fréquences rayonnées par la source centrale de traverser la surface dans un certain pourcentage. Par conséquent, la largeur de bande de la surface sélective en fréquence doit être supérieure à la largeur de bande de la source pour permettre la pénétration des fréquences de la source. La plupart de ces fréquences passent à travers le bouclier de surface sélective en fréquence seulement si la bande passante de la surface sélective en fréquence est supérieure à la largeur de bande de la source centrale. Si la bande passante de la surface sélective en fréquence est inférieure à la largeur de bande de la source, alors la bande passante de l'antenne reconfigurable sera limitée à la bande passante de la surface sélective en fréquence à l'état transparent. En effet, la surface sélective en fréquence ne permet pas la pénétration des fréquences de source qui se trouvent en dehors de bande de fréquence des surfaces sélectives en fréquence. Les derniers paramètres efficaces sont les dimensions du cylindre ; sa hauteur et son rayon. Ces deux paramètres influencent sur la mise en correspondance d'impédance et de gain d'une manière opposée. Il faut faire un compromis de rayon et

de la hauteur pour obtenir la performance souhaitée de l'antenne reconfigurable. Pour l'antenne proposée, Figures 7-5, 7-7 montrent que la largeur de bande de la surface sélective en fréquence est plus grande que la largeur de bande de la source de rayonnement. Par conséquent, une amélioration de la largeur de bande est atteinte.

**Tableau 7-1 Comparaison des antennes**

Comparaison	Antenne proposée	Antenne de [65]	Antenne de [31]
Bande passante fractionnelle	8.45%	4.08%	4.49%
Largeur de faisceau à 3-dB	34°	47°	77°
Fréquence centrale en GHz	3.55	2.45	1.78

D'après les résultats obtenus, la conception de l'antenne actuelle fournit une bande passante plus élevée par rapport aux autres travaux antérieurs [65, 31]. Le Tableau 7-1 montre la comparaison entre l'antenne proposée et les conceptions d'antennes dans [65, 31] en termes de largeur de faisceau et de la fréquence de bande passante. En outre, elle fournit un faisceau étroit, ce qui signifie plus de directivité dans le plan H.

## 7.7 La deuxième antenne reconfigurable en diagramme de rayonnement

### 7.7.1 Introduction

Après avoir présenté une antenne reconfigurable avec un bouclier de surface sélective en fréquence à la fréquence  $f_2$ , une antenne reconfigurable de forme cylindrique qui utilise le concept à la fréquence  $f_1$  est présenté dans cette section pour la première fois dans la littérature. Ces deux antennes sont présentées pour montrer l'impact de la surface sélective en fréquence commutable sur la performance de l'antenne quand elles sont conçus dans les deux bandes de fréquences  $f_1$  et  $f_2$ .

### 7.7.2 La Cellule de FSS à la fréquence $f_1$

La cellule de surface sélective en fréquence utilisée dans cette conception de l'antenne est représentée sur la Fig. 7-12. Cette cellule unitaire sera utilisée pour construire une surface sélective en fréquence autour d'une source cylindrique rayonnante centrale pour fonctionner comme une antenne à balayage de faisceau contrôlée par commutation de la surface sélective en fréquence. Si les cellules unitaires de surface sélective en fréquence sont connectées comme à la Fig. 7-12b, elles fonctionneront comme une surface réfléchissante. D'autre part, si un écart existe entre les cellules unitaires successives, comme représenté sur la Fig. 7-12a, elles agissent comme une surface transparente. L'intégration de la diode PIN (GMP 4202) [63] dans la position de la fente va permettre à la cellule de commuter électroniquement entre les états réfléchissants et transparents. En conséquence, lorsque la diode PIN est mise en OFF, la surface sélective en fréquence est une surface transparente, et lorsque la diode PIN est activée, elle devient une surface réfléchissante.

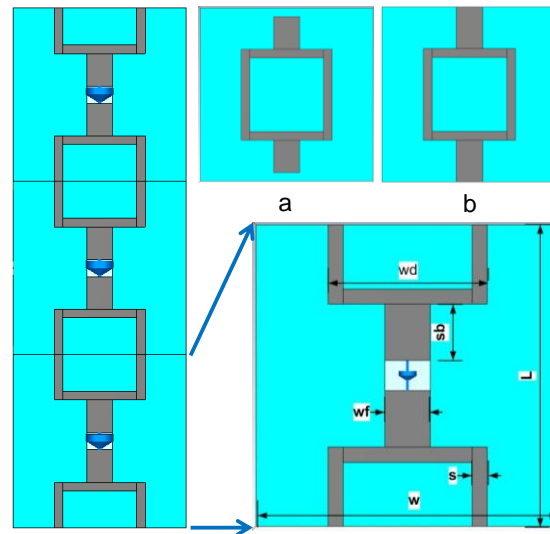


**Figure 7-12 La structure de la cellule FSS proposée. (a) état transparent. (b) état réfléchissant.**

La Fig. 7-13 compare le coefficient de transmission des cellules de surface sélective en fréquence lorsque les diodes PIN sont intégrés dans les états ON et OFF et quand il n'y a pas de diodes intégrées à la cellule unitaire. La figure montre également une échelle

de décibels pour faciliter les comparaisons avec d'autres cellules unitaires dans la littérature. En fait, la simulation de la diode PIN est modélisée par son circuit des éléments équivalents. Lorsque la diode est sous tension dans la polarisation en sens direct, le modèle est équivalent à une résistance  $R = 1.80 \Omega$ , et lorsque la diode est éteinte dans la polarisation inverse, elle est modélisée dans la simulation en tant que connexion en série de la capacité parasite et l'inductance [54] avec  $C = 0.07 \text{ pF}$  et  $L = 0.5 \text{ nH}$ . A noter que, lorsque les diodes PIN sont intégrées à la surface sélective en fréquence, la puissance est réduite dans les deux états réfléchissants et transparents en raison de l'effet dégradant des diodes PIN. L'état transparent est plus affecté par cette dégradation que l'état de réflexion en raison des caractéristiques de diodes PIN; cela pourrait être améliorée en choisissant des diodes PIN de haute qualité avec une meilleure performance. Si en travaillant dans le concept *f2*, l'état de réflexion serait touché plus que l'état transparent, car il a une performance réciproque, et la fréquence de résonance de réflexion serait décalée vers une fréquence basse de 8.616 GHz. A partir de la Fig. 7-14, on peut observer que la largeur de bande de FSS est diminuée lors de l'intégration des diodes aux cellules unitaires. Les diodes avec des caractéristiques élevées et le style d'emballage approprié pourraient être très coûteux, surtout si 160 diodes sont nécessaires, comme dans notre cas. Toutefois, la diode PIN choisie est adéquate à notre antenne parce que l'antenne fonctionne à une fréquence maximale de 2.4 GHz. À cette bande de fréquence, la puissance transmise minimale est d'environ 88% de la puissance incidente lorsque la diode PIN est bloquée, alors qu'une puissance minimale de 93% est réfléchie lorsque la diode PIN est activée. Ces pourcentages sont considérées comme suffisants pour d'antenne reconfigurable cylindrique proposée.

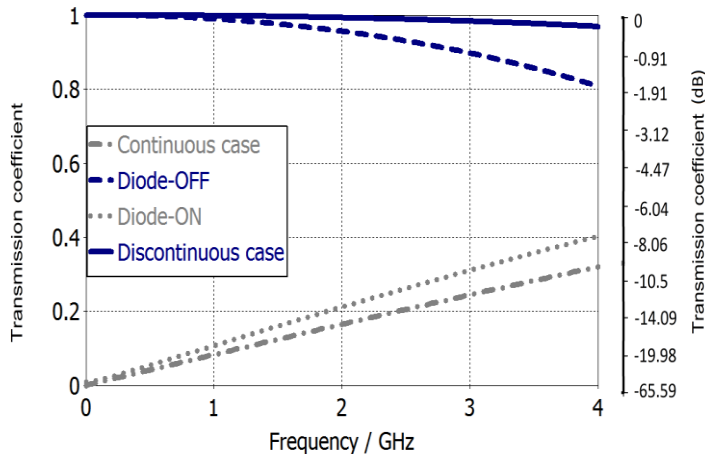


**Figure 7-13 les coefficients de transmission des FSS pour les états transparent et réfléchissant, avec et sans les diodes PIN intégrées.**

La figure. 7-14 représente le coefficient de transmission simulé et mesuré en dB de la surface sélective en fréquence commutable à l'état transparent. Le prototype présente des lacunes comme le montre la Fig. 7-12a, sans les diodes connectés. Le dispositif de mesure se compose de deux antennes cornets de chaque côté où prototype de surface sélectif en fréquence est installé entre eux. La taille du prototype est de 16x10 cellules unitaires. Le substrat utilisé pour la mise en œuvre est de type RO3003 flexible. La surface sélective en fréquence commutable est implémentée avec écarts de sorte que les diodes PIN peuvent être soudées à eux plus tard pour le prototype d'antenne. La longueur de l'intervalle est d'un 1 mm, ce qui est compatible avec la taille de la diode PIN.

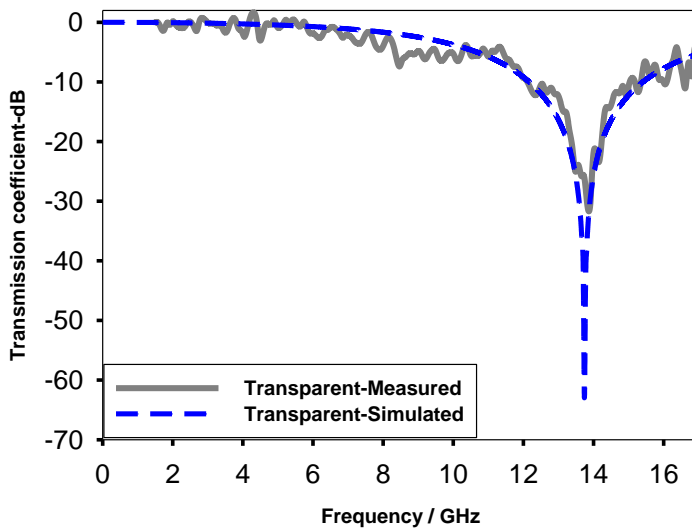


**Figure 7-14 Les coefficients de transmissions simulés et mesures pour l'état transparent**

Après le soudage des diodes PIN, des mesures expérimentales ont été effectuées. La Fig. 7-15 représente le coefficient de transmission en dB pour les états transparent et réfléchissant des surfaces sélectives fréquences. Deux lignes horizontales d'alimentation DC sont ajoutées en haut et en bas de la surface sélective de fréquence pour alimenter les diodes. Une résistance de forte valeur  $5\text{ K}\Omega$  est montée avant chaque série de diodes sur chaque panneau pour protéger les diodes de forts courants de polarisation et de faire en sorte que la même quantité de courant circule dans chaque panneau. La figure illustre le coefficient de transmission de la cellule élémentaire FSS lorsque les états des diodes PIN sont ON et OFF. Les mesures sont effectuées à l'intérieur d'une chambre anéchoïque et montrent une bonne concordance avec ceux de la simulation, en particulier dans les états transparents. Les résultats de l'état réfléchissant montrent une légère différence de l'ordre de 1 dB. Des résultats améliorés peuvent être obtenus avec une plus grande surface de prototype afin qu'elle puisse saisir toute la puissance générée par les antennes cornets.

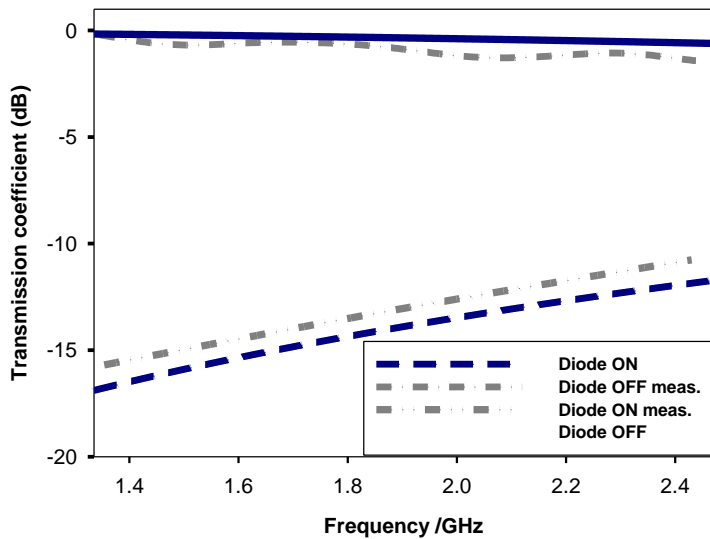


**Figure 7-15 Les coefficients de transmission simulés et mesurés de la cellule FSS dans l'état réfléchissant et transparent.**

Les Figures. 7-16a et b montrent la répartition du champ électrique pour les états transparents et réfléchissants à la fréquence 2.25 GHz dans le plan central Y-Z de la FSS proposée avec les diodes intégrées, comme le montre la Fig. 7-12. La ligne verticale noire dans le centre représente le substrat d'épaisseur de 0.13 mm. Les conditions aux limites périodiques subissent l'onde électromagnétique générée à partir du côté gauche ( $Z<0$ ) pour être absorbée sur le côté droit ( $Z>0$ ). Il est noté que les deux graphiques ont la même valeur de l'onde générée. La figure 7-16a représente la distribution du champ électrique dans le plan Y-Z de la cellule élémentaire FSS lorsque la diode est commutée vers l'état OFF. La majeure partie de l'onde incidente pénètre dans la cellule unitaire dans la région indiquée en rouge, ce qui correspond à l'emplacement de la diode. Au même temps, le champ électrique se propage faiblement à travers les faces supérieure et inférieure, en d'autres termes à travers la boucle. De même, la Figure 7-16b montre la répartition du champ électrique pour l'état de réflexion lorsque la diode est ON. Dans cet état, la cellule unitaire reflète une grande partie du champ électrique incident vers l'arrière à la direction ( $Z<0$ ). À partir de l'échelle, il est clair que la plus faible densité de champ électrique est présentée en bleu foncé tandis que la couleur rouge foncé représente la densité de champ électrique la plus haute. On

peut observer qu'il y a une différence dans les barres d'échelle entre les valeurs maximales pour les figures de la distribution de champ électrique dans les cas transparent et réfléchissant. Ces échelles ont été choisies pour montrer le niveau maximum dans les deux états. Dans la Figure 7-16a, l'échelle maximale apparaît dans le côté de l'onde générée ( $Z<0$ ) et à l'emplacement de la diode. Cette valeur diminue au fur et à mesure que l'onde pénètre à travers la surface sélective en fréquence de l'autre côté ( $Z>0$ ). En revanche, sur la Figure 7-16b l'échelle maximale est dans la région de l'onde générée ( $Z<0$ ). La différence entre les deux échelles indique la quantité du champ électrique réfléchi par la surface sélective en fréquence vers le côté gauche ( $Z<0$ ) dans l'état réfléchissant. Ces figures sont présentées pour démontrer les différences de concentration de champ électrique entre les états réfléchissants et transparents, et en particulier, pour caractériser la quantité de champ électrique réfléchi qui est ajouté à l'onde incidente au ( $Z<0$ ) côté dans l'état réfléchissant. Cette quantité va influer sur la performance de l'antenne, comme il est détaillé dans la section suivante.

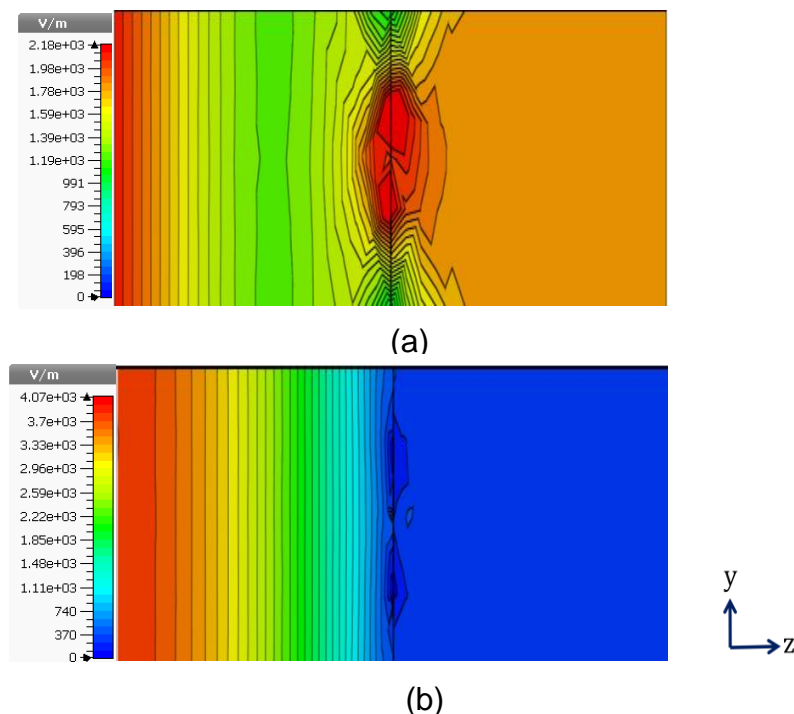


**Figure 7-16 (a)** La distribution du champ électrique à l'état transparent dans le plan Y-Z. **(b)** La distribution du champ électrique à l'état réfléchissant dans le plan Y-Z.

### 7.7.3 Configuration de l'antenne cylindrique reconfigurable

Dans cette section, la cellule FSS proposée avec diodes intégrées, démontré dans la dernière section, est utilisée dans la conception d'une antenne reconfigurable de forme cylindrique. Les performances de l'antenne reconfigurable sont influencées par les caractéristiques de la cellule unitaire FSS. Le concept de la cellule élémentaire à la fréquence  $f_1$  est choisi pour cette application pour les raisons suivantes:

- a. A fin d'assurer l'amélioration des performances de l'antenne reconfigurable en diagramme de rayonnement, la surface sélective en fréquence devrait montrer une forte réflexion de puissance à l'état réfléchissant et une transmission élevée de puissance dans l'état transparent. La transmission élevée de puissance dans la surface sélective en fréquence conduit à plus de puissance transmise sur le coté transparent de l'antenne, et donc plus de gain d'antenne. La puissance réfléchie élevée dans la surface sélective en fréquence offre deux caractéristiques. Premièrement, elle réduit le niveau du lobe arrière du diagramme de rayonnement de l'antenne. En plus, elle augmente le gain parce que la puissance réfléchie est redirigée vers la direction de la partie transparente de l'antenne. Il est important de mentionner que ces deux caractéristiques de la surface sélective en fréquence doivent avoir des fréquences correspondant et être dans la bande de fréquence de fonctionnement de l'antenne.
- b. La surface sélective en fréquence a une large bande de fréquence de fonctionnement avec une puissance réfléchie et transmise suffisantes. Cela rend possible pour l'antenne de transmettre toute la bande de fréquence de la source de rayonnement, qui est le dipôle dans notre concept. La surface sélective en fréquence agit comme un filtre sur les fréquences centrales de la source de rayonnement, si la bande de fréquence de la surface sélective en fréquence est supérieure à la largeur de bande de la source centrale, il permettra à toutes les fréquences de la source de pénétrer dans la partie transparente de l'antenne. De ce fait, l'antenne peut comprendre une large

bande passante de fonctionnement.

- c. La dimension de la cellule élémentaire FSS est réduite, et cela a conduit à une réduction de la taille de l'antenne tout en fonctionnant dans des bandes de basses fréquences. Habituellement, la réduction de la taille de l'antenne affectera négativement ses paramètres de fonctionnement. Néanmoins, l'antenne proposée a amélioré les paramètres avec une taille compacte. En outre, en raison de la taille de cellule unitaire FSS réduite, 16 panneaux peuvent être adaptés à l'antenne. L'antenne peut ainsi fonctionner avec des fonctionnalités de directivité supplémentaire et couvrir un grand nombre d'angle dans le plan d'azimut.

L'antenne est conçue selon les procédures disponibles dans la littérature, et elle est optimisée pour atteindre une taille compacte et des performances nécessaires. Le rayon d'antenne cylindrique  $R = 25.4648$  mm est plus petit que les autres modèles d'antennes similaires dans la littérature. Cela a conduit à la nécessité d'investigation si le modèle de la surface sélective en fréquence de la forme planaire valable pour le modèle conforme utilisé dans la conception de l'antenne. **B** est considéré comme le point central sur la surface sélective en fréquence planaire et **A** est un point situé sur le bord gauche ou droit de la surface sélective en fréquence plane et se trouve sur le cylindre comme représenté également sur la Fig. 7-17. Les calculs montrent que le déphasage entre le point **A** et **B** est négligeable et qui est égale  $1.34^\circ$ . Par conséquent, l'approche proposée avec une surface sélective en fréquence plane pourrait être modélisée pour le cas conforme pour l'antenne cylindrique.

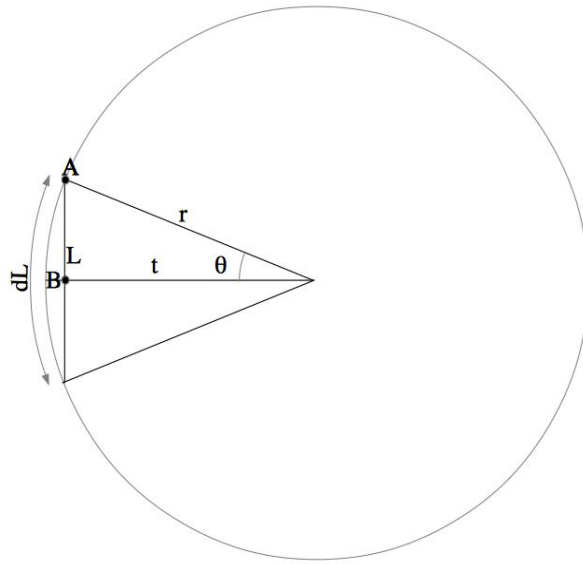


**Figure 7-17 Vue d'en haut de la structure cylindrique**  $dL$  est la largeur de la cellule FSS,  $\theta=0.1976$  rad = $11.32^\circ$ ,  $t=24.969\text{mm}$ ,  $r=25.4648\text{mm}$ ,  $F=2.25\text{GHz}$ ,  $k_0=47.156 \text{ m}^{-1}$ ,  $\Delta\phi=k_0(r-t)=0.0233 \text{ rad} = 1.34^\circ$  (le déphasage entre le point A and B)

L'antenne proposée a une forme cylindrique constituée des cellules de surface sélective en fréquence. Un élément rayonnant omnidirectionnel est placée au centre du cylindre. Il s'agit d'un simple dipôle fonctionnant autour de 2,25 GHz. Le groupe de cellules de surface sélective en fréquence formant le cylindre est composé de 16 panneaux, et chaque panneau comprend 10 cellules FSS, qui forment 10 lignes et 16 colonnes. L'antenne est réalisée sur un substrat flexible RO3003 avec une constante diélectrique de 3 et une épaisseur de 0,13 mm. La longueur totale de l'antenne est de 110 mm, et son rayon est d'environ 25 mm. Les faces supérieure et inférieure du cylindre sont fermées par une plaque métallique circulaire qui est recouverte d'un matériau non métallique sur le côté extérieur. Ces deux plaques sont ajoutées pour empêcher toute perte d'énergie qui pourrait réduire le gain de l'antenne. La Fig. 7-18 montre le concept de l'antenne et le prototype de l'antenne fabriquée.

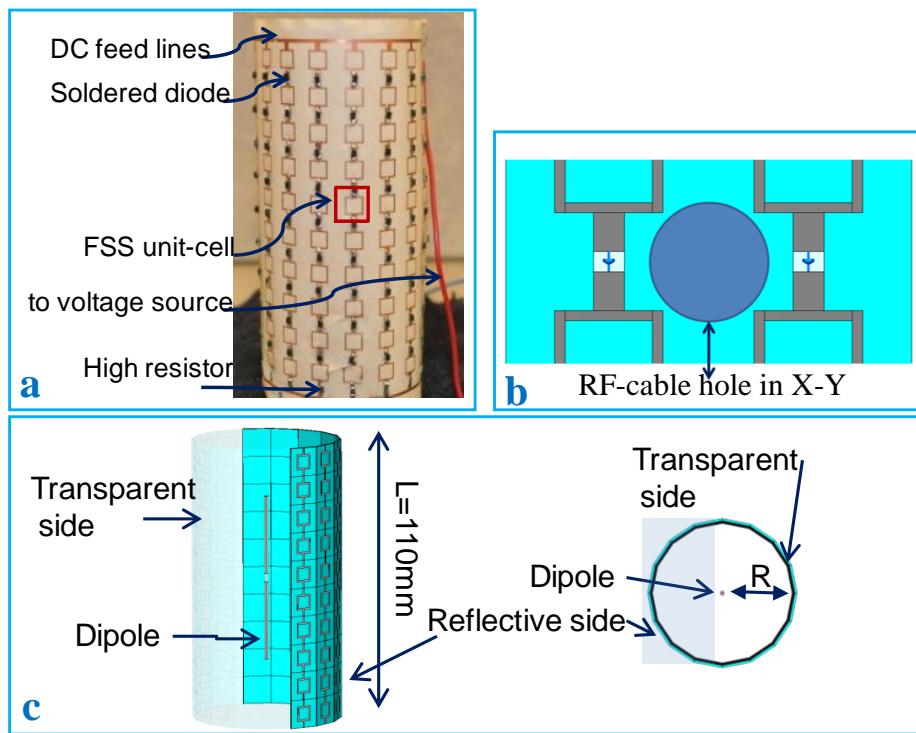


**Figure 7-18 Antenne proposée (a) Photographie de l'antenne fabriquée, (b) Le trou du bouclier FSS pour le câble RF de l'entrée.**

L'antenne possède huit panneaux sur le côté transparent et huit sur le côté de réflexion à chaque position d'orientation du faisceau reconfigurable. La direction du faisceau de rayonnement est obtenue en commutant les éléments actifs dans les panneaux dans la direction souhaitée. Les diodes PIN de huit panneaux sont activées à chaque étape, et les diodes PIN des huit autres panneaux sont désactivées. L'antenne couvre 16 positions à travers l'ensemble de la rotation d'azimut avec un pas de  $22.5^\circ$  d'angle. Ce petit pas d'angle donne à l'antenne des fonctionnalités supplémentaires pour couvrir plus de positions que les autres antennes similaires proposées dans [31, 34, 54, 65] grâce à la petite taille de la cellule de surface sélective en fréquence. La Fig. 7-19 montre le diagramme de rayonnement reconfigurable dans le plan H lorsqu'on considère que six positions angulaires.

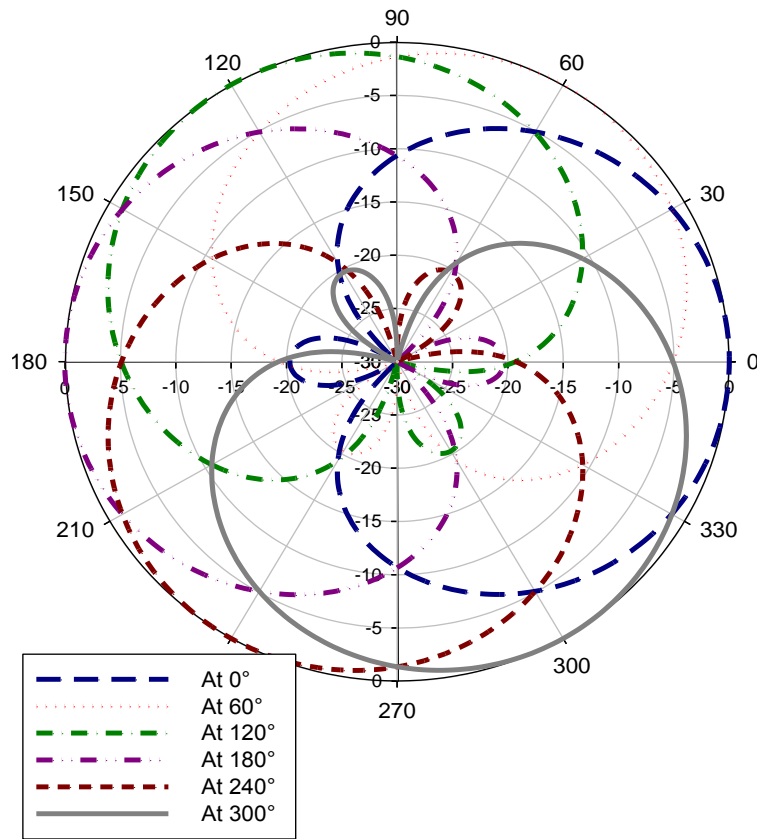


Figure 7-19 Diagramme de rayonnement pour six angle

La Fig. 7-20 illustre le mécanisme de pilotage du faisceau de l'antenne proposée. Les PC représentés sur la figure présentent les récepteurs, ce qui pourrait être tout type de dispositif de réception. La figure montre que l'antenne peut couvrir un maximum de 16 positions différentes, présentées comme des arcs de couleurs. La largeur de chaque arc est liée à la largeur de faisceau (demi-puissance), qui est de 70 °.

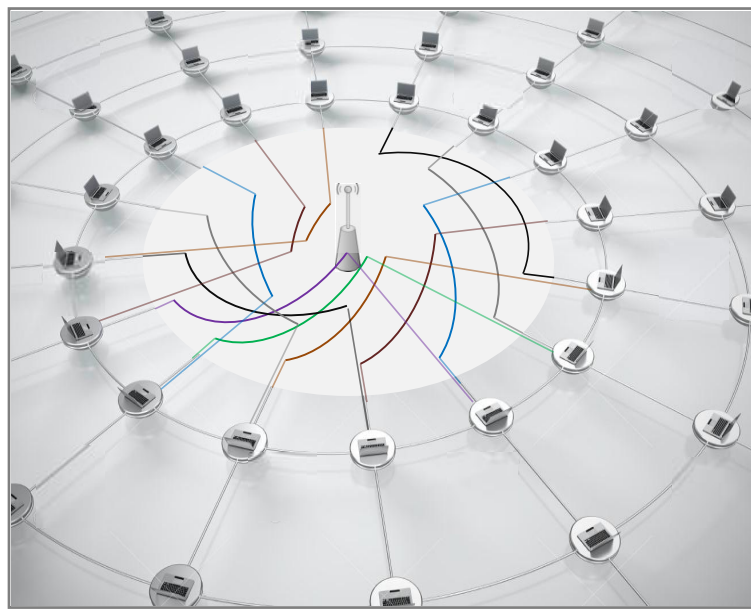


Figure 7-20 Mécanisme de pilotage de faisceau de l'antenne

#### 7.7.4 Résultats expérimentaux et discussions

La Fig. 7-21 montre les coefficients de réflexion mesurés pour le dipôle seul et pour l'antenne reconfigurable en diagramme avec le bouclier de surface sélective en fréquence. L'antenne est dans le cas directionnel lorsque huit panneaux sont réfléchissants et huit autres panneaux sont transparents. L'antenne est dans le cas omnidirectionnel lorsque toutes les diodes de cylindres sont désactivées et toutes les cellules unitaires sont à l'état transparent. A partir de la Fig. 7-21, on peut voir que l'antenne en cas de rayonnement directive possède plus de bande passante que les cas omnidirectionnelle et de dipôle simple. Cela est dû à l'influence de la surface sélective en fréquence sur la performance de la source de rayonnement.

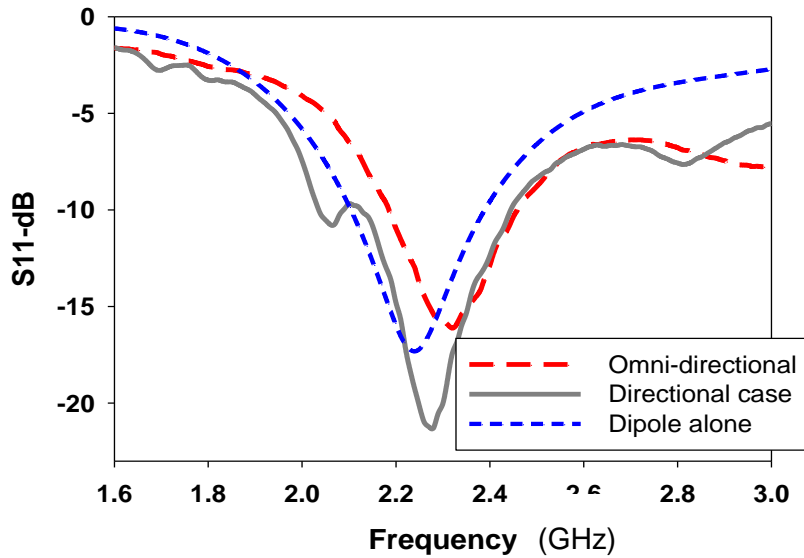
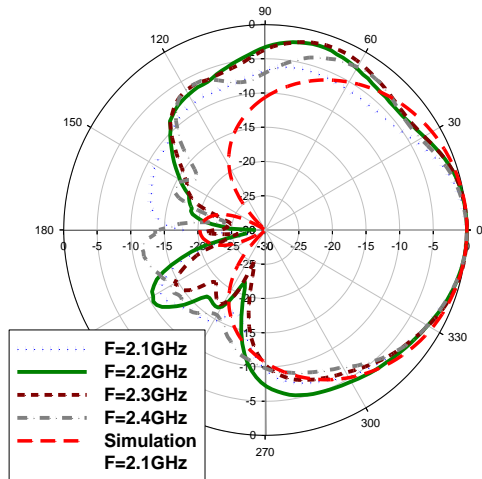
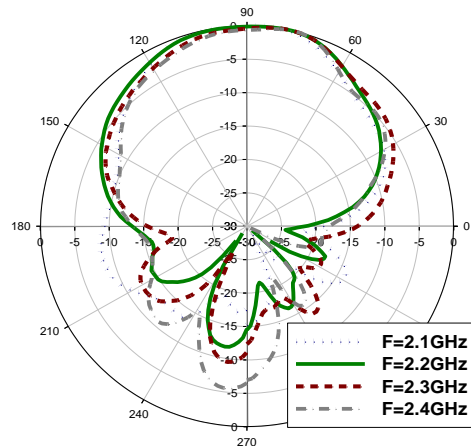


Figure 7-21 Coefficient de réflexion mesuré

A cause de la géométrie symétrique, l'antenne a un diagramme de rayonnement semblable dans toutes les directions à travers les 16 positions qu'elle couvre. Par conséquent, une seule position directionnelle est présentée dans le diagramme de rayonnement. Les Figs. 7-22 et 7-23 montrent les résultats mesurés et simulés des diagrammes de rayonnement dans les deux plans H et E à travers la bande entre 2.1 GHz et 2.4 GHz. Comme démontré dans ces figures, le niveau de lobe arrière est supérieur à -10 dB pour le plan H. En outre, les ouvertures de faisceau à mi-puissance sont à un maximum de  $70^\circ$  et  $62^\circ$  dans les plans H et E, respectivement, à travers la bande de fréquences de 2.1 GHz à 2.4 GHz.



**Figure 7-22 Diagramme de rayonnement mesuré dans le plan H, à travers 300 MHz.**



**Figure 7-23 Diagramme de rayonnement mesuré dans le plan E, à travers 300 MHz**

Il n'y a pas de définition unique de la bande passante. Par conséquent, la bande passante d'une antenne se réfère à des fréquences où l'antenne fonctionne avec les caractéristiques souhaitées. Dans ce type d'antenne de la bande passante la plus critique est la largeur de bande du diagramme de rayonnement. Ceci est à cause des lobes indésirables qui apparaissent dans certaines fréquences dans le plan E. Ainsi, ces fréquences limitent la bande passante de fonctionnement de l'antenne et ne peuvent pas être prises en compte dans les fréquences de fonctionnement, ce point a été discuté en détail dans le chapitre quatre.

Les résultats de la simulation et de mesure des diagrammes de rayonnement dans la

Fig 7-22 montrent un bon accord, à l'exception d'une légère différence liée à la symétrie du diagramme de rayonnement dans le plan H. Cette asymétrie est due à l'alimentation nécessaire pour le dipôle central. Le dipôle à l'intérieur du bouclier cylindrique sélectif en fréquence est alimenté par un connecteur SMA relié à un câble RF. Le câble RF pénètre dans le cylindre à l'horizontale à travers un trou dans la surface sélective en fréquence à la position centrale du dipôle, comme le montre la Figure 7-18b. Le trou est situé au milieu de quatre cellules FSS ajustées pour réduire son effet sur la structure et la performance des cellules. Cet effet de l'alimentation de dipôle n'est pas tenu compte dans les simulations.

Le gain maximal de l'antenne proposée est de 9 dB, ce qui est considéré comme un gain élevé pour ce type d'antenne, en gardant à l'esprit qu'un dipôle à faible gain fonctionne comme l'élément rayonnant de la source. Cette bonne valeur de gain est une conséquence de la forte puissance transmise dans l'état transparent et à la puissance réfléchie dans l'état réfléchissant.

## 7.8 Conclusions

Une nouvelle antenne reconfigurable est proposée avec une surface sélective en fréquence qui fonctionne dans la première bande de fréquence à la Section 7.6. En outre, une nouvelle antenne proposée avec une surface sélective en fréquence fonctionnant à la fréquence de résonance dans la Section 7.5. Les résultats présentés dans les deux sections démontrent la différence dans les deux performances de l'antenne. Le tableau 7-2 montre clairement l'amélioration de la fonctionnalité de la seconde antenne proposée par rapport à la première. L'amélioration la plus importante est l'augmentation de la largeur de bande qui est améliorée de 13,33%. Cela montre que cette antenne a plus de bande passante que les antennes présentées dans la littérature, le Tableau 7-2 qui montre la première amélioration de l'antenne sur les autres antennes de la littérature. La seconde antenne proposée de faisceau directionnel est large par rapport à la première antenne ayant un rayon plus directif. En outre, le gain est de 9 dB dans la bande passante de l'antenne dans le cas directionnel. Il est

important de souligner que l'on a une meilleure réduction de la taille de l'antenne, c'est-à-dire le rayon et la longueur obtenue. En effet, la deuxième fréquence de fonctionnement de l'antenne est inférieure à la première. Un autre avantage de la seconde antenne est qu'elle peut couvrir plusieurs positions reconfigurables dans le plan d'azimut. Le seul inconvénient de la seconde antenne est qu'elle consomme plus d'énergie en raison du nombre supplémentaire de diodes PIN qui est lié au nombre supplémentaire de cellules élémentaires nécessaires en raison de la taille réduite de la cellule. D'après les résultats obtenus dans la première et la seconde antenne, on peut conclure que les performances de ce type d'antenne hautement liées à la conception de la surface sélective en fréquence utilisée pour former le bouclier autour de la source centrale de rayonnement. Le pourcentage de la puissance transmise et réfléchie de la surface sélective en fréquence influe sur les caractéristiques de l'antenne et la bande passante commune des deux états ont un impact sur la bande passante et la performance de l'antenne.

*Tableau 7-2 Comparaison des antennes*

Comparaison	Première antenne du Ch-4		Deuxième antenne du Ch-5	
<b>Bande passante fractionnelle</b>	<b>8.45%</b>		<b>13.33%</b>	
<b>Largeur de faisceau à 3-dB</b>	H	E	H	E
	34°	27°	70°	62°
<b>Fréquence centrale en GHz</b>	<b>3.55</b>		<b>2.25</b>	
<b>Longueur électrique &amp; rayon</b>	<b>2.01λ X 0.355λ</b>		<b>0.825λ X 0.19λ</b>	
<b>Angle de balayage</b>	<b>40°</b>		<b>22.5°</b>	
<b>Nombre de positions directives</b>	<b>9</b>		<b>16</b>	
<b>Gain (dB)</b>	<b>8.6</b>		<b>9</b>	
<b>Pourcentage de la section transparente</b>	<b>44.44%</b>		<b>50%</b>	
<b>Nombre des diodes PIN</b>	<b>99</b>		<b>160</b>	

## 8 REFERENCES

- [1] D. Sievenpiper, J. Schaffner, R. Loo, G. Tangonan, et al., "A Tunable Impedance Surface Performing as a Reconfigurable Beam Steering Reflector," *IEEE Trans. on Ant. and Propag.*, vol. 50, no. 3, pp. 384-390, 2002.
- [2] G. I. Kiani, K. L. Ford, L. G. Olsson, K. P. Esselle, and C. J. Panagamuwa, "Switchable frequency selective surface for reconfigurable electromagnetic architecture of buildings," *IEEE Trans. on Ant. and Propag.*, vol. 58, no. 2, pp. 581–584, Feb. 2010.
- [3] A. Edalati and T. A. Denidni, "Reconfigurable beam-width antenna based on active partially reflective surfaces," *IEEE Ant. Wireless Propag. Lett.*, vol. 8, pp. 1087–1090, 2009.
- [4] R. L. Haupt, and M. Lanagan," Reconfigurable antennas," *IEEE Ant. Propag. Mag.*, vol. 55, no. 1, pp. 46-61, Feb. 2013.
- [5] J. T. Bernhard, *Reconfigurable Antennas*. San Rafael, CA: Morgan & Claypool, 2007.
- [6] Cisco Visual Networking Index: Global Mobile Data Traffic Forecast Update 2014–2019 White Paper. Feb. 2015 available at <http://www.cisco.com>
- [7] J. Huang and J. A. Encinar, *Reflectarray Antennas*, John Wiley & Sons, New York, 2008.
- [8] T. K. Wu, *Frequency-selective surface and grid array*, John Wiley & Sons, New York, 1995.
- [9] H. T. Friis, C. B. Feldman, and W. M. Sharpless, "The determination of the direction of arrival of short radio waves," *Proc. Institute of Radio Engineers*, vol. 22, no.1, pp. 47-78, Jan. 1934.
- [10] P. S. Hall, P. Gardner, J. Kelly, E. Ebrahimi, M. R. Hamid, F. Ghanem, F. J. Martinez, and D. Vargas, "Reconfigurable antenna challenges for future radio systems." *Proc. Eur. Conf. Ant. and Propag.*, pp. 949-955, Mar. 2009.
- [11] C. Caloz, and T. Itoh, *Electromagnetic metamaterials: transmission line theory and microwave applications*, John Wiley & Sons, New York, 2005.
- [12] R. Mittra, C. H. Chan and T. Cwik, "Techniques for analyzing frequency selective surfaces-a review," *Proceedings of the IEEE*, vol. 76, pp. 1593-1615, Dec. 1988.

- [13] B. A. Munk, Frequency Selective Surfaces Theory and Design. John Wiley & Sons, New York, 2000.
- [14] J. C. Vardaxoglou, "Frequency-selective surfaces: Analysis and design," Research Studies Press, Ltd., Taunton, UK, 1997.
- [15] D. Sievenpiper, L. Zhang, R. F. J. Broas, N. G. Alexopolous, and E. Yablonovitch. "High-impedance electromagnetic surfaces with a forbidden frequency band." IEEE Trans. Microw. Theory Tech., vol. 47, pp. 2059-2074, Nov. 1999.
- [16] B. Hooberman, "Everything you ever wanted to know about frequency selective surface filters but were afraid to Ask," Technical report. May 2005.
- [17] F. Yang, and Y. Rahmat-Samii, Electromagnetic band gap structures in antenna engineering, Cambridge, Cambridge University Press, 2009.
- [18] C. A. Balanis and P. I. Ioannides, Introduction to Smart Antennas, Morgan & Claypool publications series, 2007.
- [19] E. W. Matthews, C. L. Cuccia, and M. D. Rubin, "Technology Considerations for the Use of Multiple Beam Antenna Systems in Communications Satellites," IEEE Trans. Microw. Theory Tech., vol. 27, pp. 998-1004, Dec. 1979.
- [20] Edalati, T. A. Denidni, "Frequency Selective Surfaces for BeamSwitching Applications", IEEE Trans. Ant. and Propag., vol. 61, no. 1, pp. 195-200, 2013.
- [21] F. Capolino, Theory and Phenomena of Metamaterials, CRC Press, Taylor and Francis Group, 2009.
- [22] G. K. Palikaras, A. P. Feresidis and J. C. Vardaxoglou, "Cylindrical Electromagnetic Bandgap Structures for Directive Base Station Antennas", IEEE Ant. Wireless Propag. Lett., vol.3, no. 1, pp-87-89, 2004.
- [23] G.K Palikaras, A.P Feresidis and J.C Vardaxoglou. "Cylindrical EBG surface for omni-directional wireless LAN antennas" IEEE Ant. and Propag. Society International Symposium, pp. 339-342, Jul. 2005.

- [24] H. Boutayeb, T.A. Denidni, K. Mahdjoubi, Anne-Claude Tarot, A. Sebak, and L. Talbi, "Analysis and Design of Cylindrical EBG Structures and their Applications to Directive Antennas ", IEEE Trans. Ant. and Propag., vol. 54, No. 1, pp. 211-219, Jan. 2006.
- [25] H. Boutayeb and T.A. Denidni, "Band Structure of Crystals with Periodically Loaded Metallic Wires," IEEE Ant. and Propag. Society International Symposium, pp.4501-4504, Jul. 2006.  
doi: 10.1109/APS.2006.1711636
- [26] A. Edalati, H. Boutayeb, and T. A. Denidni, "Band structure analysis of reconfigurable metallic crystals: Effect of active elements," J. Electromagn. Waves Applicat., vol. 21, no. 15, pp. 2421–2430, 2007.
- [27] A. Edalati and T. A. Denidni, "High-Gain Reconfigurable Sectoral Antenna Using an Active Cylindrical FSS Structure", IEEE Trans. Ant. Propag., vol. 59, no. 7, pp. 2464 - 2472 , Jul. 2011.
- [28] Y. L. Tsai, R. B. Hwang, and Y. D. Lin, "A reconfigurable beam-switching antenna base on active FSS." International Symposium Antenna Technology and Applied Electromagnetic (ANTEM), Toulouse, France, pp. 1-4. 2012.
- [29] B. Liang, S. L. Benito, J. C. Batchelor, and A. Bogliolo. "Active FSS enclosed beam-switching node for wireless sensor networks." European Conference in Antennas and Propagation (EuCAP), pp. 1348-1352. Apr. 2014.
- [30] A. Bostani and T.A. Denidni,, "Design and implementation of a beam scanning reconfigurable antenna," IEEE Ant. and Propag. Society International Symposium, pp.1-4, 2009.
- [31] L. Zhang, Q. Wu, and T. Denidni. "Electronically Radiation Pattern Steerable Antennas Using Active Frequency Selective Surfaces." IEEE Trans. Ant. and Propag., vol. 6, pp. 6000 – 6007, Dec. 2013.
- [32] M. A. Habib, M. N. Jazi, A. Djaiz, M. Nedil, and T. A. Denidni, "Switched-beam antenna based on EBG periodic structures," Proc. IEEE Int. Microwave Symp., pp. 813–816, Jun. 2009
- [33] M. A. Habib and T. A. Denidni. "Directive cylindrical electromagnetic band gap antenna with microstrip technology." IEEE Ant. and Propag. Society International Symposium, 2007.

- [34] M. Niroo-Jazi and T. A. Denidni, "Electronically sweeping-beam antenna using a new cylindrical frequency-selective surface," IEEE Trans. Ant. and Propag, vol. 61, pp.666-676, Sep. 2013.
- [35] ASD Reports. (2014, April). Metamaterials Market - Trends & Global Forecasts to 2025. [Online]. Available : <https://www.asdreports.com/market-research-report-105693/metamaterials-market-trends-global-forecasts>
- [36] Wikipedia. Stealth aircraft. [Online]. Available : [https://en.wikipedia.org/wiki/Stealth\\_aircraft](https://en.wikipedia.org/wiki/Stealth_aircraft)
- [37] Wikipedia. French ship Surcouf . [Online]. Available : [https://en.wikipedia.org/wiki/French\\_ship\\_Surcouf](https://en.wikipedia.org/wiki/French_ship_Surcouf)
- [38] Misawa, Japan Misawa NSA Echelon Station [Online]. Available : [http://www.thelivingmoon.com/45jack\\_files/03files/ECHELON\\_Misawa.html](http://www.thelivingmoon.com/45jack_files/03files/ECHELON_Misawa.html)
- [39] Wikipedia. USS San Antonio (LPD-17) [Online]. Available : [https://en.wikipedia.org/wiki/USS\\_San\\_Antonio\\_\(LPD-17\)](https://en.wikipedia.org/wiki/USS_San_Antonio_(LPD-17))
- [40] F. Bayatpur," Metamaterial-Inspired Frequency-Selective Surfaces ,”Ph.D. dissertation, Dept. Elect. Eng., Michigan Univ., Michigan, 2009.
- [41] [Online]. Available : <http://dasan.sejong.ac.kr/~dongkim/subject2.html>
- [42] M. Raspopoulos and S. Stavrou, “Frequency selective buildings through frequency selective surfaces,” IEEE Trans. Ant. Propag., vol. 59, no. 8, pp. 2998–3005, Aug. 2011.
- [43] Knott, Eugene F., John F. Schaeffer, and Michael T. Tuley: Radar Cross Section. SciTech Publishing, Raleigh, NC, 2nd edition, 2004, ISBN 978-1-891121-25-8.
- [44] G. Marconi and C.S. Franklin, “Reflector for use in wireless telegraphy and telephony,”U.S. Patent 1 301 473, 1919.
- [45] V. D. Agrawal and W. A. Imbriale, “Design of a dichroic Cassegrah subreflector,” IEEE Trans. Ant. Propag., vol. 27, no. 4, pp. 466-473, Jul. 1979.
- [46] T. K. Wu, “Four-band frequency selective surface with double-square-loop patch,” IEEE Trans. Ant. Propag., vol. 42, no. 12, pp. 1659-1663, Dec. 1994.

- [47] D. R. Jackson and N. G. Alexopoulos, "Gain enhancement methods for printed circuit antennas," IEEE Trans. Ant. Propag., vol. 33, no. 9, pp. 976-987, 1985.
- [48] A. K. Rashid and B. Li, Z. Shen, "An overview of three-dimensional frequency-selective structures," IEEE Trans. Ant. Propag. Mag., vol. 56, pp. 43-67, Jun. 2014.
- [49] B. A. Munk, Finite Antenna Arrays and FSS, John Wiley & Sons, New York, 2003.
- [50] J. Thirumal Murugan and T. R. Suresh Kumar, "Frequency selective transparent frontdoor for microwave-oven," Int. J. Elec & Electr. Eng & Telecoms, vol. 3, no. 3, pp. 120-123, 2014.
- [51] G. Poilasne, P. Pouliquen, K. Mahdjoubi, L. Desclos and C. Terret, "Active Metallic Photonic Band-Gap Materials (MPBG): Experimental Results on Beam Shaper," IEEE Trans. Ant. Propag., vol. 48, no. 1, pp. 117-119, 2000.
- [52] C. A. Balanis, Modern Antenna Handbook. , John Wiley & Sons, New York, 2008.
- [53] T. K.. Chang, R. J. Langley and E. A. Parker, "An active square loop frequency selective surface," IEEE Microw. Guided Wave Lett., vol. 3, no. 10, pp. 387–388, 1993.
- [54] Jazi, M. N. and T. A. Denidni, "Frequency selective surfaces and their applications for nimbleradiation-pattern antennas," IEEE Trans. Ant. Propag., vol. 58, no. 7, pp. 2227–2237, 2010.
- [55] G. I. Kiani, K. L. Ford, and K. P. Esselle et al., "Single-layer bandpass active frequency selective surface," Microw. Opt. Tech. Lett., vol. 50, no. 8, pp. 2149–2151, Aug. 2008.
- [56] P. S. Taylor, E. A. Parker, and J. C. Batchelor, "An active annular ring frequency selective surface," IEEE Trans. Ant. Propag., vol. 59, pp. 3265–3271, Sep. 2011.
- [57] B. Sanz-Izquierdo, E. A. Parker, and J. C. Batchelor. "Switchable technique for frequency selective slots," IEEE Ant. and Propag. Society International Symposium, pp. 1-4, 2010.
- [58] F. J. Zucker ,Antenna Engineering Handbook, McGraw Hill, New York, 1961.

- [59] N. Engheta and R. W. Ziolkowski, Metamaterials: Physics and Engineering Explorations, John Wiley & Sons, New York, 2006.
- [60] J. Costantine, Y. Tawk, and C. G. Christodoulou, "Design of reconfigurable antennas using graph models." Morgan and Claypool Publishers, Synthesis Lectures on Antennas 2013.
- [61] D. Uttamchandani, Handbook of MEMS for Wireless and Mobile Applications, Woodhead publishing, 2013.
- [62] M. A. Matin, Wideband, Multiband, and Smart Reconfigurable Antennas for Modern Wireless Communications, IGI Global, 2015.
- [63] GMP4200 PIN-Diode Series, [Online]. Available:  
<http://www.microsemi.com/datasheets/gmp4200%20series.pdf>.
- [64] CST Microwave Studio. "User Manual Version 2011." CST Computer Simulation Technology, Darmstadt, Germany, 2011.
- [65] B. Liang, B. Sanz-Izquierdo, E. A. Parker, and J. C. Batchelor, "Cylindrical Slot FSS Configuration for Beam-Switching Applications," IEEE Trans. Ant. Propag., vol. 63, no. 1, pp. 166-173, Jan. 2015.
- [66] R. L. Yadava, Antenna and Wave Propagation, PHI Learning Pvt. Ltd, 2011.
- [67] A. Balamis Constantine, Antenna theory : analysis and design, John Wiley & Sons, New York, 2012.
- [68] D. M. Pozar, Microwave Engineering, John Wiley & Sons, New York, 2004.
- [69] Indian railways launch free WiFi service on trains, [Online]. Available :  
<http://www.netvuze.com/2013/04/indian-railways-launch-free-wifi.html>

## **Publications**

1. S. M. Mahmood and T. A. Denidni, "Pattern Reconfigurable Antenna using a Switchable Frequency Selective Surface with Improved Bandwidth" IEEE Ant. Wireless Propag. Lett., no.99, pp.1, Oct. 2015. doi: 10.1109/LAWP.2015.2496501
2. Suhair M. Mahmood and Tayeb A. Denidni "Switchable Square Loop Frequency Selective Surface," Progress In Electromagnetic Research Letters, vol. 57, pp 61–64, Oct. 2015.
3. S. M. Mahmood and T. A. Denidni, "A Comparative Study on Switchable Frequency Selective Surfaces" Microwave and Optical Technology Letters, vol. 58, Issue 4, pp. 839 Feb. 2016.
4. S. M. Mahmood and T. A. Denidni, Switchable Square Frequency Selective Surfaces" Microwave and Optical Technology Letters. vol. 58, Issue 6, pp. 1446. Mar. 2016.

## **Conferences:**

5. S. M. Mahmood, T. A. Denidni, "A novel three-dimensional wideband active frequency selective surface unit-cell," IEEE Ant. and Propag. International Symposium pp.1256-1257, Jul. 2015. Doi: 10.1109/APS.2015.7305017
6. S. M. Mahmood and T. A. Denidni," Switchable Single-Slot Ring Frequency Selective Surface" Ubiquitous Wireless Broadband (ICUWB), IEEE International Conference 2015. Doi: 10.1109/ICUWB.2015.7324517
7. S. M. Mahmood and T. A. Denidni, "Reconfigurable antenna using novel active frequency selective surface" IEEE Ant. and Propag. International Symposium, pp. 1236 - 1237, 2014. Doi: 10.1109/APS.2014.6904945.
8. S. M. Mahmood and T. A. Denidni, "Design and Implementation of Substarte-Free Frequency Selective Surfaces", Antenna Technology and Applied Electromagnetics (ANTEM), Montréal, Canada, Jul. 2016.